The Dissertation Committee for Shannon Renee Sweeney Certifies that this is the approved version of the following dissertation:

Elucidating metabolic vulnerabilities to improve outcomes in pediatric precursor B-cell acute lymphoblastic leukemia

Committee:

Stefano Tiziani, Supervisor

Dean R. Appling

Jennifer S. Brodbelt

John DiGiovanni

Marina Y. Konopleva

Elucidating metabolic vulnerabilities to improve outcomes in pediatric precursor B-cell acute lymphoblastic leukemia

by

Shannon Renee Sweeney

Dissertation

Presented to the Faculty of the Graduate School of

The University of Texas at Austin

in Partial Fulfillment

of the Requirements

for the Degree of

Doctor of Philosophy

The University of Texas at Austin

May 2020

Dedication

To my parents for always believing I was exceptional and inspiring me to prove them right. To my sisters – Lauren for keeping me grounded, Erin for making me want to fly – together you have taught me innumerable lessons. Thank you for teaching me how to mediate, negotiate, and above all, choose my battles. And to Nicholas, you make me better; none of this would have been possible without you.

Acknowledgements

I will be forever grateful and indebted to the many people who have guided me with endless encouragement and unwavering support. The most incredible tribe of brilliant women – Dr. Nathalie Muñoz, Dr. Maria José Romo Palafox, Dr. Gloria Cecilia Galván, Dr. Lauren D. Mangini, Dr. Deborah Salvo Domínguez, and soon to be doctors, Diana E. Gutierrez Lopez and Amy R. Nichols. It took me a while to find you, but in the end, your timing was impeccable. My lab family – Dr. Renu Pandey, Xiyuan Lu, Jennifer Chiou, Meghan Collins, Paul Gries, and Lavender Hackman. Thank you for sharing your gifts and being on this journey with me. Dr. Enrique Sentandreu, thank you for mentoring me long beyond our time together at the bench. Your guidance has been one of the greatest gifts. Dr. Alessia Lodi, thank you for your insightful observations, computational magic, and ability to visualize data so beautifully. To my committee members, I acknowledge that truly none of this is possible without you; thank you for sharing your precious time and insights with me. Last, but certainly not least, deepest gratitude to my advisor, Dr. Stefano Tiziani, for endlessly encouraging me to find my passion and realize my potential.

Abstract

Elucidating metabolic vulnerabilities to improve outcomes in pediatric precursor B-cell acute lymphoblastic leukemia

Shannon Renee Sweeney, PhD

The University of Texas at Austin, 2020

Supervisor: Stefano Tiziani

Cancer continues to be the leading cause of disease-related death in children. Improving treatment protocols and outcomes for pediatric leukemia patients is of critical importance as acute lymphoblastic leukemia (ALL) accounts for 25% of all childhood cancers. ALL five-year relative survival rates have improved significantly in recent decades. However, many survivors suffer severe chronic physiological and psychological health problems, as well as poor social and economic outcomes. These consequences exemplify the continuing need to develop targeted, less toxic alternative therapeutics. Metabolomics, an emerging tool for precision medicine, can be used to analyze intracellular and extracellular environments, metabolic response to treatment, and pathway regulation in order to expand our understanding of the molecular mechanisms that drive pediatric cancer biology and identify and evaluate novel therapeutics. This study applied metabolomics approaches to precursor B-cell ALL (BCP-ALL) which accounts for 80% of ALL cases in children and adolescents. First, high-throughput screening (HTS) was used to identify a synergistic combination of non-toxic therapeutic alternatives to chemotherapy. Metabolomics and metabolic flux analyses of dimethylaminoparthenolide (DMAPT) and

shikonin (SHK) in BCP-ALL showed changes in amino acid, antioxidant, TCA cycle, and nucleotide metabolism. The shunting of glycolytic intermediates and glutaminolysis-related metabolites to support proliferation was inhibited by DMAPT and SHK leading to apoptosis in BCP-ALL cells. Second, bone marrow-derived leukemia cells were collected from pediatric BCP-ALL patients at diagnosis. Stratifying patients by cytogenetic anomalies yielded unique metabolic profiles. Aberrations at the IGH locus are associated with poor outcomes, but no clear therapeutic targets have been identified. Assessment of individual metabolites indicated that amino acids, amino acid-related compounds, and some sugars were more abundant in patients with IGH locus aberrations. Phosphatidylcholines, phosphatidylethanolamines, and polar compounds involved in lipid metabolism were also increased, while nucleotides, diglycerides, and triglycerides were decreased in the IGH group. Pathway interrogation confirmed metabolic dysregulation. HTS indicated IGH mutant sensitivity to HSP, proteasome, mTOR, and HDAC inhibitors. Together, these analyses indicate the flexibility and utility of metabolomics to elucidate the underlying biology of pediatric leukemia and evaluate novel therapeutics to improve quality of life and long-term outcomes for childhood leukemia patients and adult survivors.

Table of Contents

List of Tables

List of Figures

Chapter 1: Introduction

1.1 CANCER

It is estimated that in 2020, there will be nearly 2 million (1,806,590) cancer diagnoses and over half a million (606,520) cancer deaths in the United States (U.S.) [1]. Despite an overall decline in cancer-related deaths in recent decades, cancer remains the second leading cause of death overall, second only to heart disease. It is also the leading cause of death in Hispanic and Asian Americans, and individuals younger than 80 years of age [1, 2]. Moreover, the most recently reported five-year survival rate is 67% overall (2009 – 2015), indicating that nearly one third of people diagnosed with cancer succumb to the disease within the first five years [1].

Cancer comprises a vast diversity of neoplastic diseases defined most simply by the uncontrolled proliferation of abnormal cells. Biologically, cancers share at least six well-established characteristics: resisting cell death, sustained proliferative signaling, evading growth suppressors, activating invasion and metastasis, enabled replicative immortality, and inducing angiogenesis [3, 4]. More recently, deregulating cellular energetics and avoiding immune destruction have appeared as emerging 'hallmarks' and genome instability and tumor-promoting inflammation have been identified as enabling characteristics [4]. In the last few decades, a great deal of research has focused on the genetic anomalies that permit and promote these shared cancer cell characteristics. From a genetics perspective, cancer can be understood as the accumulation of genetic lesions over time, giving rise to abnormal cellular proliferation [4-6]. The multi-stage model of carcinogenesis – encompassing initiation, promotion, and progression – is well-recognized

---

Portions of this chapter have been previously published as the book chapter "Metabolomics, Bioactives, and Cancer" in the 2nd edition of *Genomics, Proteomics, and Metabolomics in Neutraceuticals and Functional Food*. Author contributions: Sweeney SR: Manuscript composition. DiGiovanni J: Critical revisions of the article. Tiziani S: PI, critical revisions of the article.

and has been widely accepted for many years [7-9]. As cells replicate, they become more prone to errors. Many errors naturally result in apoptosis or cellular senescence. In cancer, however, the accumulation of oncogenic errors results in tumor development [5, 6, 10, 11]. Current evidence suggests that genomic instability continues and may be accelerated during tumor progression, leading not only to the accumulation of submicroscopic lesions, but the loss of chromosomal integrity as well [8, 12]. Accordingly, cancer is typically thought of as a disease of old age or aging. The acceleration of the process that results in cancer in young individuals is not well understood. It cannot be attributed to germline mutations, or heritable cancers, as they only account for 7–8 % of childhood cancers [13, 14]. There is compelling evidence that genetic mutations found predominantly in infants are initiated *in utero* (i.e. *MLL* translocations), but there is little indication that this is the case in most pediatric cancers [15, 16]. Pan-cancer genome and transcriptome analyses of pediatric leukemias and solid tumors found that only 45% of common genetic driver genes in children and adolescents overlapped with those found in adult studies [17]. Thus, translating findings from research and clinical trials in adults may not represent the best approach for treating pediatric cancer patients. Pediatric cancers may require distinct and unique techniques and approaches to understand the disease biology, develop treatment protocols, and improve long-term outcomes for childhood survivors. In fact, the National Cancer Institute (NCI) at the Nation Institutes of Health (NIH) has advocated for the investigation of the biological foundation for age-related differences in cancer outcomes [18].

1.2 PEDIATRIC CANCER

Cancer is the second leading cause of death in American children aged 1 to 14 years, surpassed only by accidents [1, 2]. Moreover, cancer is responsible for more than half (57%) of disease-related deaths in children [2]. For reasons that remain unclear, childhood cancer rates have steadily increased by 0.7% per year since 1975 [1]. Although diagnoses continue to rise, childhood cancer survival rates have improved significantly in recent decades. The increase in overall numbers has been driven by progress in five-year survival rates in leukemia, which are currently 87% for children (birth to 14 years) and 73% for adolescents (15 to 19 years) [1]. However, many survivors suffer from poor long-term outcomes including excess mortality and a wide range of late effects as a result of cancer treatment [19]. Pediatric cancer survivors have a significant increase in risk of all-cause mortality up to 30 years after diagnosis [20]. When evaluated clinically, 98.2% of long-term survivors had at least one chronic health condition [21]. Adult survivors of childhood cancers suffer from a variety of life-threatening chronic health conditions including, pulmonary, cardiac, endocrine, and neurological disorders [21, 22]. Adult survivors are also prone to chronic conditions effecting quality of life including vision loss, hearing impairment, reproductive complications, diminished cognitive function, and mental health concerns [21, 23-25]. Optimization of timing, dosages, and combinations of existing therapeutics are predominantly responsible for improvements in patient outcomes [1, 26, 27]. However, less progress has been made in understanding the causes of childhood and adolescent cancers [20]. Further reducing cancer mortality will rely on new treatment paradigms based on childhood-specific cancer biology and targeted therapy [26].

1.3 LEUKEMIA

1.3.1 Background

Leukemia arises when white blood cells undergo malignant transformation while in circulation or in the bone marrow [28]. Because these cells are not confined to a single tissue, they do not form solid tumors [29]. Rather, immature malignant cells overpopulate the blood and bone marrow microenvironment, interfere with normal hematopoiesis, and ultimately overwhelm the circulatory and lymphatic systems [28, 30]. Thus, hematologic malignancies are unique in presentation [28, 29]. Leukemias are categorized as either lymphoblastic or myeloid depending on the cellular origin of malignant cells [30]. Lymphoblastic and myeloid leukemias are further categorized as either acute or chronic. Acute leukemias are characterized by the rapid proliferation of immature blast cells whereas chronic leukemias proliferate more slowly and malignant cells are more mature [28]. Acute lymphoblastic leukemia (ALL) and acute myeloid leukemia (AML) require immediate intensive chemotherapeutic treatment to avoid the spread of malignant cells to vital organs and the central nervous system (CNS) [28, 30]. Conversely, chronic myeloid leukemia (CML) proliferates less rapidly and up to half of cases are diagnosed incidentally. Approximately 95% of CML cases can be managed with tyrosine kinase inhibitors, which specifically target malignant cells. Finally, chronic lymphoblastic leukemia (CLL) is diagnosed almost exclusively in older adults (65 years and older) and often requires little to no treatment to manage symptoms [29].

In 2020, an estimated 60,530 people will be diagnosed with leukemia in the U.S. [1]. It is also estimated that leukemia will result in the deaths of 23,100 people in 2020 [1]. Acute leukemia incidence is high in both children (0–14 years) and adolescents (15–19 years). Together, they account for 74% of cases, making ALL predominantly a childhood

disease [20, 31]. In addition, ALL is also the most common malignancy in young people, accounting for 28% of all cancer incidence in children [1, 19, 20]. Acute myeloid leukemia (AML) is the fifth most common malignancy, accounting for approximately 5% of all cancers in children. Overall, incidence of ALL and AML decrease with age. For adolescent boys between 15 and 19 years of age, ALL is the fourth most common cancer accounting for 9% of all cancers and AML is the seventh most common cancer accounting for 4% of cancer incidence. Together, ALL and AML make leukemia one of the most common cancers in adolescent males. In adolescent girls, ALL is the sixth most common cancer accounting for 5% of incidence and AML is eighth, also with approximately 5% of cancer incidence [19].

In the last three decades, significant improvements in chemotherapeutic regimens have vastly improved leukemia patient prognosis. The five-year survival rates for children and adolescents rose from 41% in the 1970s to 71% in the early 2000s [20, 26, 32]. Presently, five-year survival rates are 87% and 73% for children and adolescents, respectively [1]. Nonetheless, cancer, including leukemia, continues to be the leading cause of disease-related death in children [1, 33].

1.3.2 Urgent need to improve long-term outcomes for pediatric leukemia survivors

Despite high rates of remission, the Childhood Cancer Survivor Study reported that the primary cause of death in leukemia survivors was disease recurrence and secondary tumorigenesis [34]. Additionally, pediatric leukemia survivors suffer from a number of severe chronic health problems including musculoskeletal, cardiac, and neurological conditions [34-36]. Childhood survivors also struggle with social, emotional, psychological, academic, and economic challenges, including lower rates of marriage and college graduation when compared to their healthy siblings [34, 37-39]. These

consequences are directly connected to the administration of highly toxic chemotherapeutics at young age [35-37, 39]. Thus, new strategies are needed to improve long-term quality of life for childhood cancer survivors [34, 40].

1.3.3 Risk stratification has reduced pediatric leukemia mortality

Patient stratification based on risk-directed treatment, coupled with improvements in supportive care for children and adolescents, has greatly reduced mortality over the last three decades [33, 40]. For risk-directed treatment, leukemia patients are assigned a preliminary risk group based on select clinical parameters prior to induction therapy [41]. Most commonly, patients are classified into two groups: standard risk (SR) or high risk (HR), or four groups by the addition of: very high risk (VHR) and low risk (LR). Conventional, widely-accepted risk factors at diagnosis include: sex, age, white blood cell count (WBC count), and immunophenotype (B-cell or T-cell), where male, increasing age, higher WBC count, and T-ALL are considered unfavorable [41, 42]. More recently, response to induction therapy has been factored into patient risk assessment [40, 42]. Treatment response, measured as minimal residual disease (MRD), has proven to be a useful tool for risk stratification during treatment. MRD can be assessed by either polymerase chain reaction (PCR) or flow cytometry to determine the number of remaining leukemia cells following induction therapy. PCR is more sensitive than flow cytometry but is more costly and time consuming. Most commonly, MRD negative is defined as one or fewer leukemia cells per 10,000 healthy cells, or $\leq 10^{-4}$, which is largely determined by the limit of detection (LOD) of the assays [43]. In the U.S. and most industrialized countries, pediatric institutions, including major research consortiums like Children's Oncology Group (COG) and St. Jude's Children's Research Hospital, stratify patients by MRD following induction therapy [40, 43]. It should be noted that no consensus has been reached

establishing ideal timing and thresholds for MRD measurements [42, 43]. Genetic anomalies have also been used to stratify patients for risk-directed therapy [40, 42]. Much like MRD, little consensus has been reached regarding the best way to integrate established clinical parameters and genetic risk factors to maximize improvements in patient outcomes [42]. Nonetheless, stratification by genetic and molecular factors can be useful for both risk-directed therapy and targeted drug development to maximize HR (and VHR) patient survival and improve long-term quality of life for all leukemia patients [40].

1.3.4 Leukemia is characterized by significant genetic alterations

Hematological malignancies, like solid tumors, are characterized by genomic instability and mutations that cooperate to promote leukemogenesis [4, 44-47]. Nearly all leukemias are driven by a limited number of gross chromosomal changes [42, 45-47]. There are two main categories of chromosomal aberrations, changes in chromosome number giving rise to aneuploidy and structural changes which include translocations, deletions, insertions, and inversions [42, 46-49]. Although most leukemias have a small number of mutations, in experimental models, most primary chromosomal alterations do not induce leukemia alone. Instead, they require one or more secondary mutations that cooperatively result in leukemogenesis [42, 47]. Most gross chromosomal anomalies have not been thoroughly investigated as therapeutic targets because they do not result in leukemogenesis alone. Furthermore, explicit targets can be challenging to identify since large regions of the genome are effected [15]. Nevertheless, rates of incidence and correlations with patient outcomes suggest chromosomal anomalies are crucial for leukemogenesis and future research should focus on elucidating the underlying molecular mechanisms and identifying potential therapeutic targets [15, 48].

Several complimentary molecular techniques have been employed to characterize genetic anomalies in leukemia and improvements in cytogenetic tools have made it possible to identify chromosomal anomalies with a high degree of accuracy and specificity [47, 48]. Standard cytogenetic techniques used clinically include karyotyping, Giemsa banding (G-banding), fluorescence *in situ* hybridization (FISH), and comparative genome hybridization (CGH) [47]. In conjunction with karyotyping, FISH is most commonly employed clinically to detect the presence and location of specific gene sequences on chromosomes [50]. G-banding and multiplex FISH can both be used for detecting chromosome number and morphology, but at the cost of lower resolution and sensitivity [47]. Locus-specific FISH has higher resolution and sensitivity, and can detect specific DNA sequences, but has narrower application [47]. CGH can detect a broad array of unbalanced losses or gains of genetic material across the genome with very high resolution [47, 51]. These techniques can also be combined with PCR and multiplex ligation-dependent probe amplification (MLPA) which provide additional high-resolution genetic information [47]. Lastly, the falling costs of whole genome sequencing has made it possible to sequence all or large parts of individual genomes to identify the unique genetic profile of patients. While genomic sequencing techniques employed by researchers have identified an impressive number of novel anomalies, none of these techniques have become routine in clinical application [52, 53].

1.4 CANCER AS A DISEASE OF ABERRANT METABOLISM

Prior to a modern understanding of molecular biology and the genetic mutations and chromosomal anomalies associated with cancer, it was thought to be a metabolic disorder. In 1956, Otto Warburg observed that cancer cells produced copious amounts of

lactate from glucose even in the presence of adequate oxygen [54, 55]. Warburg hypothesized that cancer was caused by defective mitochondria leaving cells unable to efficiently produce energy via the canonical Tricarboxylic Acid Cycle (TCA) and Oxidative Phosphorylation (OXPHOS) pathways, both of which take place in the mitochondria. More recently, metabolic reprogramming (along with evasion of immune destruction) has been recognized as an emerging hallmark of cancer [3, 4]. Cancer cells do not engage in anaerobic glycolysis because they lack the ability to completely oxidize glucose. Instead they engage in both anaerobic and aerobic metabolism simultaneously to meet their energetic and proliferation needs. Cancer cells reprogram their metabolism to enhance the uptake of both glucose and glutamine to promote biomass production and sustained proliferation without the complete oxidation of substrates [54-59]. Reprogramming of major metabolic pathways can produce sufficient energy via glycolysis while simultaneously exploiting the TCA cycle for the interconversion of metabolites to be harvested for biosynthesis of macromolecules [59, 60].

In addition, cancer cells have been shown to reprogram the metabolism of neighboring cells for their own benefit [4]. For example, leukemia cells can evade and overcome asparaginase-induced stress with the support of other cells in the microenvironment [61, 62]. Mesenchymal stem cells (MSC) protect acute lymphoblastic leukemia (ALL) cells from asparaginase treatment by upregulating their own asparagine synthetase (ASNS) in co-culture experiments [63]. Similarly, adipocytes, which are abundant in the bone marrow tumor microenvironment, also provide asparaginase resistance for ALL cells by secreting glutamine into the extracellular matrix [64]. And, CLL cells depend on stromal cell-derived cysteine to synthesize glutathione for protection from stress induced by reactive oxygen species (ROS) [65].

Cancer research has come full circle and returned to understanding cancer not only in the context of mutations and faulty proteins, but also as a metabolic disease where cellular energetics are used to feed the insatiable appetites of malignant cells, metabolites are hijacked and used to stoke the flames of cancer factories, and healthy cells are reprogrammed to support their greedy neighbors. In this way, cancer can be understood as a disease that is initiated by an accumulation of mutations that culminate in the metabolic dysregulation of cancer cells and surrounding normal cells that have been recruited and reprogrammed to support the growth and proliferation of their malignant neighbors.

1.5 METABOLOMICS

1.5.1 The short history of metabolomics

While the identification and monitoring of metabolites is not a new concept in science or medicine, untargeted, comprehensive metabolite analysis, commonly designated metabolomics, has only become possible in more recent years [66]. For decades, biochemists have evaluated metabolites found in blood, urine, and tissue samples to diagnose diseases, monitor cellular response to treatments, and understand pathway regulation [67, 68]. In fact, with the proper tools, metabolites can provide insight into processes occurring at subcellular, cellular, tissue, organ, and organism levels [66, 69]. Historically, the instrumentation and computational technologies available have meant that it was only possible to measure a small number of metabolites or classes of metabolites that were determined *a priori* [70, 71]. As a consequence, metabolite identification gained little attention. Rather, biological research has focused on identification of novel genetic mutations and later aberrant protein activities [72]. The complete sequencing of the human genome gave rise to the systems biology approach and ‘omics’ disciplines were born.

Metabolomics is the newest of the pure 'omics' (genomics, transcriptomics, proteomics, and metabolomics) [72-74]. In 1999, Nicholson and colleagues proposed the term *metabonomics*, which they defined as "the quantitative measurement of the dynamic multiparametric metabolic response of living systems to pathophysiological stimuli or genetic modification" [75]. Shortly after, Oliver Fiehn presented a simpler and broader alternative, describing *metabolomics* as the "…comprehensive analysis in which all the metabolites of a biological system are identified and quantified" [66]. Metabolomics has become the more universally accepted term when addressing the complexity of comprehensively evaluating metabolites and will be used in this sense henceforth [70]. Great efforts have been made to create libraries of complete genomes, proteomes, transcriptomes, and metabolomes in order to provide standards for comparison [76-78]. Furthermore, future integration of libraries will elucidate biological perturbations across all levels of expression [79]. Much work still remains, for the metabolome in particular, as it is by far the most complex in terms of chemical diversity, abundance, and dynamism. Moreover, consensus regarding reporting standards and analytical methods are still under development [71, 77, 80, 81]. The number of metabolites in mammalian samples is enormous and remains mostly unknown, with estimates ranging from thousands to hundreds of thousands of small molecules [67]. Combining several analytical platforms, 4229 and 2651 metabolites have been identified in the human serum and urine metabolomes, respectively [82, 83]. Even more metabolites are detectable in both serum and urine, but have not yet been annotated [71, 81]. Furthermore, the chemical diversity of the metabolome coupled with the concentration range of metabolites in biological samples make it virtually impossible to comprehensively measure every metabolite with a single platform or analysis [67, 71, 74, 84, 85]. Instead, platforms and analyses should be applied in concert to provide complementary data sets [86]. Advancements in nuclear magnetic

resonance (NMR) spectroscopy and mass spectrometry (MS) instrumentation have contributed most significantly to the emergence and development of metabolomics [70, 86, 87]. In addition, because these instruments generate large amounts of data, in some cases tens of thousands of data points in a single scan, advances in computation and statistical methods have made it possible to address the complexity and size of the information generated [81, 88, 89].

1.5.2 Nuclear magnetic resonance spectroscopy

High-resolution NMR spectroscopy is a popular analytical technique that continues to be widely used in metabolomics research [90-92]. NMR, also known as MRS (magnetic resonance spectroscopy) [93], takes advantage of the inherent magnetic properties of certain nuclei [94]. In particular, nuclei that have a nuclear spin, I, equal to ½ are easily detected with NMR spectroscopy. Common spin ½ nuclei include ^{1}H, ^{13}C, ^{15}N, and ^{31}P; the most abundant and widely used in metabolomics is ^{1}H-NMR. Under normal conditions nuclear spins are completely random and, therefore, do not lead to bulk magnetic properties. However, when subjected to a strong, static magnetic field, typically denoted B_0, the nuclear spins will align and precess around the magnetic field at a characteristic frequency, known as their Larmor frequency [95]. Application of a much weaker, transient oscillating radio frequency (RF) pulse results in the excitation of the nuclei [96]. Pulses are typically applied perpendicular to the static magnetic field, B_0, which changes the orientation of the magnetization. The removal of the RF pulse causes the excited nuclear spins to relax according to their T_1, spin-lattice, and T_2, spin-spin relaxation times. T_1 is a measure of the time it takes for the spins to return to their lower energy states and T_2 is a measure of the loss of coherence of the spins that occurs after the removal of the RF pulse [97]. This relaxation is observed as a free induction decay (FID). After collection, the FID

can be Fourier transformed to convert the signal from the time domain into the frequency domain, resulting in a classic NMR spectrum, typically given in ppm.

The NMR spectrum contains a wealth of information including the structure and abundance of the molecules present. The chemical shift of peaks in an NMR spectrum depends on the local environment the nucleus experiences [94]. Nuclei that have greater electron densities will be found at lower ppm, whereas electron deficient nuclei will be shifted to higher ppm [98]. Furthermore, sensitive nuclei can couple with neighboring nuclei to create a multiplet instead of a single peak [94]. This phenomenon, known as J-coupling, is due to overlapping electron orbitals and can be used for structural identification [99, 100]. Due to these characteristic properties, NMR continues to be a powerful analytical chemistry tool to elucidate molecular structure [94, 101]. In fact, it is still used extensively for structural and functional analysis of proteins [102]. In addition, NMR peak areas are directly proportional to the number of sensitive nuclei making it an inherently quantitative technique. Incorporating a single standard compound, usually TSP (Trimethylsilyl propanoic acid) or DSS (4,4-dimethyl-4-silapentane-1-sulfonic acid), at a known concentration is sufficient to correct chemical shift and extrapolate absolute concentrations of all positively identified metabolites [91].

NMR spectroscopy is one of the most extensively used analytical techniques for metabolite identification because it is so well suited for molecular analysis. The application of NMR to biological samples was first explored by Nicholson *et al.* in the late 1990s [103]. It is particularly well suited for an 'omics' approach because it is naturally untargeted and thus, completely unbiased [91]. If a metabolite is present at an adequate concentration, it will be detected. Furthermore, relatively minimal sample preparation is required [90, 91]. This results in highly efficient and reproducible sample preparation [86]. As a result, NMR is extremely reliable and ideal for absolute quantification of metabolites [89, 90]. The

inherently untargeted nature of NMR spectroscopy allows for the identification of both metabolites of interest and those outside hypothesized outcomes.

The most significant limitation of NMR spectroscopy is sensitivity [91, 96]. While advances in superconducting materials, magnet strength and quality, cryogenic probe technology, and pulse sequences have vastly improved sensitivity, MS remains superior for detection of very low abundance metabolites [91, 96, 101]. Superconducting materials and improvements in magnetic field homogeneity have created extremely powerful instruments. There are now magnets that can generate a magnetic field of 25.9 Tesla which gives a resonance frequency of 1.1 GHz (gigahertz). Technological advances in pulse sequences and pulsed-field gradients, used to select for desired signal have significantly enhanced signal quality [101, 104, 105]. Likewise, advanced water suppression techniques, such as excitation sculpting, have also improved NMR spectra [106]. Lastly, advances in probe quality and size have improved excitation profiles and sensitivity, and decreased sample volumes [96]. Typically, NMR requires rather large sample volumes, on the order of 200 μL, but newer probes can obtain high quality signals with as little as 30 μL [107]. Nonetheless, spectra are still dominated by higher abundance metabolites and complex samples often require some degree of deconvolution to identify less abundant molecules [91]. Additionally, because no separation techniques are employed, lower abundance metabolites may be undetectable due to overlap with more abundant molecules.

1.5.3 Mass spectrometry

In the simplest terms, mass spectrometers manipulate electromagnetic fields that apply forces to ionized particles. Because the forces being applied are dependent on the mass and the charge of molecules, mass analyzers are designed to separate ions by their mass-to-charge ratio (*m/z*). While NMR spectrometers primarily vary in the magnetic field

strength and the properties of the probe, there is a great deal of diversity in mass analyzers. Because each have their strengths and weaknesses, different instrumentation can be selected depending on the desired properties. Common mass analyzers utilized in metabolomics research include: Triple Quadrupole (QqQ-MS), Time of Flight (TOF-MS), Quadrupole Time of Flight (QTOF-MS), Fourier Transform Ion Cyclotron Resonance (FT-ICR/MS), and Orbitrap [69]. Quadrupole mass analyzers function similar to a filter, only stabilizing a selected mass-to-charge ratio that will reach the detector. On the other hand, time of flight mass analyzers separate ions based on the time it takes to reach the detector. FT-ICR/MS and Orbitrap mass analyzers trap and manipulate ions, which provides the highest mass accuracies, whereas others are preferred because of their rapid scanning rates and broad *m/z* detection ranges [69].

Although direct injection methods, often called 'shotgun' techniques, are used in metabolomics, more often mass spectrometers are coupled with either gas (GC) or liquid chromatography (LC), especially ultra-high performance liquid chromatography (UPLC or UHPLC), to enhance chemical separation of complex biological matrices [69, 108]. This adds an additional layer of diversity to developing and applying MS methods to metabolomics. Although GC-MS was developed and gained popularity before LC-MS, the latter has been shown to deliver superior separation to a broader diversity of compounds, whereas GC-MS is primarily limited to volatile molecules or requires derivatization of non-volatile compounds [71]. LC-MS requires an interface between the chromatography column and the mass analyzer because the eluted metabolite must be ionized and converted into the gas phase before detection. There are three common interfaces: atmospheric pressure photo ionization (APPI), atmospheric pressure chemical ionization (APCI), and pneumatically assisted electrospray ionization (ESI). Of these, ESI is by far the most commonly used in metabolomics analyses and across other disciplines [69, 108].

To add another layer of complexity, mass spectrometers can be used in tandem (MS/MS) to positively identify ions by their fragmentation pattern. Typically, the first MS isolates molecular ions and the second MS detects ion fragments in order to positively identify metabolites by combining the data from the molecular ion and its characteristic fragmentation pattern. Alternatively, positive identification can be performed by matching the retention time to a standard reference library of compounds. Internal standards can be spiked directly into the sample matrix or a mass spectral metabolite library of standards can be acquired under identical parameters to build a reference library of accurate masses and retention times.

Mass spectrometers have the advantage of essentially unparalleled sensitivity, making MS an ideal complement to NMR. In addition, lipid analysis, which is difficult with NMR, is possible with MS, making it an extremely valuable technique for lipidomics [109-112]. MS analysis is not without of challenges. Aside from the great diversity in mass analyzer types and coupled techniques, sample preparation is often tedious and can result in significant metabolite loss [90]. Furthermore, chromatography column selection, elution solvents, and analysis time all introduce limitations for untargeted analysis and can lead to undesired matrix effects [71]. While it is currently impossible for a single MS analysis to detect all the metabolites in any given sample, the remarkable sensitivity coupled with chromatographic techniques that separate overlapping metabolites make GC-MS and LC-MS valuable techniques for metabolomics. MS analysis is not well suited for absolute quantification due to variable ionization efficiencies which significantly limits its application, in particular for biomarker identification [90]. For this reason, concentration curves and internal standards labeled with stable isotopes are required to accurately quantify metabolites, when necessary [90].

1.5.4 Technological advancements

Advances in computer programming and processing speeds have made untargeted metabolite analysis possible [70, 74]. For example, a single NMR spectrum can contain more than 64,000 complex data points [76, 113]. Similarly, LC-MS is able to separate and detect tens of thousands of features from a single complex sample [71, 86, 114]. Without computers and software capable of processing this information, it would be impossible to advance the field of metabolomics.

Multivariate analysis can be applied to multiple spectra for pattern recognition [70]. These methods fall under two broad categories, unsupervised and supervised, the most common of which are principal component analysis (PCA) and partial least squares discriminant analysis (PLSDA), respectively [89, 90]. Both are powerful statistical tools that can be used to observe global differences among groups [90, 115]. Supervised and unsupervised methods analyze entire spectra to evaluate statistical trends without identification of individual metabolites. PCA is typically considered more powerful than PLSDA because it is completely unbiased and is usually applied first to determine if inherent grouping exists within the data [85]. On the other hand, with PLSDA, grouping is predetermined and a predictive model is developed based on the common characteristics of each group [85, 116]. A related supervised method, orthogonal PLSDA (O-PLSDA), is common in metabolomics research [85, 115, 117]. In order to avoid bias from higher abundance metabolites, it is important to apply normalization and scaling functions prior to evaluation with either supervised or unsupervised methods [78]. Care must be taken to avoid overfitting the data when applying supervised methods to prevent false positive results [118].

Metabolite identification is one of the biggest challenges in metabolomics [81, 114]. Progress in the development of metabolome databases and libraries has significantly

improved identification of metabolites detected by either NMR or MS [77, 80]. The most comprehensive human database is the Human Metabolome Database (HMDB) with a catalog of more than 100,000 metabolites [119-122]. Several smaller databases have also become publicly available in recent years. These resources often vary by organism or analytical platform. Some of the most valuable are metabolic pathway databases, such as Kyoto Encyclopedia of Genes and Genomes (KEGG) [123-125] and HumanCyc [126], and spectral libraries, such as Metlin [127] and mzCloud. More recently, faster tools have been developed to interrogate these databases including R-Metabolist [128, 129]. Frequently, the majority of compounds detected are not present in any database [71, 81]. To alleviate this deficiency, the Metabolomics Standards Initiative (MSI) has been formed and proposes thorough minimum reporting standards to maintain consistency between laboratories employing different instruments and methods [130, 131].

1.5.5 Integration of clinical parameters and metabolic profiling

Large-scale, untargeted profiling methods, including genomics, transcriptomics, proteomics, and metabolomics have been successfully used to elucidate molecular and metabolic cellular processes that are altered in disease states and identify potential targets for therapy [132, 133]. Metabolite concentrations have already been shown to be sensitive markers for genomic changes and in the context of cancer, an increasing amount of evidence indicates that major alterations in cancer cell metabolism contribute to oncogenic signaling and support cancer cell proliferation [134]. The main analytical platforms for metabolic profiling are mass spectrometry (MS) and nuclear magnetic resonance spectroscopy (NMR). MS, especially coupled to liquid chromatography (LC), is characterized by unparalleled sensitivity, while NMR is inherently quantitative and seamlessly translates *in vivo* [135, 136]. High-throughput, untargeted experiments allow

for the mining of not only known, but also unknown, unpredicted, and novel pathways of interest to provide new insights into disease [92, 137, 138].

Chapter 2: Identification of a synergistic combination of dimethylaminoparthenolide and shikonin alters metabolism and inhibits proliferation of pediatric precursor B-cell acute lymphoblastic leukemia

2.1 ABSTRACT

Exploiting metabolic vulnerabilities of cancer cells with non-toxic, plant derived compounds constitutes a novel strategy for both chemoprevention and treatment. A high-throughput screening approach was used to evaluate a library of natural products to determine the most synergistic combination in precursor B-cell acute lymphoblast leukemia. Dimethylaminoparthenolide and shikonin effectively inhibited proliferation resulting in cell death in primary and immortalized leukemia cells, while having negligible effects on normal cells. Dimethylaminoparthenolide and shikonin have been shown separately to inhibit cell survival and proliferative signaling and activate tumor suppressors and pro-apoptotic pathways. Untargeted metabolomics and metabolic flux analysis with stable isotopically labeled glucose and glutamine exhibited a global shift in metabolism following treatment. Pathway analysis indicated significant differences in amino acid, antioxidant, TCA cycle, and nucleotide metabolism. Together, dimethylaminoparthenolide and shikonin reduced the shunting of glycolytic intermediates into the pentose phosphate pathway for biosynthetic purposes. Similarly, the incorporation of glutamine and glutamine-derived metabolites into purine and pyrimidine synthesis was inhibited by the combination of dimethylaminoparthenolide and shikonin, effectively impeding biosynthetic pathways critical for leukemia cell survival. This approach demonstrates that

This chapter has been published previously under the same title in *Molecular Carcinogenesis*. DOI: 10.1002/mc.23163 Author contributions: Sweeney SR: Study concept and design, data acquisition, analysis, and results interpretation, manuscript composition. Collins M: Study concept and design, data acquisition, analysis, and results interpretation. Pandey R: Analytical method development. Chiou J: Data acquisition and analysis. Lodi A: Data analysis and results interpretation. Tiziani S: PI, study concept and design, critical revisions of the article.

a synergistic pair of compounds with malignant cell specificity can effectively target metabolic pathways crucial to leukemia cell proliferation and induce apoptosis.

2.2 INTRODUCTION

Cancer is the primary cause of death in children and adolescents ages 1 – 19 [26]. Leukemia is the most common pediatric cancer, accounting for nearly one-third of all cancers in children [19]. Current treatment strategies involve a very intense, risk-directed induction phase at the outset of treatment [139]. This approach effectively induces remission in most patients but is highly toxic and consequently results in significant short- and long-term side effects [34, 140]. Among childhood leukemia survivors, 75% report a least one chronic condition 5 – 14 years post-diagnosis, a figure that climbs to 85% by 25 – 36 years [141]. Even more concerning, incidence rates have continued to rise since 1975, indicating a persistent and growing problem [19]. Given the numerous adverse effects of current strategies, there is a continued need to identify compounds that are chemopreventive and can be used as adjuvant therapies to ameliorate the consequences of treatment [142-144].

Diets rich in fruits and vegetables have been shown to reduce cancer risk due to an abundance of phytochemicals – non-nutritive, plant-based bioactive chemical compounds [142]. *In vitro* experiments and *in vivo* animal models of cancer prevention and progression have established that many phytochemicals, also called natural products, possess potent anti-cancer activities [142, 145]. These compounds have a variety of biological activities including functioning as antioxidants [146], reducing inflammation [147], regulating signal transduction pathways [148], promoting terminal differentiation [149], inhibiting proliferation [150], inducing apoptosis [151], and suppressing angiogenesis [152]. Natural

products have also inspired the pharmaceutical industry for mimetics and synthetic analogs [153]. Many drugs approved by the US Food and Drug Administration in recent decades have been natural products and derivatives thereof; Chemotherapeutic examples include etoposide, vincristine, vinblastine, and paclitaxel [145, 153].

Early research characterized cancer as a disease of aberrant metabolism [54, 55]. In recent years, this characterization has been reinvigorated and metabolomics has become a valuable tool for the study of cancer cell metabolism, the tumor microenvironment, drug discovery, and biomarker investigation [154]. Metabolomics is the analysis of all the small molecules present in a biological sample. Metabolite levels reflect the amalgamation of gene variants, gene expression, pathway activity, and enzyme kinetics, and as such, serve as a direct signature of biochemical activity in a cell, tissue, organ, or organism [81].

In this study, a high-throughput screening (HTS) approach was used to simultaneously analyze 136 compounds in a natural product library (NPL) in patient-derived precursor B-cell acute lymphoblastic leukemia (BCP-ALL), immortalized BCP-ALL cell lines, and bone marrow-derived normal cells. This technique has been used extensively in drug discovery because it allows concurrent analysis without determining *a priori* which compound to investigate in-depth [150, 155]. The top candidate compounds were evaluated at varying concentrations and ratios to identify the optimal combination. Dimethylaminoparthenolide (DMAPT) and shikonin (SHK) were selected as the most promising synergistic pair. Untargeted metabolomics and metabolic flux analysis (MFA) were performed following single and combination treatment of DMAPT and SHK to determine the global impact these compounds have on BCP-ALL metabolism. The results of this research demonstrate the efficiency and efficacy of combining untargeted analyses in a data-driven process to identify chemotherapeutic strategies that ameliorate the global toxicity of currently employed compounds.

2.3 MATERIALS AND METHODS

2.3.1 Reagents and chemicals

A natural product library (NPL) consisting of 131 structurally diverse compounds (**Table A1**) was purchased from Selleck Chemicals (Houston, TX, USA). Five additional natural products were purchased from Cayman Chemical Company (Ann Arbor, MI, USA): betulinic acid, caffeic acid phenylethyl ester, genistein, resveratrol, and shikonin. The library was diluted and configured from a 96-well format into 384-well microplates at a stock concentration of 2.5 mM in dimethyl sulfoxide (DMSO). Each stock plate contained two treatment replicates and control wells. Microplates were sealed and stored at -80°C until use. Plates were only thawed and used once to prevent efficacy loss from repeated freeze-thaw cycles. Tissue culture reagents were purchased from GE Healthcare Biosciences (Pittsburg, PA, USA) unless specified otherwise. Mass spectrometry grade water, acetonitrile, methanol, 2-propanol, chloroform, ammonium acetate, ammonium formate, and formic acid, as well as molecular biology grade ethanol, hydrochloric acid (HCl), DMSO, and 2,6-di-tert-butyl-4-methylphenol (BHT) were purchased from Thermo Fisher Scientific (Waltham, MA, USA). Commercial calibration solutions for the mass spectrometer were also purchased from Thermo Fisher Scientific. Ammonium bicarbonate was purchased from Sigma-Aldrich Corporation (St. Louis, MO, USA). The following isotopically labeled compounds were purchased from Cambridge Isotope Laboratories (Tewksbury, MA, USA): $^{13}C_5$,$^{15}N_2$-glutamine, $^{13}C_6$-glucose, $^{13}C_1$-glucose, D_4-alanine, D_3-serine, D_2-glycine, D_4-citric acid, D_3-malic acid, D_4-succinic acid, D_2-fumaric acid, D_3-aspartic acid, D_4-L-lysine, D_4-cystine, D_3-DL-glutamic acid, D_5-glutamine, and D_5-L-tryptophan.

2.3.2 Cell culture

Eight human cell lines were used for screening purposes, five pediatric BCP-ALL and three bone marrow-derived normal (**Table 2.1**). Patient-derived BCP-ALL cells from a collaboration with Dell Children's Blood and Cancer Center (CBCC; Austin, TX, USA) were isolated from fresh bone marrow aspirates by Ficoll-Paque (GE Healthcare Bio-sciences AB, Uppsala, Sweden) density centrifugation at the time of diagnosis and cultured for 24 – 48 hours prior to screening. IRB approval was granted prior to collection of patient-derived samples all of which were de-identified by CBCC staff before transfer to the laboratory.

Table 2.1: Human cells screened with NPL and top candidate combinations are representative of the bone marrow microenvironment in pediatric leukemia
Immortalized cell lines were expanded, tested for mycoplasma, and stored cryogenically prior to screening. Primary cells were collected fresh from bone marrow aspirates and cryogenically stored until screening. Cells were cultured under standard conditions for a minimum of 48 hours prior to screening. BCP-ALL, precursor B-cell acute lymphoblastic leukemia.

Name	*Type*	*Status*
Kasumi-2	BCP-ALL	Pediatric, Immortalized
KOPN-8	BCP-ALL	Pediatric, Immortalized
NALM-6	BCP-ALL	Pediatric, Immortalized
RCH-ACV	BCP-ALL	Pediatric, Immortalized
Reh	BCP-ALL	Pediatric, Immortalized
Patient 1	BCP-ALL	Pediatric, Primary
Patient 2	BCP-ALL	Pediatric, Primary
Patient 3	BCP-ALL	Pediatric, Primary
Patient 4	BCP-ALL	Pediatric, Primary
MSC	Mesenchymal Stem Cell	Bone marrow derived, Primary
HS-5	Stromal	Bone marrow derived, Immortalized
HS-27A	Stromal	Bone marrow derived, Immortalized

Immortalized cell lines were expanded, tested for mycoplasma, and stored cryogenically prior to screening. Primary cells were collected fresh from bone marrow aspirates and cryogenically stored until screening. Cells were cultured under standard conditions for a minimum of 48 hours prior to screening. Suspension cell lines were cultured in RPMI-1640 medium supplemented with 10% characterized fetal bovine serum (FBS) and 2 mM L-glutamine. Adherent cell lines were cultured in DMEM medium supplemented with 10% mesenchymal stem cell-qualified FBS and 2 mM L-glutamine. Patient-derived cells were cultured in Stem Span II Serum-Free Expansion Medium (StemCell Technologies, Vancouver, Canada). Stable isotope labeling experiments were performed in RPMI-1640 medium without glucose or glutamine (MP Biomedicals, Santa Ana, CA, USA) supplemented with 10% dialyzed FBS and either $^{13}C_5$,$^{15}N_2$-glutamine or $^{13}C_6$-glucose. All cells were incubated under standard conditions at 37°C and 5% CO_2. Suspension cells were maintained at a concentration range of 200,000 to 2 x 10^6 cells/mL and adherent cells were split via trypsinization at 70 – 90% confluency.

2.3.3 High-throughput screening

To minimize variability, cells were pre-conditioned for 48 hours in fresh medium. An automatic pipetting system (VIAFLO ASSIST; INTEGRA Biosciences, Hudson, NH, USA) was used to ensure consistent cell seeding. Cells were seeded into 384-well white polystyrene microplates (Thermo Fisher Scientific, Waltham, MA, USA) at either 2,500 or 5,000 cells/well for leukemia and normal cells, respectively. A lower seeding density was used for leukemia cells due to their high proliferation rates relative to non-malignant cells. A cell density experiment was performed initially to ensure appropriate seeding for all cell lines despite differences in doubling times. For each cell line, a total of 6 plates were seeded to obtain four replicates at three time points: 12, 24, and 48 hours. Following plating, cells

were incubated for 8 – 12 hours to equilibrate. Next, each well was treated simultaneously using a 384-channel electronic pipette platform (VIAFLO 384; INTEGRA Biosciences) at a final concentration of 10 μM.

Cell viability was assessed at each timepoint by ATP luminescence (CellTiter-Glo; Promega, Madison, WI, USA) with a multimode microplate reader (Tecan Spark; Tecan, Männedorf, Switzerland). The manufacturer's protocol was followed for the CellTiter-Glo (CTG) assay. Briefly, in a dark room, plates were equilibrated to room temperature for 30 minutes prior to the addition of the CTG reagent. Reagent was dispensed using the automatic pipetting system described above. Plates were placed on a platform mixer (MixMate; Eppendorf, Hamburg, Germany) for two minutes at 700 rpm to homogenize lysate. Following mixing, plates were equilibrated for an additional 10 minutes to allow the luminescence signal to stabilize. Endpoint luminescence with a 1000 ms integration time was recorded as a surrogate for cell viability. A Dixon's Q test was applied to all raw data points prior to normalization to identify outliers that could lead to potential false positive or false negative results [156]. Luminescence intensities were normalized to the vehicle control for each plate. Averages and standard deviations were calculated for each compound, time point, and cell line. Statistical significance was determined using a two-tailed, Student's t-test with a standard α of 0.05.

2.3.4 Combination screening

A second round of screening was performed on the top candidates identified from the single compound screening. To be considered a candidate for combination screening, compounds were required to meet a threshold of >25% growth inhibition in patient-derived leukemia cells. The candidate compounds were then divided into two groups based on their toxicity in normal cells. Compounds that inhibited normal cell growth <50% were

considered selectively toxic to leukemia cells whereas those that inhibited normal cell growth >50% were categorized as broadly toxic at 10 μM. Additionally, for each of the candidate compounds, the difference in toxicity between leukemia and normal cells was calculated. The compound with the greatest viability difference was selected as the top candidate. For combination screening, selectively toxic compounds were evaluated at concentrations ranging from 250 nM – 15 μM (250 nM, 500 nM, 750 nM, 1 μM, 5 μM, 10 μM, 15 μM). Compounds categorized as broadly toxic were evaluated in the concentration range of 10 nM – 5 μM (10 nM, 50 nM, 100 nM, 250 nM, 500 nM, 1 μM, 5 μM). The top candidate compound was evaluated in combination with the other candidate compounds at concentrations ranging from 50 nM – 5 μM (50 nM, 100 nM, 250 nM, 500 nM, 1 μM, 5 μM). Combination studies followed the same protocol as single compound screening. Cells were incubated for 24 hours prior to ATP luminescence assays. Synergy between combinations was assessed by the Bliss independence model and Chou-Talalay combination index (CI) [157, 158]. In conjunction with cell viability, these mathematical methods were used to identify the most effective and synergistic combination for metabolomics analysis. Bliss values were calculated within the R programming environment [159]. Chou-Talalay CI values were calculated with CompuSyn [160].

2.3.5 Ultrahigh performance liquid chromatography-mass spectrometry (UPLC-MS) analysis

Following the identification of the most synergistic combination, metabolomics analysis was performed. RCH-ACV and Reh cell lines were chosen for metabolomics analysis because they most closely mimicked the response of patient-derived cells. Cells were seeded in 6-well plates (Corning Incorporated, Corning, NY, USA) in triplicate. Four groups were assessed: vehicle control, DMAPT, SHK, and combination. This experiment

was performed under three different labeling conditions: unlabeled glucose and glutamine, $^{13}C_6$-glucose and unlabeled glutamine, or unlabeled glucose and $^{13}C_5$,$^{15}N_2$-glutamine. Following a 24-hour treatment period, cells were aspirated, washed with phosphate buffered solution, harvested by centrifugation, and snap frozen in liquid nitrogen. Metabolite extraction was performed by modified Bligh-Dyer, similar to previously reported [138]. In brief, cell pellets were extracted with 1:1 water:methanol with 10 mM ammonium bicarbonate and equal parts chloroform. BHT was added to the extraction buffer to preserve metabolites susceptible to oxidation.

The polar fractions were transferred to LC-MS vials for immediate analysis. Metabolite extracts were spiked with a mixture of deuterated internal standards (IS) to monitor retention time, ionization efficiency, and instrument stability. Chromatographic separation was achieved on an Accela 1250 UPLC system equipped with a quaternary pump, vacuum degasser, and an open autosampler with temperature controller (6°C, Fisher Scientific, San Jose, CA, USA) coupled to a UPLC column. First, a SeQuant ZIC-HILIC 3.5 µm, 100 Å, 150 x 2.1 mm PEEK coated HPLC column (Millipore Sigma, Burlington, MA, USA) was used to analyze redox cofactors. Mobile phase A was 10 mM ammonium acetate in water and mobile phase B was acetonitrile. An isocratic separation was performed at a flow rate of 150 µL/min with 90% A and 10% B for 12 minutes with an injection volume of 4 µL. Second, a Synergi 4 µm Hydro-RP 80 Å, 150 x 2 mm HPLC column (Phenomenex, Torrance, CA, USA) was used for additional polar metabolites. Mobile phase A was water with 0.2% formic acid and mobile phase B was methanol. A gradient separation was performed holding 1% B for 2 minutes, then linear 30-80% B in 8 minutes, washing with 98% B for 5 minutes, and column equilibration with 1% B for 15 minutes. The total run time was 30 minutes with a flow rate of 250 µL/min and an injection volume of 5 µL. In both cases, eluent was coupled to a Q Exactive Hybrid Quadrupole

Orbitrap mass spectrometer with an electrospray ionization (ESI) source simultaneously operating in fast negative/positive ion switching mode (Thermo Scientific, Bremen, Germany). The following acquisition settings were used for data collection in full MS mode: spray voltage, 3.5 kV; capillary temperature, 320°C; sheath gas, 45 (arbitrary units); auxiliary gas, 10 (arbitrary units); *m/z* range, 70-1000 (HILIC), 50-750 (RP); data acquisition, centroid mode; microscans, 10; AGC target, 1e6; maximum injection time, 200 ms; mass resolution, 70,000 FWHM at *m/z* 200. Accuracy of MS analysis was ensured by calibrating the detector prior to analysis. Non-polar fractions were evaporated to dryness in a CentriVap refrigerated vacuum concentrator (Labconco, Kansas City, MO, USA) at 4°C. Metabolites were subsequently resuspended in 95:5 ethanol:6N HCl for analysis. Chromatographic separation was achieved with a Kinetex 2.6 µm C_{18} 100 Å, 150 x 2.1 mm column (Phenomenex, Torrance, CA, USA) running at a flow rate of 260 µL/min of 60:40 2-propanol:methanol with 5 mM ammonium formate for 4 minutes and a 5 µL injection volume, as previously reported [161]. Eluent was coupled to the instrumentation above. Acquisition parameters for full MS/AIF were as follows: ionization mode, positive; spray voltage, 4.0 kV; capillary temperature, 300°C; sheath gas, 50 (arbitrary units); auxiliary gas, 10 (arbitrary units); *m/z* range, 150-1000; data acquisition, centroid mode; microscans, 1; AGC target, 1e6/5e5; maximum injection time, 200 ms; mass resolution, 140,000/70,000 FWHM at *m/z* 200; higher energy collisional dissociation (HCD), 22 eV. Mass tolerance was maintained at 5 ppm for all analyses.

The UPLC-MS analytical platform was controlled by a computer operating the Xcalibur v. 2.2 SP1.48 software package (Thermo Scientific, San Jose, CA, USA). Raw files were processed using SIEVE 2.2.0 SP2 (Thermo Scientific, San Jose, CA, USA) and an in-house script that operates in the MATLAB programming environment. Spectral alignment and peak picking were performed in SIEVE. Integrated intensities, monoisotopic

masses, and retention times were exported for further analysis. In MATLAB, metabolite identifications were determined by matching accurate masses and retention times to a mass spectral metabolite library of standards. A pooled quality control (QC) was used to monitor instrument stability and a blank was used for background subtraction. Peaks were included in analysis if the coefficient of variance (CV) was <0.25 and >0 in the QC replicates. Probabilistic quotient normalization (PQN) was performed prior to statistical analysis [162]. Pathway analysis was performed with MetaboAnalyst on confirmed features [163].

2.4 RESULTS

2.4.1 Natural product library (NPL) screening

An NPL composed of 136 unique compounds (**Table A1**) was assessed for cytotoxicity (measured by ATP luminescence) in 12 cell populations (Summary in **Table 2.1**). Normal cells were used to evaluate the specificity of cytotoxic compounds for cancer cells. Cells were treated with a 10 μM final concentration for 12, 24, and 48 hours. Overall, time course data showed that 12 hours was too early to see persistent effects on cell viability and 48 hours was too long to differentiate the effects of cytotoxic compounds (data not shown). Therefore, 24 hours was selected as indicative of robust cytotoxicity.

Seven compounds resulted in viability inhibition of >25% in leukemia cells derived from patients: 10-hydroxycamptothecin, cyclocytidine, dioscin, parthenolide, shikonin, tetrandrine, and triptolide (**Figure 2.1A**). Interestingly, immortalized BCP-ALL cells were sensitive to a greater number of compounds, with an additional 21 achieving >25% viability inhibition (**Figure 2.1B**) . *In vitro* experiments can overestimate the anti-cancer activities of compounds leading to poor clinical outcomes [164]. Thus, the inherent

resistance of primary cells was used as a guide. Only compounds considered effective in primary BCP-ALL cells were evaluated further.

To assess specificity for cancer cells, viability inhibition of leukemia versus normal cells was plotted for all 136 compounds (**Figure 2.1**). Of the seven compounds considered cytotoxic in primary leukemia cells, dioscin, shikonin, and tetrandrine inhibited normal cell viability above 50% suggesting the concentration should be reduced in subsequent experiments. These compounds were classified as broadly toxic at 10 µM. Conversely, 10-hydroxycamptothecin, cyclocytidine, parthenolide, and triptolide were less toxic to normal cells (<50% viability inhibition) and were categorized selectively cytotoxic to leukemia cells.

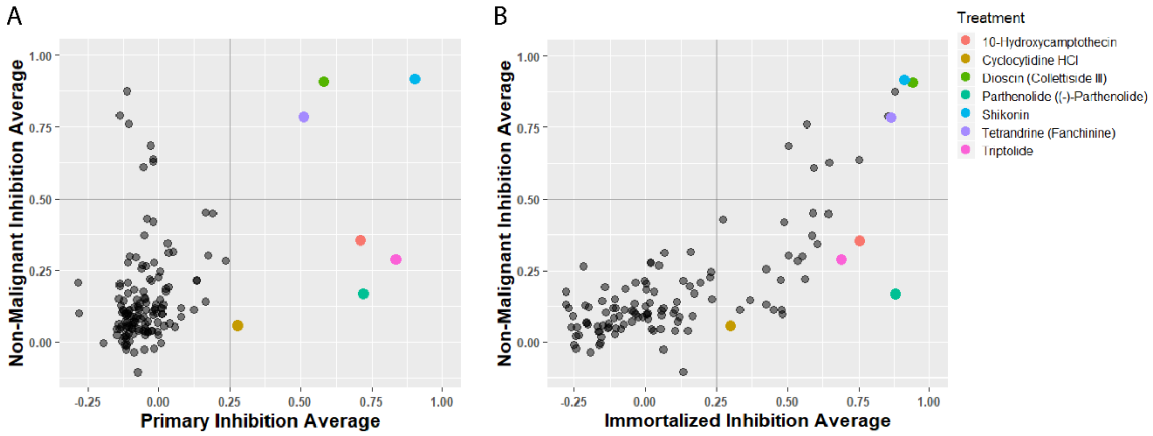

Figure 2.1: Growth inhibition patterns in BCP-ALL compared to normal indicate similar trends in compound efficacy
Compounds that inhibited primary cell growth (A) by more than 25% were comparably effective in immortalized cell lines (B). Compounds with an average growth inhibition above 50% were considered cytotoxic at 10 µM. Compounds that demonstrated less than 50% growth inhibition in normal cells while exhibiting efficacy in malignant populations were considered selective for leukemia cells. Growth inhibition was calculated from ATP luminescence. BCP-ALL, precursor B-cell acute lymphoblastic leukemia.

The difference in viability between leukemia and normal cells was calculated for the seven candidate compounds. Parthenolide (PTL) achieved the greatest average difference in both primary and immortalized cells. PTL growth inhibition was <20% in normal cells and >70% in primary malignant cells. In immortalized leukemia cells, the difference was even greater with PTL achieving >80% growth inhibition. Thus, PTL was selected as the leading candidate compound due to its high efficacy in primary and immortalized leukemia cells coupled with exceptionally low toxicity in normal cells. For each combination, a range of concentrations was evaluated to assess synergy. Concentration ranges were 50 nM – 5 μM (6 concentrations) for PTL, 10 nM – 5 μM (7 concentrations) for broadly toxic compounds, and 250 nM – 15 μM (7 concentrations) for selectively toxic compounds. In total, 42 combinations were assessed for each of the six compounds evaluated in combination with PTL.

The Bliss independence model was used to evaluate synergy for each compound and concentration pair. In the Bliss model, negative values indicate antagonism, zero implies an additive effect, and positive values denote synergism [157]. High confidence values were defined as ≥0.1, thus strongly indicative of synergism. Of the six compounds analyzed in combination with PTL, all but triptolide demonstrated some level of synergism in BCP-ALL (**Table A2**). Tetrandrine and 10-hydroxycamptothecin both had a small number of synergistic combinations, but neither were observed across all leukemia cells. Shikonin and dioscin resulted in synergistic combinations with PTL at several concentrations in all leukemia cells. In general, synergism between PTL and shikonin was higher in magnitude and frequency than PTL and dioscin. Consequently, the combination of PTL and shikonin (SHK) was selected for further evaluation. The synergy between PTL and SHK increased with increasing concentrations of both compounds and peaked between 750 nM – 1 μM PTL and 500 nM – 1 μM SHK (**Figure 2.2A**). At concentrations >1 μM,

synergy dropped precipitously, likely due to high cytotoxicity in some cells. The maximum Bliss values for Reh and NALM-6 were observed at 1 μM PTL:SHK. RCH-ACV was the most resistant cell line with a maximum Bliss index at 5 μM dose for each compound. However, concentrations this high were not found to be synergistic in other cell line. KOPN-8 was particularly sensitive to SHK with a maximum Bliss value at 1 μM:250 nM PTL:SHK. Nonetheless, the maximal Bliss index was only marginally higher than at 1 μM PTL:SHK. Kasumi-2 cells were the most sensitive to both PTL and SHK with a maximum Bliss value at 750 nM:100 nM PTL:SHK. This combination was not synergistic in any other cell line. Similar to KOPN-8, synergism decreased but was not lost at 1 μM each in Kasumi-2 (**Figure 2.2A, Table A2**). Consistent with the results of single compound screening, primary cells were more resistant to the combinations than immortalized cell lines. Importantly, in normal cells there were no discernible patterns of synergism indicating leukemia-specific activity. Taken together these data suggest that 1 μM PTL:SHK would be strongly synergistic across pediatric BCP-ALL cells without sacrificing viability in normal bone marrow cells.

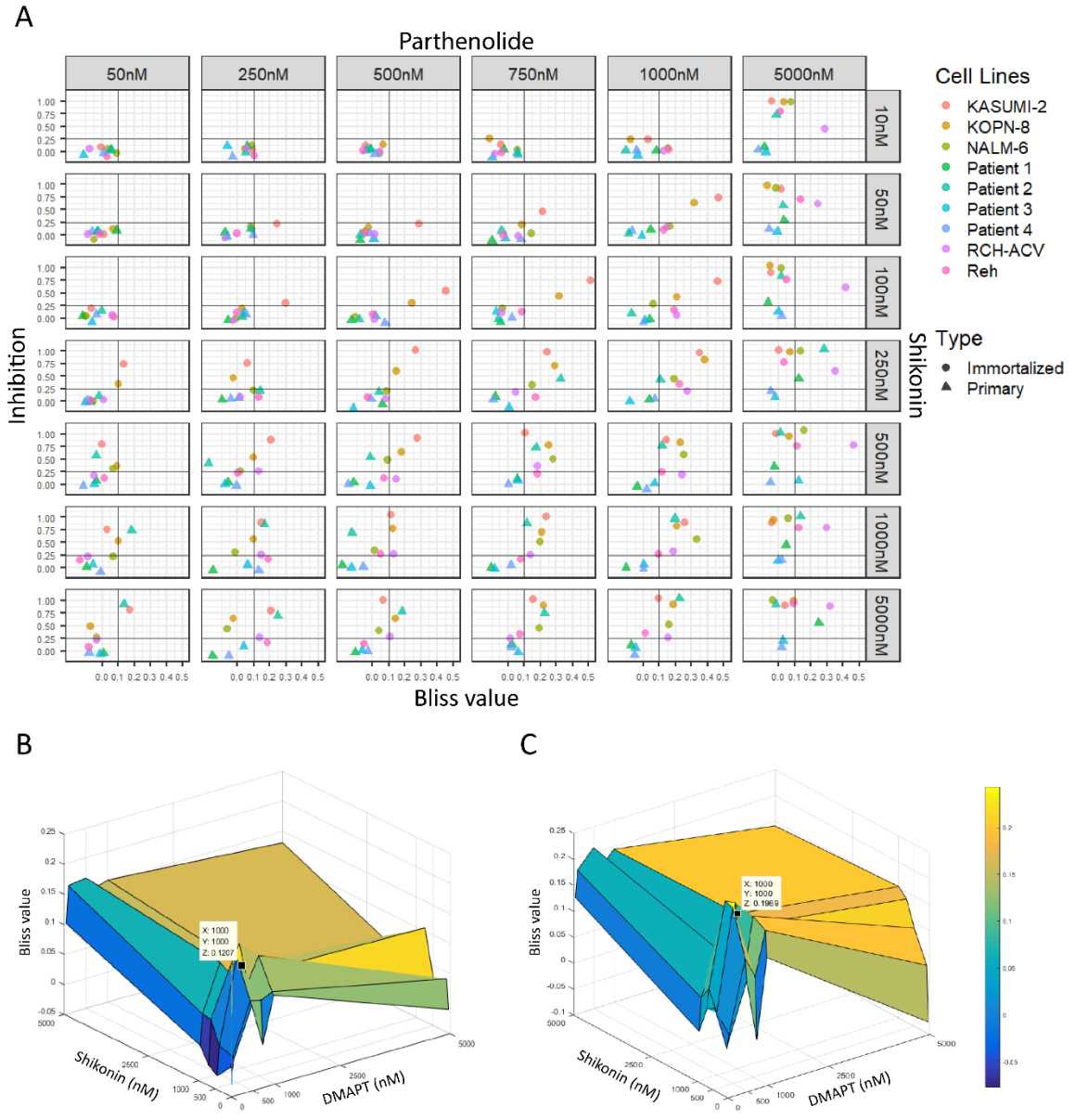

Figure 2.2: Bliss independence model determination of the most synergistic combination of parthenolide and dimethylaminoparthenolide with shikonin
(A) Viability inhibition and Bliss indices were calculated for each combination of PTL and SHK in immortalized and primary cells. Subplots exhibit shifting efficacy and synergy across concentrations and compound ratios. Bliss indices for tertiary screening of 1:1 ratio of the synthetic PTL analog DMAPT and SHK visualized as surface plots indicate maximal synergy near 1 µM DMAPT:SHK in RCH-ACV (B) and Reh (C) cells. PTL, parthenolide; DMAPT, dimethylaminoparthenolide, SHK, shikonin.

PTL is known to have limited bioavailability *in vivo*, a clinical application challenge for many natural products. An orally bioavailable analog was previously developed to overcome this limitation [165]. DMAPT has been shown to have improved water solubility (1000-fold) and bioavailability, as well as, comparable chemical specificity and *in vitro* efficacy as PTL *[165, 166]*. Our analysis confirmed that DMAPT and PTL demonstrated comparable activity in BCP-ALL and normal cells (**Figure B1**). The combination of 1 μM DMAPT:SHK also exhibited minimal toxicity in normal cells (data not shown). To confirm synergism observed in PTL and SHK was also maintained with DMAPT, a final round of screening was performed with 1:1 DMAPT:SHK ranging from 50 nM – 5 μM. Bliss indices exhibited similar synergism to PTL (**Figure 2.2B, C**). Additionally, the Chou-Talalay CI was calculated for this combination. For Chou-Talalay, CI >1 denotes antagonism, CI equal to one indicates an additive effect, and CI <1 one represents synergism. The CI for RCH-ACV was 0.90102 for 1:1 DMAPT:SHK at 1 μM each. The CI for Reh was 0.34616 for the same concentration. Interestingly, in this model increasing the dose beyond 1 μM each was predicted to shift towards antagonism in RCH-ACV cells. The synergistic window spanned from 0.1 to 0.6 Fa (fraction affected) (**Figure B2A, B**). In Reh cells, the CI was predicted to decrease steadily with dose escalation indicating no upper limit to the synergistic effect (**Figure B2C, D**). Based on the combined results of the Bliss independence model and the Chou-Talalay CI, 1 μM:1 μM DMAPT:SHK was selected for further investigation.

2.4.2 Metabolomics and metabolic flux analysis

Following the selection of DMAPT:SHK as the top synergistic combination, metabolomics analysis was performed. Reh and RCH-ACV cell lines most closely mirrored the viability inhibition and synergistic compound sensitivity of primary cells in

both single and combination screening. As such, they were chosen for metabolomics experiments to best recapitulate the response of primary BCP-ALL cells. Similar to screening conditions, cells were incubated for 24 hours with 1 μM DMAPT, SHK, or both. Intracellular profiles were analyzed by ultrahigh performance liquid chromatography-mass spectrometry (UPLC-MS). Features extracted from UPLC-MS analyses were matched to a mass spectral metabolite library of standards containing accurate masses and chromatographic retention times. This resulted in the positive identification of 83 and 81 metabolites confirmed in all treatment groups in RCH-ACV and Reh cells, respectively. Fold-change (FC) was calculated relative to vehicle control for DMAPT, SHK, and the combination (**Figure 2.3**). Several metabolites involved in energy metabolism and proliferation were reduced in the combination group relative to control. In addition, pathway analysis was performed to contextualize the results of UPLC-MS analysis (RCH-ACV, **Table 2.2**; Reh, **Table 2.3**). These results quantified the significance of the DMAPT, SHK, and DMAPT:SHK on intracellular metabolism. Single treatment with DMAPT did not result in any statistically significant pathways (calculated by FDR q-value) with an impact greater than 0.2 or that included ≥10 annotated metabolites. SHK alone did not result in any significant pathways in Reh cells. In RCH-ACV cells, single treatment with SHK was less remarkable than the combination, but nonetheless resulted in significant q-values ($q < 0.01$). Specifically, *alanine, aspartate, and glutamate metabolism*, *taurine and hypotaurine metabolism*, *glutathione metabolism*, and the *TCA cycle* (tricarboxylic acid cycle) were significantly changed (**Table 2.2**). For the combination, statistically significant pathways with the greatest impact fell under four major categories: (1) amino acid metabolism (of which the top three were *alanine, aspartate, and glutamate metabolism*, *arginine and proline metabolism*, and *glycine, serine, and threonine metabolism*), (2) antioxidant metabolism (*taurine and hypotaurine metabolism*, *glutathione metabolism*), (3)

the *TCA cycle*, and (4) nucleotide metabolism (*pyrimidine metabolism*, *purine metabolism*) (**Tables 2.2, 2.3**).

Many amino acids were significantly decreased in the combination group. Notably, glutamine, an important oncogenic substrate[61], was not decreased in the combination group in either cell line. Intracellular glutamine was not statistically significant between treatments in RCH-ACV cells. In contrast, glutamine was significantly reduced in single treatments, but not the combination in Reh cells. Interestingly, the antioxidant tripeptide, glutathione was not significantly different between groups despite decreased glycine, cysteine, and glutamate. Taurine and hypotaurine, which are also potent antioxidants, were significantly reduced in the combination. The significance of *glutathione metabolism* and *taurine and hypotaurine metabolism* suggest oxidative stress following treatment with DMAPT:SHK. Along these lines, redox cofactors including coenzyme Q_{10} (ubiquinone) indicated a cellular environment with high reactive oxygen species (ROS). The ratio of oxidized (CoQ_{10}) to reduced ($CoQ_{10}H_2$, ubiquinol) coenzyme Q was elevated following treatment, especially in RCH-ACV cells (**Table 2.4**).

In the combination group, there was an appreciable difference between RCH-ACV and Reh cells regarding pathway q-values for the *TCA cycle*. This pathway was highly significant in RCH-ACV ($q = 0.0024$) but not statistically significant in Reh ($q = 0.8733$) cells. Consistent with this, most TCA cycle intermediates trended in the same direction with the combination being most significantly decreased in RCH-ACV cells. In contrast, none of the TCA cycle intermediates were statistically significant in the combination in Reh cells. Rather, citrate, malate, and fumarate were more depressed following single compound treatment.

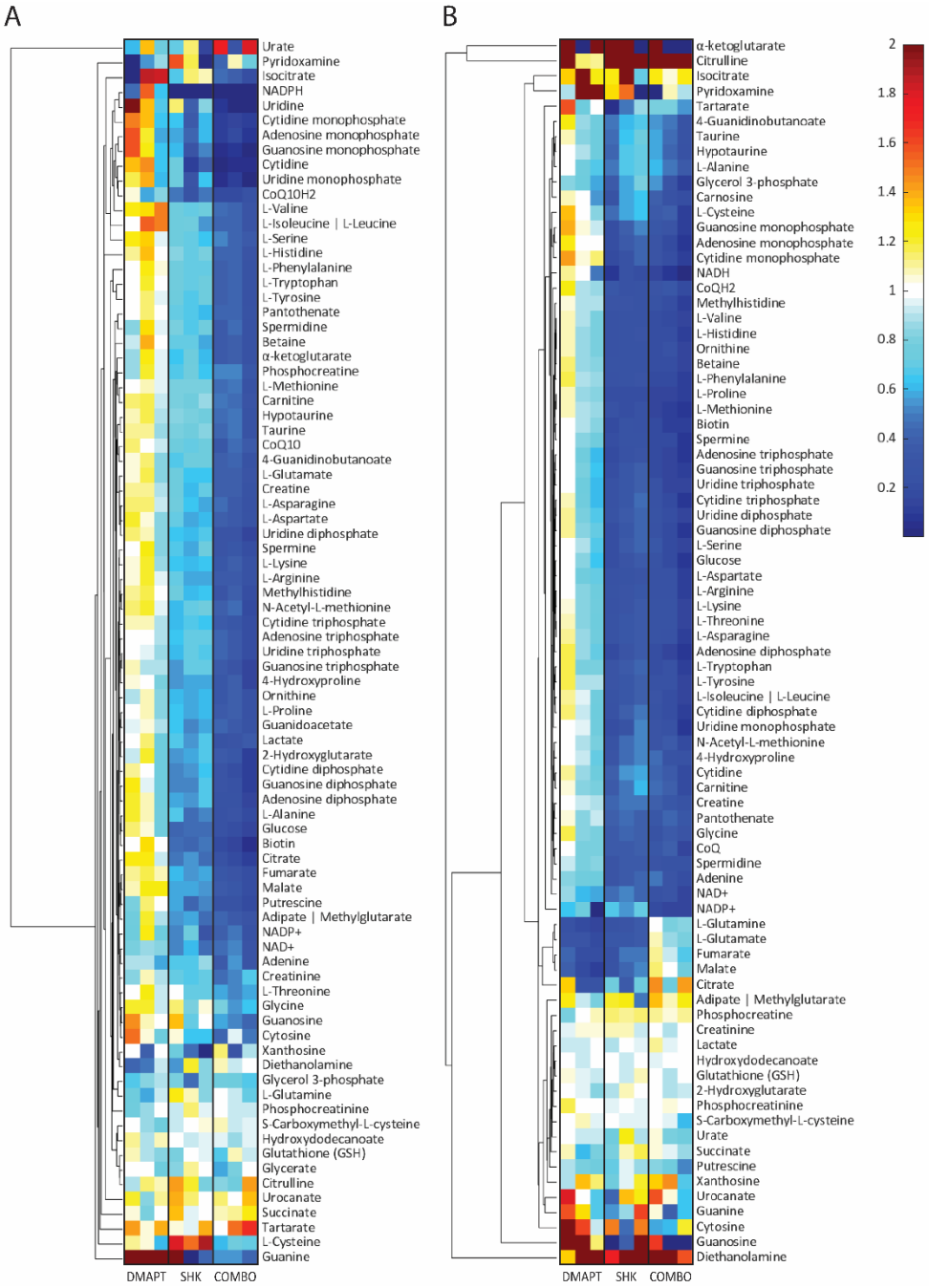

Figure 2.3: Modulation of unique metabolites demonstrates global changes in cellular metabolism following treatment with DMAPT, SHK, or both

Metabolites extracted from (A) RCH-ACV and (B) Reh leukemia cell lines are expressed in fold change (FC) compared to vehicle control as measured by UPLC-MS of intracellular extracts following 24-hour treatment. Hierarchical clustering was performed by Euclidean distance and average linkage methods. DMAPT, Dimethylaminoparthenolide; SHK, Shikonin; COMBO, combination.

Table 2.2: Metabolic pathway analysis in RCH-ACV cells
Pathway analysis was performed on UPLC-MS features positively identified by accurate mass and retention time. *Hits* indicates the number of identified compounds over the total number of compounds in the specified pathway. Pathways were included if the impact was >0.2 and/or ≥10 annotated compounds. FDR q-values <0.01 are in **bold**. UPLC-MS, ultrahigh performance liquid chromatography-mass spectrometry; DMAPT, dimethylaminoparthenolide; SHK, shikonin; TCA cycle, tricarboxylic acid cycle.

Pathway	*Hits*	*Impact*	*DMAPT*	*SHK*	*Combination*
Alanine, aspartate, and glutamate metabolism	8/24	0.7540	0.9859	**0.0017**	**0.0021**
Arginine and proline metabolism	17/77	0.6381	0.9859	0.0107	**0.0025**
Glycine, serine, and threonine metabolism	11/48	0.4693	0.9859	0.0115	**0.0021**
Taurine and hypotaurine metabolism	4/20	0.4443	0.9859	**0.0037**	**0.0052**
Glutathione metabolism	11/38	0.4343	0.9859	**0.0038**	**0.0067**
Pyrimidine metabolism	10/60	0.2944	0.9859	0.0563	**0.0062**
Histidine metabolism	8/44	0.2604	0.9859	0.0107	**0.0006**
Pantothenate and CoA biosynthesis	7/27	0.2447	0.9859	0.0102	**0.0062**
TCA cycle	6/20	0.2386	0.9859	**0.0017**	**0.0024**
Aminoacyl-tRNA biosynthesis	19/75	0.2254	0.9859	0.0107	**0.0024**
Glycerolipid metabolism	3/32	0.2162	0.9859	0.7258	0.5619
Purine metabolism	15/92	0.2050	0.9859	0.0107	**0.0047**
Biotin metabolism	2/11	0.2033	0.9859	0.0219	**0.0046**
Nitrogen metabolism	11/39	0.0083	0.9859	0.0285	**0.0024**

Table 2.3: Metabolic pathway analysis in Reh cells
Pathway analysis was performed on UPLC-MS features positively identified by accurate mass and retention time. *Hits* indicates the number of identified compounds over the total number of compounds in the specified pathway. Pathways were included if the impact was >0.2 and/or ≥10 annotated compounds. FDR q-values <0.01 are in **bold**. UPLC-MS, ultrahigh performance liquid chromatography-mass spectrometry; DMAPT, dimethylaminoparthenolide; SHK, shikonin; TCA cycle, tricarboxylic acid cycle.

Pathway	*Hits*	*Impact*	*DMAPT*	*SHK*	*Combination*
Alanine, aspartate, and glutamate metabolism	9/24	0.7778	0.4039	0.4039	0.0260
Arginine and proline metabolism	16/77	0.6166	0.4039	0.4039	**0.0015**
Taurine and hypotaurine metabolism	5/20	0.5414	0.5173	0.5173	**0.0077**
Glycine, serine, and threonine metabolism	9/48	0.4636	0.5173	0.5173	**0.0003**
Glutathione metabolism	10/38	0.3474	0.4039	0.4039	**0.0067**
Pyrimidine metabolism	10/60	0.2814	0.4039	0.4039	**0.0006**
TCA cycle	6/20	0.2386	0.4039	0.4039	0.8733
Aminoacyl-tRNA biosynthesis	19/75	0.2254	0.4548	0.4548	**0.0006**
Histidine metabolism	8/44	0.2115	0.4271	0.4271	**0.0026**
Biotin metabolism	2/11	0.2033	0.4039	0.4039	**0.0003**
Lysine degradation	5/47	0.2025	0.4271	0.4271	**0.0026**
Purine metabolism	16/92	0.1962	0.4039	0.4039	**0.0029**
Nitrogen metabolism	13/39	0.0998	0.4271	0.4271	**0.0008**

Table 2.4: Redox cofactor ratios indicate mitochondrial dysfunction following treatment

NAD^+ captures energy released from biological processes as NADH and transfers it to the electron transport chain (ETC) for ATP synthesis. Coenzyme Q_{10} is an electron carrier in the ETC. Electrons are transferred from NADH to generate reduced coenzyme $Q_{10}H_2$. Depletion of NADH and $CoQH_2$ are indicative of reduced oxidative phosphorylation and elevated oxidative stress. p-values <0.05 are in **bold.** Con, control; DMAPT, dimethylaminoparthenolide; SHK, shikonin; Comb, combination; ND, not detected.

	RCH-ACV				Reh			
Cofactor Ratio	*Con*	*DMAPT*	*SHK*	*Comb*	*Con*	*DMAPT*	*SHK*	*Comb*
[CoQ10]/[CoQ10H2]	12	15	22	**24**	9	8	12	9
[NAD^+]/[NADH]	34	35	ND	ND	15	12	**48**	39

Lastly, nucleotide metabolism was most significantly reduced in the combination. Q-values for *pyrimidine metabolism* and *purine metabolism* were 0.0062 and 0.0042, respectively, for RCH-ACV cells. Similarly, in Reh cells, the q-values were 0.0006 and 0.0029 for pyrimidine and purine metabolism, respectively. Treatment with DMAPT:SHK resulted in a consistent reduction in nucleotide mono-, di-, and triphosphates. Nucleosides, nitrogenous bases, and amino acids required for nucleotide synthesis were not as clearly clustered but were generally decreased in the combination as well.

To elucidate the mechanisms of these changes, MFA was performed with $^{13}C_6$-glucose and $^{13}C_5$,$^{15}N_2$-glutamine (**Figure 2.4**). The DMAPT:SHK combination reduced overall glucose utilization, but glucose-derived ^{13}C incorporation was not significantly different in glycolysis or the TCA cycle. In the combination group, a small increase in label incorporation was observed for some metabolites in RCH-ACV, but consistent with the unlabeled data, this was not observed in Reh cells. The most pronounced difference in glucose label incorporation was the shunting of ^{13}C-labeled sugars (predominantly M+5) into nucleotide synthesis through the pentose phosphate pathway (PPP). Label incorporation in nucleotide metabolism was significantly decreased by the combination,

most substantially in pyrimidine synthesis. Glutamine incorporation differed greatly between RCH-ACV and Reh cells. Leukemia cells typically divert glutamine towards biosynthetic and energy production pathways via glutaminolysis, first converting glutamine to glutamate and then to α-ketoglutarate which can enter the TCA cycle. In RCH-ACV cells, treatment with the combination (and SHK alone) diminished the conversion of glutamine to glutamate. This was propagated downstream in the TCA cycle seen through the reduction of label incorporation in fumarate and malate as well as a reduction in aspartate (synthesized from the TCA cycle intermediate oxaloacetate). Incorporation of ^{13}C and ^{15}N from glutamine was most significantly diminished in purine and pyrimidine nucleotides. In contrast, asparagine synthesis, which also utilizes carbon and nitrogen from aspartate was not affected in any group. No significant difference in TCA cycle intermediates was observed in Reh cells treated with the combination. Nonetheless, at the level of pyrimidine synthesis there was a substantial decrease in label incorporation suggesting an inhibitory mechanism downstream from aspartate in these cells. These results are consistent with pathway analysis which indicated that *alanine, aspartate, and glutamate metabolism* and the *TCA cycle* were not significantly changed in Reh cells but were significantly different in RCH-ACV cells. In addition to the canonical oxidative TCA cycle metabolism, the reductive flux of ^{13}C-labeled carbon was observed in RCH-ACV cells. Glutamine-derived label incorporation from reductive flux was observed in citrate, aspartate, malate, and the oncometabolite 2-hydroxyglutarate [167].

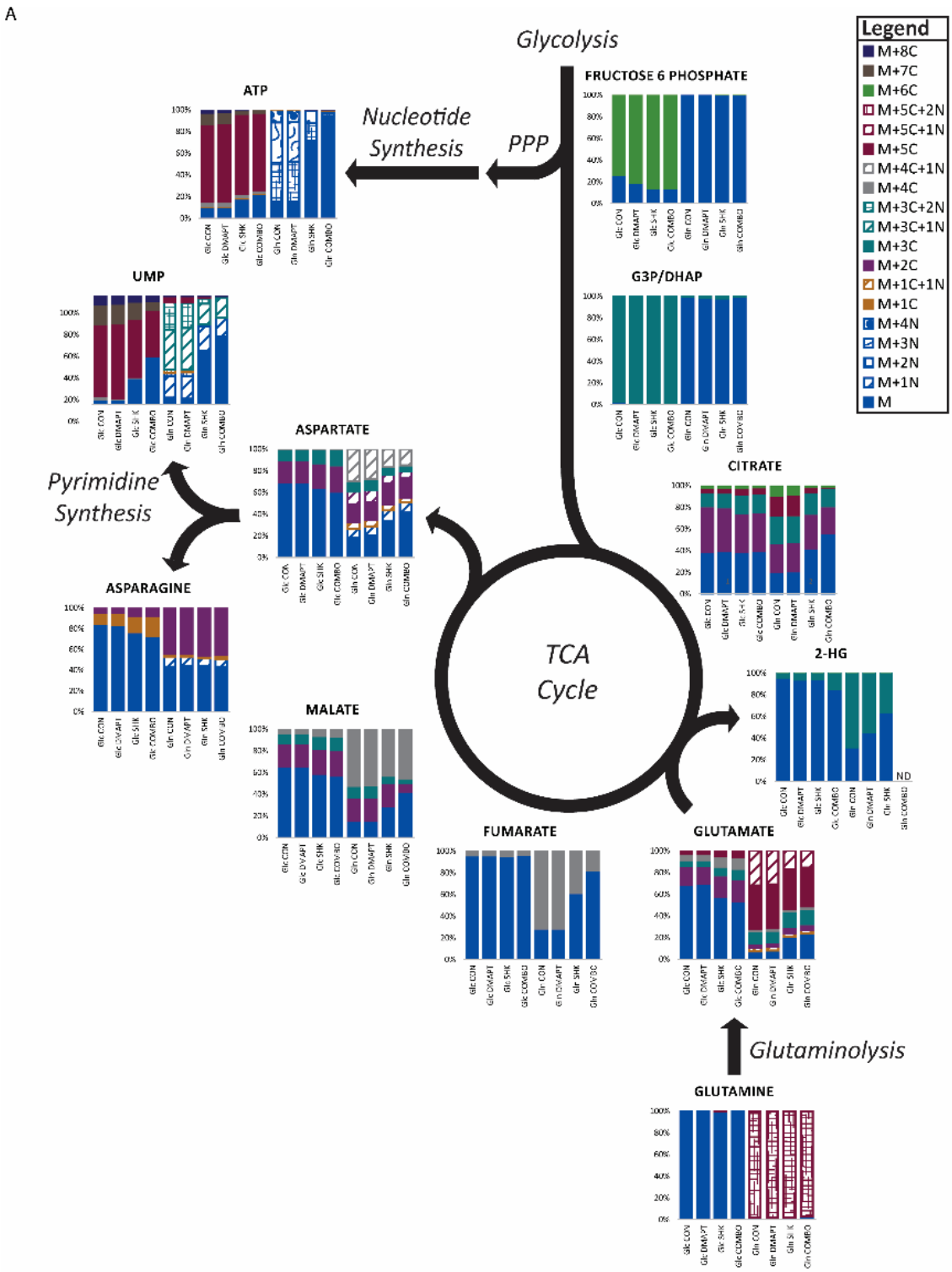

Figure 2.4: DMAPT and SHK induce changes in intracellular glucose and glutamine flux in precursor B-cell leukemia

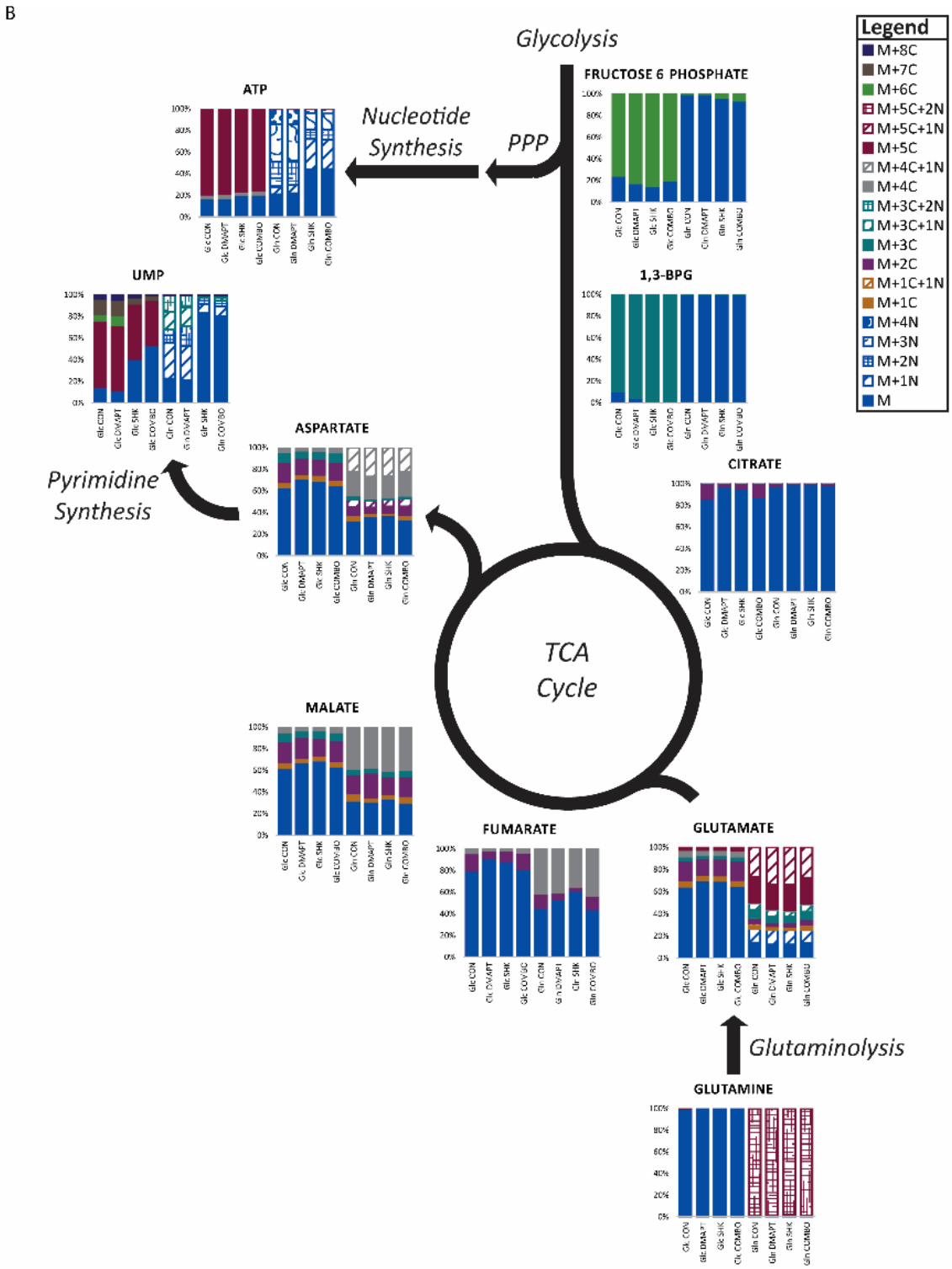

Figure 2.4: DMAPT and SHK induce changes in intracellular glucose and glutamine flux in precursor B-cell leukemia, continued

Figure 2.4: DMAPT and SHK induce changes in intracellular glucose and glutamine flux in precursor B-cell leukemia, continued

(A) RCH-ACV and (B) Reh cells were cultured in medium containing $^{13}C_6$-glucose or $^{13}C_5$,$^{15}N_2$-glutamine and treated with vehicle, DMAPT, SHK, or both. Stable isotope enrichment is shown as a fraction of the total metabolite pool averaged over three replicates. Glc, $^{13}C_6$-glucose; Gln, $^{13}C_5$,$^{15}N_2$-glutamine; CON, vehicle control; DMAPT, dimethylaminoparthenolide; SHK, shikonin; COMBO, combination; G3P, glyceraldehyde 3-phosphate; DHAP, dihydroxyacetone phosphate; 1,3-BPG, 1,3-bisphosphoglyceric acid; 2-HG, 2-hydroxyglutarate; UMP, uridine monophosphate; ATP, adenosine triphosphate; PPP, pentose phosphate pathway; TCA cycle, tricarboxylic acid cycle.

2.5 DISCUSSION

In this study, a library of natural products was screened for cytotoxicity in BCP-ALL and normal bone marrow-derived cells. Most chemotherapeutics are broadly toxic to cancer and normal cells alike, which leads to short- and long-term consequences for patients, especially very young ones [34, 140]. Thus, differences in BCP-ALL and normal cells viability were critical for identifying compounds that exhibited selective activity in leukemia cells. The effect of each NPL compound on cell viability was monitored by ATP luminescence. Intracellular ATP is essential for cancer cell survival and depletion has been linked to apoptosis in a number of cancer cells [168]. Furthermore, SHK has previously been shown to decrease ATP and lead to cell death in hepatocellular carcinoma and melanoma [169, 170]. The first round of screening resulted in seven candidate compounds, with PTL having the greatest difference in viability between normal and BCP-ALL cells. A secondary screen was performed combining PTL with the six other candidate compounds to investigate synergistic combinations. Bliss indices narrowed the candidate pool to PTL and SHK. Importantly, normal cells we equally unaffected by the synergistic combination indicating that leukemia cell specificity was maintained with PTL and SHK.

PTL has been shown to be effective against acute leukemias but has limited solubility and bioavailability [171, 172]. To ameliorate this limitation, an orally bioavailable, water-soluble analog (DMAPT) was developed previously and found to induce cell death in acute myeloid leukemia cells [165, 166]. This study demonstrated that PTL and DMAPT also have comparable activity in BCP-ALL. Next, DMAPT was evaluated in combination with SHK to confirm comparable synergism to PTL and SHK. Evaluation by two methods, Bliss and Chou-Talalay, indicated synergy between DMAPT and SHK near maximal at 1 μM DMAPT:SHK for both cell lines. Subsequent experiments

were performed under these conditions to elucidate the metabolic consequences of DMAPT:SHK treatment.

Metabolomics analysis revealed a significant impact on global metabolite levels in single and combination groups. Metabolites central to sustaining the energetic and biosynthetic needs of leukemia cells were modulated by DMAPT, SHK, and the combination. Pathway analysis confirmed that amino acid, antioxidant, TCA cycle (in RCH-ACV cells), and nucleotide metabolism were central to the biological effects of the combination. MFA with $^{13}C_6$-glucose revealed a limited influence on the incorporation of glucose in glycolysis or the TCA cycle. Overall, glycolysis and the TCA cycle were downregulated, but label incorporation was uniform. Instead, treatment resulted in a significant decrease in ^{13}C-label incorporation into nucleotides, particularly in the combination and SHK alone. SHK has been shown to inhibit PKM2 (pyruvate kinase M2) which is key in diverting glucose into PPP [169]. Inhibition of PKM2 leads to suppression of metabolism, decreased proliferation, and ultimately apoptosis [173, 174]. Label incorporation from $^{13}C_5$,$^{15}N_2$-glutamine differed between cell lines. In RCH-ACV cells, the combination group (and SHK alone) had reduced label incorporation that propagated from glutamine through glutaminolysis, the TCA cycle, and nucleotide synthesis. The net effect of these pathways is both energy generation and biosynthesis of macromolecules for proliferation. DMAPT has been shown to directly inhibit cell survival and proliferative signals from NF-κB (nuclear factor kappa-light-chain-enhancer of activated B cells) [166, 171], STAT (signal transducer and activator of transcription) [175], and MAPK (mitogen-activated protein kinases) [176]. At the same time, DMAPT activates pro-apoptotic signaling through JNK (c-Jun N-terminal kinases) and p53 [165, 166, 177]. This simultaneous shifting of metabolism away from pro-survival and proliferative signals was seen via reduced biosynthetic label incorporation, most remarkably in nucleotides.

Reductive flux through the TCA cycle was also limited as seen by diminished label incorporation (M+5, M+3) 2-hydroxyglutarate, citrate, aspartate, and malate. In Reh cells, minimal differences in label incorporation in the TCA cycle were seen between groups. Consistent with the unlabeled data, DMAPT and SHK appear to have a greater impact individually on TCA cycle intermediates. Although no difference was observed in TCA cycle flux, the significant reduction in nucleotide synthesis was similarly observed in Reh cells, suggesting an inhibitory mechanism further downstream. Other studies have also shown a stronger response in purine and pyrimidine metabolism than other pathways in response to metabolic stress [178]. Synergism between DMAPT and SHK may be explained by inhibition of the PI3K/AKT/mTOR (phosphoinositide 3-kinase/protein kinase B, mammalian target of rapamycin) signaling cascade by SHK. mTOR regulates cancer cell anabolism and drives nucleotide synthesis for ribosome biogenesis and DNA synthesis. Inhibition of this process leads to the depletion of nucleotides, DNA damage, and selective cytotoxicity [179]. Furthermore, DMAPT has been shown to be synergistic with mTOR inhibitors in acute myeloid leukemia [180, 181]. Thus, despite minimal differences in energy metabolism, biosynthetic pathways central to leukemia cell survival were nonetheless significantly inhibited resulting in arrested proliferation and ultimately cell death.

In this study, successive rounds of compound screenings led to the identification of a synergistic combination of natural products that exhibited strong effects on BCP-ALL cell viability with minimal consequences in normal cells. DMAPT and SHK altered total metabolite pools and inhibited flux through key pathways involving amino acids, antioxidants, the TCA cycle, and nucleotides. Together DMAPT and SHK exploited the metabolic vulnerabilities of BCP-ALL. This combination indicates a promising avenue for BCP-ALL treatment with less toxic, leukemia-specific treatments. To assess clinical

applicability, future studies could evaluate DMAPT and SHK in combination with standard and reduced doses of current therapeutics.

Chapter 3: Stratification of pediatric leukemia patients by combining clinical parameters and metabolic signatures to identify exploitable pathway dysregulation for a personalized therapeutic approach

3.1 ABSTRACT

Cytogenetic analyses have revealed that most pediatric precursor B-cell acute lymphoblastic leukemia (BCP-ALL) cells possess gross chromosomal alterations, many of which have been correlated with patient outcomes. Aberrations in the IGH locus have been associated with poor prognosis in pediatric patients, likely due to the frequency of oncogene translocations into proximity of the IGH promotor. Yet, little is known about the phenotypic consequences of these mutations. Chromosomal anomalies have a significant effect on both cancer phenotype and response to therapeutics. Here, we utilized a metabolomics approach to characterize the global metabolic effects of genetic aberrations at the IGH locus. This study investigated the relationship between traditional clinical markers, cytogenetics, and intracellular metabolite profiles in pediatric leukemia patients at diagnosis. Metabolites extracted from fresh bone marrow (BM) aspirates of 41 BCP-ALL patients were analyzed by ultrahigh performance liquid chromatography-mass spectrometry (UPLC-MS). Multivariate analysis demonstrated that global metabolic profiles were significantly altered by anomalies at the IGH locus. We observed unique metabolic profiles suggesting dysregulation of several major pathways when patients were stratified by their primary cytogenetic anomalies. Assessment of individual metabolites indicated nucleotides and energy metabolism intermediates were decreased in the BM of patients with IGH anomalies. Conversely, levels of amino acids, amino acid-related metabolites, and some sugars were increased in these patients. Phosphatidylcholines, phosphatidylethanolamines, and polar metabolites involved in lipid transport and metabolism were also increased in IGH mutants. These data suggest that aberrations at the

IGH locus result in characteristic dysregulation of central metabolic pathways involving both polar metabolites and lipids. Screening of a cancer compound library in BCP-ALL cells harboring an IGH locus aberration indicated that therapeutics targeting heat shock protein, proteasome, mTOR, and HDAC activities is an effective strategy for inhibiting leukemia cell proliferation. Interrogation of metabolic dysregulation and the identification of novel therapeutics is a promising step towards personalized treatment for patients carrying this mutation, an essential development for improving the quality of life and long-term outcomes of pediatric leukemia patients.

3.2 INTRODUCTION

Cancer is the leading cause of disease-related death in children and adolescents ages 1–19 years [1, 26]. Leukemia is the most common pediatric cancer, accounting for 28% of all cancers in children [1, 19]. Current treatment strategies involve a very intense, risk-directed induction phase at the outset of treatment followed by a series of consolidation, intensification, and maintenance therapies that typically spans 2–3 years [15, 27, 49, 139]. This approach effectively induces remission in most patients but is highly toxic and consequently results in significant short- and long-term side effects [34-40, 140]. Among childhood leukemia survivors, 75% report a least one chronic condition 5–14 years post-diagnosis, a figure that climbs to 85% by 25–36 years [141]. Even more staggering, when evaluated clinically, 98.2% of long-term survivors were diagnosed with at least one chronic health condition [21]. Patient outcomes have improved as a result of optimization of current treatment protocols in recent decades [1]. In particular, risk-directed treatment incorporating minimal residual disease (MRD) and cytogenetic anomalies that correlate with prognosis have greatly improved patient stratification [15, 40, 42, 47].

There is a significant amount of genetic diversity in BCP-ALL [182]. Many recurrent cytogenetic anomalies in BCP-ALL have been shown to correlate with patient outcomes [15, 17, 48, 183-190]. The World Health Organization (WHO) recognizes seven established BCP-ALL cytogenetic subtypes: t(9;22)(q34.1;q11.2)/*BCR-ABL1*, t(12;21)(p13.2;q22.1)/*ETV6-RUNX1*, t(v;11q23.3)/*KMT2A* rearranged (previously *MLL* translocations), t(1;19)(q23;p13.3)/*TCF-PBX1*, t(5;14)(q31.1;q32.3)/*IGH@-IL3*, and high hyperdiploidy (HeH), hypodiploidy, and two provisional subtypes: *BCR-ABL1-like* and *iAMP21* [47, 182]. In BCP-ALL, two anomalies have consistently been associated with high rates of remission and 5-year relative survival, hyperdiploidy and *ETV6-RUNX1* translocation. The definition of HeH varies with research protocol, but the two most common definitions are the gain of five or more chromosomes (51+) or the specific gain of chromosomes 4 and 10 (or 4, 10, and 17). Inversely, hypodiploidy, typically defined as fewer than 40 chromosomes, is associated with poor prognosis. Patients with *MLL* translocations are also considered high risk and individuals with this anomaly are predominantly less than one year old [15, 40, 42, 47, 48]. Likewise, patients carrying the *BCR-ABL1* mutation are considered very high risk and assigned to a separate protocol that utilizes tyrosine kinase inhibitors (TKI) [191-193]. However, less than half of the recurrent chromosomal anomalies that have been correlated with clinical outcomes are presently used clinically for patient stratification and risk-directed treatment. There is a growing body of evidence that suggests chromosomal anomalies beyond the classifications recognized by the WHO represent important clinical markers as well as potential targets for novel therapeutics [42, 194].

While most chromosomal aberrations occur with high fidelity, likely due to chromatin structure, translocations at the IGH locus are quite promiscuous [44, 184, 195-198]. Translocation and other anomalies at the IGH locus result in bringing target genes

into proximity of the IGH enhancer region, thus resulting in dysregulation of genes downstream of IGH [184, 195, 196, 199-202]. Aberrations at the IGH locus, located on chromosome 14, occur at varying rates depending on patient age [42, 48]. Different anomalies are common at this locus including translocations, separations, insertions, deletions, and copy number variants. Despite the promiscuity of the IGH locus, translocation partners are not random. In BCP-ALL, the IGH locus has several recurrent partner genes including: MYC, CRLF2, BCL-2, ID4, EPOR, IL3, IGF2BP1, and CEBP family members [44, 47, 185, 197, 203-208]. These genes serve several purposes and are broadly involved in cell cycle regulation, apoptosis evasion, proliferation, differentiation, immunity, and metabolism. Aberrations at the IGH locus have been associated with poor prognosis in pediatric patients, but little is known of the phenotypic consequences of these mutations [44, 184, 201, 209, 210].

While cytogenetics has provided important information about chromosomal aberrations and oncogenes, it has failed to fully explain the biological consequences of many anomalies. In fact, one of the biggest challenges to incorporating cytogenetic data into clinical practice is that cellular response to gross genetic abnormalities remains largely unknown. Here we use metabolomics to demonstrate that regardless of translocation partner, patient-derived BCP-ALL cells harboring IGH locus anomalies demonstrate similar dysregulations in metabolism indicating potential targets for novel therapeutics.

3.3 MATERIALS AND METHODS

3.3.1 Reagents and chemicals

Tissue culture reagents were purchased from GE Healthcare Biosciences (Pittsburg, PA, USA) unless specified otherwise. Mass spectrometry grade water, methanol,

acetonitrile, 2-propanol, chloroform, ammonium formate, and formic acid, as well as molecular biology grade ethanol, dimethyl sulfoxide (DMSO), and 2,6-di-tert-butyl-4-methylphenol (BHT) were purchased from Thermo Fisher Scientific (Waltham, MA, USA). Hanks' Balanced Salt Solution (HBSS), Ficoll-Paque Plus, and commercial calibration solutions for the mass spectrometer were also purchased from Thermo Fisher Scientific. A library containing 291 unique anti-cancer compounds was purchased for high-throughput screening (**Table A3**; Cambridge Cancer Compound Library (CCL); Selleck Chemicals, LLC, Houston, TX, USA). The following isotopically labeled compounds were purchased from Cambridge Isotope Laboratories (Tewksbury, MA, USA): $^{13}C_1$-glucose, D_4-alanine, D_3-serine, D_2-glycine, D_4-citric acid, D_3-malic acid, D_4-succinic acid, D_2-fumaric acid, D_3-aspartic acid, D_4-L-lysine, D_4-cystine, D_3-DL-glutamic acid, D_5-glutamine, and D_5-L-tryptophan. For non-polar analyses, SPLASH LipidoMix mass spectrometry standard was purchased from Avanti Polar Lipids (Alabaster, AL, USA).

3.3.2 Declaration of ethical approval

Clinical investigations were conducted in accordance with the Declaration of Helsinki principles. Human studies were approved by both the UT Austin Health Science (2013-06-0047, 2018-05-0129) and Ascension Seton (CR-13-161) Institutional Review Boards (IRB). Written informed consent and parental/guardian permission were obtained prior to specimen collection and study inclusion.

3.3.3 Patients and clinical outcomes

Patients were recruited by the clinical staff at the Children's Blood and Cancer Center at the Dell Pediatric Medical Center in Austin, Texas. Bone marrow (BM) aspirates were collected at diagnosis and throughout treatment following written and informed

consent and parental/guardian permission. Specimen collection was performed in accordance with IRB guidelines. To be eligible for the study, patients were required to be between one to 21 years of age at the time of leukemia diagnosis (new or relapse). Clinical measures including age, gender, weight, body mass index (BMI), race, ethnicity, risk classification, minimal residual disease (MRD), histopathology (flow cytometry, karyotype, and fluorescence in situ hybridization (FISH), where applicable) were reported following diagnosis. Nonparametric Wilcoxon rank sum tests were performed on patient age, weight, and BMI [211, 212]. All patients were treated following Children's Oncology Group (COG) protocols as determined by diagnosis and risk assessment (**Table 3.1**). Patients diagnosed with precursor B-cell acute lymphoblastic leukemia (BCP-ALL) were treated in accordance with COG protocol AALL0932 (standard risk), AALL1131 (high risk), or AALL1122 (Philadelphia chromosome positive). Treatment roadmaps can be found in **Appendix C**. Clinical risk assessment at diagnosis included age, sex, white blood cell count, and presence of leukemia cells in cerebrospinal fluid. A small number of cytogenetic markers are also used (once available). Last, response to therapy, as measured by minimal residual disease during or following induction is used to establish patient risk.

Table 3.1: Established parameters for clinical risk assessment of pediatric BCP-ALL patients
Very few modern markers for patient risk stratification are currently being used clinically. WBC, white blood cells; CNS, central nervous system; MRD, minimal residual disease; ND, not detected; D, detected, Ph+, Philadelphia chromosome positive; Ph-like, Philadelphia like; MLL, mixed lineage leukemia translocation.

Parameter	*Standard Risk*	*High Risk*
Age (years)	<10	≥10
Sex	Female	Male
WBC count (per μL)	<50,000	>50,000
CNS infiltration	ND	D
MRD (Induction)	Negative	Positive
Cytogenetics	Hyperdiploid	Hypodiploid, Ph+, Ph-like, *MLL*

3.3.4 Sample preparation

Patient specimens were collected in heparinized vacuum blood collection tubes (Becton, Dickenson and Company, Franklin Lakes, New Jersey, USA). Blood plasma and bone marrow supernatant were isolated by centrifugation at 400 *g* for 20 minutes at 18°C. A 1 mL aliquot of plasma or supernatant was immediately snap frozen in liquid nitrogen and stored at -80°C prior to analysis. Leukemia cells were isolated using a modified Ficoll-Paque protocol. Briefly, the remaining blood was diluted 1:1 with ice cold Hanks' Balanced Salt Solution (HBSS) and layered over 3 mL of Ficoll-Paque Plus solution. Specimens were then centrifuged at 400 *g* without brake for 30 minutes at 18°C. The mononuclear cell layer was collected and washed twice with ice cold 10 mL of HBSS. Cells were counted, pelleted, snap frozen in liquid nitrogen, and stored at -80°C prior to analysis.

For analysis of the extracellular environment, aliquots of biofluid supernatant were ultrafiltered (Nanosep 3K Omega centrifugal devices; Pall Corporation, Port Washington, NY, USA) to remove protein and lipid components as previously reported [68, 93]. In brief, centrifugal filters were washed twice within 24 hours with MilliQ water (Millipore). Biofluids were thawed on ice, vortexed, and a 600 µL aliquot was transferred to the filter. Samples were centrifuged at 14,600 *g* and 4°C for up to 24 hours. The polar filtrate was transferred on ice to LC-MS vials and spiked with 14 stable isotope-labeled polar internal standards (IS) at a final concentration of 0.2 ppm. For intracellular analysis, metabolites were extracted from cell pellets by modified Bligh-Dyer, similar to previously reported [138]. In brief, cell pellets were extracted with ice cold 1:1 water:methanol and equal parts chloroform. BHT was added to preserve metabolites susceptible to oxidation. Polar and non-polar fractions were isolated and evaporated to dryness at 4°C in a CentriVap refrigerated vacuum concentrator (Labconco, Kansas City, MO, USA). Polar fractions were resuspended in water containing 14 IS at 0.2 ppm and transferred to LC-MS vials for

immediate analysis. Aliquots of non-polar metabolites were spiked with 10 µL of SPLASH LipidoMix (supplied in methanol), resuspended in 100 mM ammonium formate in 65:35 acetonitrile:2-propanol, and were transferred into 96-well microplates (Eppendorf, Hamburg, Germany). Filled microplates were heat sealed with pierceable foil sheets (ALPS 50V Manual Heat Sealer; Thermo Fisher Scientific, Waltham, MA, USA) and kept at -80°C until analysis.

3.3.5 Ultrahigh performance liquid chromatography-mass spectrometry (UPLC-MS) analysis

Chromatographic separation was achieved on a Vanquish Flex UPLC system equipped with a quaternary pump, vacuum degasser, column compartment, and split autosampler with temperature controller (5°C; Fisher Scientific, Bremen, Germany). A Kinetex 2.6 µm C18 100 Å, 150 x 2.1 mm HPLC column (Phenomenex, Torrance, CA, USA) was used for untargeted polar metabolite analysis. Mobile phase A was water with 0.2% formic acid and mobile phase B was methanol. A gradient separation was performed holding 2% B for 4 minutes, then a linear increase to 80% B over 10 minutes, followed by another linear increase to 98% B over 1 minute, then washing with 98% B for 6 minutes, and column equilibration with 2% B for 14 minutes. The total run time was 35 minutes with a flow rate of 150 µL/min and an injection volume of 5 µL. Eluent was coupled to a Q Exactive Hybrid Quadrupole Orbitrap mass spectrometer with an electrospray ionization (ESI) source simultaneously operating in fast negative/positive ion switching mode (Thermo Scientific, Bremen, Germany). The following acquisition settings were used for data collection in full MS mode: spray voltage, 4 kV (pve), 3.5 kV (nve); capillary temperature, 320°C; sheath gas, 45 (arbitrary units); auxiliary gas, 10 (arbitrary units); *m/z* range, 50-750; data acquisition, centroid mode; microscans, 10; AGC target, 1e6;

maximum injection time, 200 ms; mass resolution, 70,000 FWHM at *m/z* 200. Accuracy of the instrument was ensured by calibrating the detector prior to analysis. Mass tolerance was maintained at 5 ppm in all cases. Internal standards were used to monitor retention time, ionization efficiency, and instrument stability during analysis.

The ultrahigh performance liquid chromatography-mass spectrometry (UPLC-MS) analytical platform was controlled by an external computer operating the Xcalibur software package (version 2.2 SP1.48; Thermo Scientific, San Jose, CA, USA). Raw files were processed using SIEVE 2.2.0 SP2 (Thermo Scientific, San Jose, CA, USA) and an in-house script that operates in the MATLAB programming environment. Spectral alignment and peak picking were performed in SIEVE. Integrated intensities, monoisotopic masses, and retention times were exported for further analysis in the MATLAB programming environment. Metabolite identifications were determined by matching accurate masses and retention times to a mass spectral metabolite library of standards (IROA 300, Mass Spectrometry Metabolite Library of Standards (MSMLS); IROA Technologies, Sea Girt, NJ, USA). A pooled quality control (QC) was used to monitor instrument stability and a blank was used for background subtraction. Peaks were only included in further analyses if the coefficient of variance (CV) was <0.25 and >0 in the QC replicates. Probabilistic quotient normalization (PQN) was performed prior to statistical analyses [162]. Pathway analysis was performed with MetaboAnalyst on confirmed features [163, 213, 214].

3.3.6 Direct infusion mass spectrometry (DIMS) analysis

Sample plates were thawed on ice and centrifuged at 2500 *g* for 10 minutes at 4°C. Acquisition was performed on a Q Exactive Hybrid Quadrupole Orbitrap mass spectrometer equipped with an automated chip-based nanoelectrospray ionization (nESI) source (TriVersa NanoMate; Advion, Ithaca, NY, USA). The direct infusion nESI was

controlled by ChipSoft software (version 8.3.3; Advion) with the following acquisition conditions: gas pressure, 0.4 psi; spray voltage, 1.3 kV; injection volume, 5 µL; acquisition time, 30 s (per mode). Simultaneously, the mass spectrometer acquisition conditions were capillary temperature, 250°C; *m/z* range, 150-2000; data acquisition, centroid mode; microscans, 1; AGC target, 3e6; mass resolution, 70,000 FWHM at *m/z* 200. The mass spectrometer was controlled with the Xcalibur software package (version 2.2 SP1.48). Calibration of the mass spectrometer was achieved as described above. Tandem mass spectrometry (MS^2) data was acquired on a pooled QC sample for metabolite annotation. Sample microplates were maintained at 4°C for the duration of analysis.

Raw files were converted into mzXML files by MSConvert [215] and processed by in-house MATLAB scripts. Following normalization, peaks were included in analysis if the coefficient of variance (CV) was <0.25 and >0 in the QC replicates. Tandem MS^2 data facilitated the differentiation of complex lipid polar head groups. Positively annotated lipids are reported with MS^2 confirmed classifications and accurate ion masses.

3.3.7 *In vitro* screening

Cell lines were expanded, tested for mycoplasma, and stored cryogenically before screening. Suspension cells were cultured in RPMI-1640 medium supplemented with 10% characterized fetal bovine serum (FBS) and 2 mM L-glutamine. Adherent cells were cultured in DMEM high glucose supplemented with 10% characterized or MSC-qualified FBS and 2 mM L-glutamine. Stromal cells, HS-5 and HS-27A, were purchased from the American Type Culture Collection (ATCC; Manassas, VA, USA). Mesenchymal stem cells (MSC) were a gift from the laboratory of Dr. Laura Suggs (The University of Texas at Austin, Austin, TX, USA). Suspension cells, BALL-1 and Tanoue, were a generous gift from Dr. Marina Konopleva (The University of Texas MD Anderson Cancer Center,

Houston, TX, USA). Cells were incubated under standard conditions at 37°C and 5% CO_2. Suspension cells were maintained at a concentration range of 200,000 to 2 x 10^6 cells/mL and adherent cells were split via trypsinization at 70 – 90% confluency.

For screening, an automated pipetting system was used to ensure the consistency of seeding (VIAFLO 384; INTEGRA Biosciences, Hudson, NH, USA). Cells were seeded into 384-well white polystyrene microplates, as previously reported [216]. Here, cells were treated with the Cambridge Cancer Compound Library (CCL) at a final concentration of 100 nM and incubated for 24 hours. For each cell line, at least four replicates were plated. Following incubation, cell viability was assessed by adenosine triphosphate (ATP) luminescence (Cell Titer Glo (CTG); Promega, Madison, WI, USA). The manufacturer's protocol was followed for the CTG assay. Briefly, in a dark room, plates were equilibrated to room temperature for 30 minutes prior to the addition of the CTG reagent. Reagent was dispensed using the automatic pipetting system described above. Plates were placed on a platform mixer (MixMate; Eppendorf, Hamburg, Germany) for two minutes at 700 rpm to homogenize lysate. Following mixing, plates were equilibrated for an additional 10 minutes to allow the luminescence signal to stabilize. Endpoint luminescence with a 1000 ms integration time was recorded as a surrogate for cell viability. A Dixon's Q test was applied to all raw data points prior to normalization to identify outliers that could lead to potential false positive or false negative results [156]. Luminescence intensities were normalized to the vehicle control for each plate. Averages, standard deviations, and z-scores were calculated for each compound and cell line combination. Statistical significance was determined using a two-tailed, Student's t-test with a standard α of 0.05.

3.4 RESULTS

3.4.1 Clinical and demographic characteristics of BCP-ALL patients

Fresh BM was collected from 41 patients with BCP-ALL at the time of diagnosis. Patient characteristics and demographics are reported in **Table 3.2**. The median age was 7 (interquartile range (IQR) = 4–12). There were more females than males (18 males, 23 females). Most patients identified as white (83%) and Hispanic (59%). Patients were nearly evenly split between high/very high and low/standard risk groups (22 and 19, respectively). Low and standard risk patients were treated by COG protocol AALL0932 (**Form C1**). Patients classified as high or very high risk were treated according to COG protocol AALL1131 (**Form C2**), with the exception of *BCR-ABL1* and *BCR-ABL1-like*, which were treated according to COG protocol AALL1122 (**Form C3**). With the exception of those on AALL1122, all patients were treated with a combination of cytarabine, vincristine, methotrexate, L-asparaginase, and a glucocorticoid (either dexamethasone or prednisone). Patients on AALL1131 also received daunorubicin.

There were minimal differences between patients with an identified anomaly at the IGH locus and those without IGH aberrations. Wilcoxon rank sum tests on age, weight, and BMI yielded p-values of 0.1395, 0.0578, and 0.1409, respectively. For clinical data, a threshold for statistical significance is often set at p-value ≤ 0.1, as opposed to the standard $\alpha \leq 0.05$, due to higher variability between patients than genetically identical mice or *in vitro* models. If the significance threshold is set at ≤ 0.1, patient weight is statistically significant between groups. However, this is likely due to two factors. First, although not statistically significant, IGH mutant patient ages trended higher and older children and adolescents tend to weight more as they grow. Second, two patients in the IGH mutant group were classified as obese with BMI >40 and weight >100 kg placing them both at or

above the 99th percentile for their respective sex and age. Sex, race, and ethnicity classifications were also similar between groups. The non-IGH group was 58% female, whereas the IGH group was evenly split between males and females. The non-IGH group also contained more patients identifying as white (87%) than the IGH group (70%). Ethnicity was very similar at 58% and 60% Hispanic for non-IGH and IGH groups, respectively. Importantly, aberrations at the IGH locus were associated with the high and very high risk disease classification (80%). Risk was more evenly distributed in the non-IGH group (45% low or standard risk and 55% high or very high risk).

Table 3.2: Pediatric BCP-ALL patient characteristics and demographics indicated that IGH locus aberrations are associated with higher risk

Patient characteristics and demographics were similar between groups. Median values with interquartile ranges (IQR) are reported for age, weight, and BMI. Sex, race, and ethnicity distributions were similar. BCP-ALL, precursor B-cell acute lymphoblastic leukemia; IGH, immunoglobulin heavy chain; BMI, body mass index.

Characteristic	*Total*	*Non-IGH*	*IGH Mutant*
Age (years)	7 (4–12)	6 (4–10)	11 (6–13)
Sex	18 Male 23 Female	13 Male 18 Female	5 Male 5 Female
Weight (kg)	25.8 (19.1–47.1)	25.4 (18.4–37.8)	38.6 (24.0–68.1)
BMI	17.1 (16.3–19.4)	17.1 (16.1–19.1)	17.7 (16.8–27.5)
Race	34 White 3 Other 2 African American 1 Asian 1 Declined	27 White 2 Other 1 Asian 1 Declined	7 White 1 Other 2 African American
Ethnicity	24 Hispanic 15 Non-Hispanic 2 Declined	18 Hispanic 11 Non-Hispanic 2 Declined	6 Hispanic 4 Non-Hispanic
Risk Stratification	22 High/Very High 19 Low/Standard	14 High/Very High 17 Low/Standard	8 High/Very High 2 Low/Standard

3.4.2 Polar metabolomics analysis by UPLC-MS

Untargeted metabolomics analysis was performed on intracellular extracts from bone marrow-derived cells collected from patients at the time of diagnosis. Features extracted from UPLC-MS acquisition were matched to a mass spectral metabolite library of standards containing accurate masses and chromatographic retention times. This resulted in the positive identification of 128 metabolites present in most samples. Twenty-four positively identified metabolites were statistically significant between patients with an aberration at the IGH locus and patients without an IGH mutation (p-value ≤ 0.1). Statistically significant metabolites included several canonical amino acids (glutamate, glutamine, threonine, tryptophan, glycine, and aspartate) and non-canonical amino acids and amino acid-related compounds (taurine, hypotaurine, homocysteine, N-acetylglucosamine, and trimethyllysine). Fold change differences between the IGH and non-IGH groups were calculated relative to the non-IGH group (**Figure 3.1**). The non-canonical amino acids, taurine, hypotaurine, and homocysteine were all increased in the IGH mutant group. Conversely, trimethyllysine and N-acetylglucosamine were decreased in IGH patient cells ($p = 0.0145$ and 0.0102, respectively). Glutathione (GSH) was also significantly increased in the IGH mutant group ($p = 0.0583$). While oxidized glutathione (GSSG) was not statistically significant, the ratio [GSH]/[GSSG] was > 2.5 times larger in the IGH mutant group. The glutathione ratio was 422 in the IGH group as compared to 160 in the non-IGH group (data not shown).

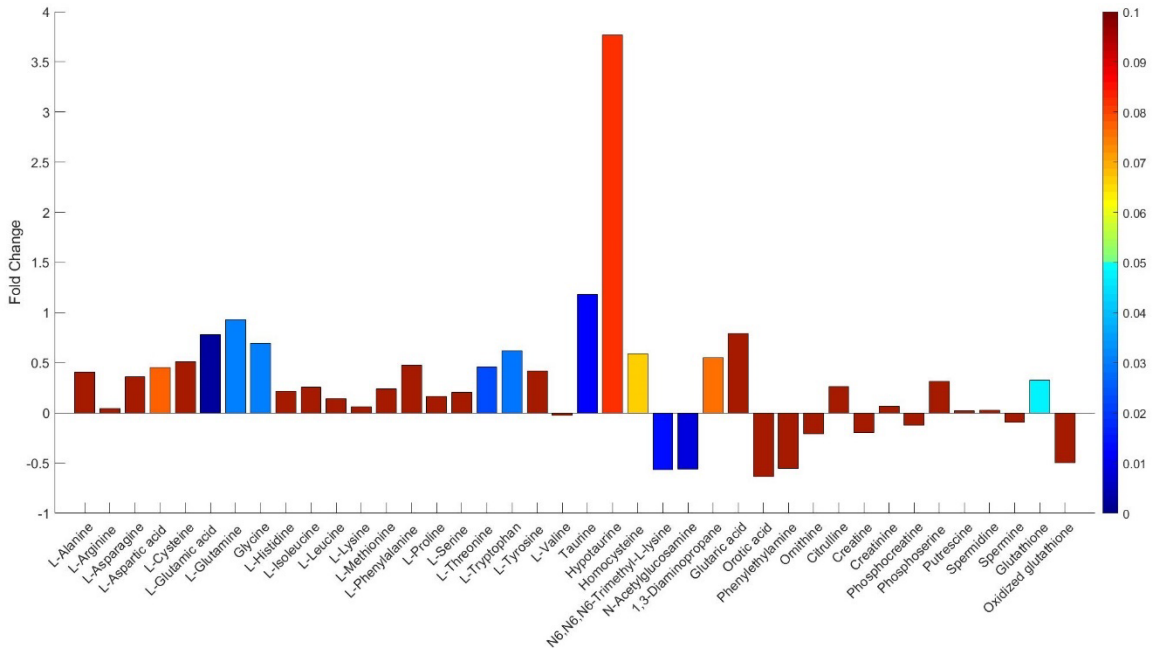

Figure 3.1: Amino acids and related metabolites were significantly elevated in pediatric BCP-ALL patients with an IGH locus aberration
Relative metabolite levels as measured by UPLC-MS. Fold change calculated relative to patients without IGH locus anomalies. Color bar indicates p-value. UPLC-MS, ultrahigh performance liquid chromatography-mass spectrometry; BCP-ALL, precursor B-cell acute lymphoblastic leukemia; IGH, immunoglobulin heavy chain.

In addition to amino acid and amino acid-related compounds, several nucleotides, energy metabolism intermediates, and polar metabolites involved in lipid metabolism were identified (**Figure 3.2**). Contrary to most amino acids, trends in nucleotides indicated decreases in the IGH mutant group relative to the non-IGH group. While only cyclic CMP (cytosine monophosphate) and GMP (guanosine monophosphate) were statistically significant ($p = 0.0201$ and 0.0664, respectively), most identified nucleotides demonstrated similar patterns. On the other hand, glucose was significantly increased in the IGH mutant group ($p = 0.0739$) but the remaining glycolytic intermediates were decreased (although not statistically significant). Similar to glucose, polar metabolites involved in lipid metabolism (ethanolamine phosphate, methyl propionate, sphinganine,

and suberic acid) were significantly increased in the IGH mutant group suggesting lipid metabolism dysregulation in these patients.

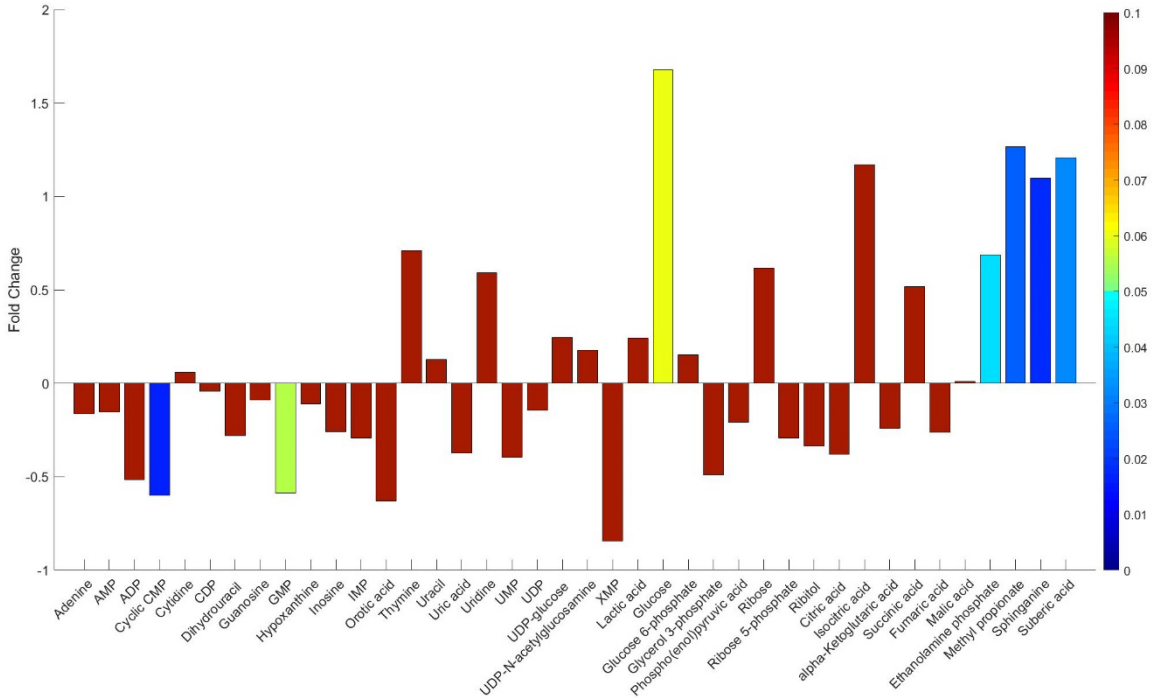

Figure 3.2: UPLC-MS analysis indicated distinct trends in nucleotide, energy, and lipid metabolism in pediatric BCP-ALL patients with an IGH locus aberration
Fold change calculated relative to patients without IGH locus anomalies. Color bar indicates p-value. UPLC-MS, ultrahigh performance liquid chromatography-mass spectrometry; BCP-ALL, precursor B-cell acute lymphoblastic leukemia; IGH, immunoglobulin heavy chain; AMP, adenosine monophosphate; ADP, adenosine diphosphate; CDP, cytidine diphosphate; GMP, guanosine monophosphate; IMP, inosine monophosphate; UMP, uridine monophosphate; UDP, uridine diphosphate; XMP, xanthosine monophosphate.

3.4.3 Pathway analysis of metabolite profiles

To contextualize the results of UPLC-MS analysis, pathway analysis was performed using the online software MetaboAnalyst [163]. Pathways implicated are reported in **Table 3.3**. Pathways were considered consequential if they had a p-value <0.1

and/or an impact >0.2. These parameters yielded 12 pathways of interest. Overall, these pathways fell under three main categories: amino acid, nucleotide, and energy metabolism. The key amino acid pathways were *glutamate metabolism* (p = 0.0080), *aspartate metabolism* (p = 0.0157), and *glutathione metabolism* (p = 0.0348). In addition to being important for protein synthesis and energy metabolism, aspartate and glutamate are also central to nucleotide synthesis. The impact of *glutathione metabolism* may be related to amino acid metabolism as glutathione is a tripeptide or may play a role in ameliorating reactive oxygen species (ROS). With regard to nucleotide synthesis, *purine metabolism* and *pyrimidine metabolism* were both statistically significant (p = 0.0082 and 0.0628, respectively). Additionally, the *pentose phosphate pathway* and the *Warburg effect* were statistically significant (p = 0.0715 and 0.0717, respectively) providing additional support that glycolytic flux was dysregulated. Several pathways involved in phospholipid metabolism were identified as statistically significant, but their impact was unclear because the number of hits was low (<5). However, this is not unexpected given that only polar metabolites were included in the pathway analysis. These findings did prompt further investigation into the role of lipid metabolism in patients with IGH locus anomalies.

Table 3.3: Pathway analysis indicated significant differences in amino acid, nucleotide, and energy metabolism
Pathway analysis was performed on UPLC-MS features positively annotated by accurate mass and retention time. Hits indicates the number of identified compounds over the total number of compounds in the specified pathway, according to SMPDB. Pathways were included if the p-value <0.1 and/or the impact was >0.2. UPLC-MS, ultrahigh performance liquid chromatography-mass spectrometry; SMPDB, small molecule pathway database; TCA, tricarboxylic acid cycle.

Pathway	*Hits*	*Impact*	*p-value*
Glutamate metabolism	10/45	0.0742	**0.0080**
Purine metabolism	13/63	0.1853	**0.0082**
Aspartate metabolism	8/34	0.8000	**0.0157**
Glutathione metabolism	5/19	0.4724	**0.0348**
Pyrimidine metabolism	9/54	0.4306	**0.0628**
Pentose phosphate pathway	6/57	0.3118	**0.0715**
Warburg effect	10/49	0.2037	**0.0717**
Urea cycle	6/23	0.3908	0.1064
TCA cycle	6/26	0.2299	0.1067
Amino sugar metabolism	6/31	0.2204	0.1310
Arginine & proline metabolism	9/48	0.2822	0.1985
Cysteine metabolism	5/24	0.4200	0.2664

3.4.4 Complex lipid analysis by DIMS

Approximately 500 complex lipid species were annotated by direct infusion mass spectrometry (DIMS). A broad range of lipid classes were identified including: monoglycerides (MG), diglycerides (DG), triglycerides (TG), phosphatidic acids (PA), phosphatidylcholines (PC), phosphatidylethanolamines (PE), phosphatidylglycerol (PG), phosphatidylinositols (PI), phosphatidylserines (PS), cholesterol esters (CE), and sphingomyelins (SM). Complex lipids are particularly difficult to assign a single molecular identification because any given species has a number of isomers that share the same accurate mass. The similarity in structures between classes and fragmentation patterns of the glycerol backbone, polar heads, and fatty acid chains of varying lengths and degrees of saturation further complicate the mass spectra of mixed samples. In order to simplify the

analysis, annotated lipids were identified by two key features: lipid classification and ion mass (*m/z*). MS^2 analysis differentiated lipid classifications. However, a small number of PC and PE species were indistinguishable and are thus reported as PC/PE for transparency. Of the nearly 500 lipids positively annotated by DIMS, 40 were statistically significant (p-value ≤0.1) between patients harboring IGH locus anomalies and those that did not have an IGH mutation (**Figure 3.3**). Fold changes were calculated between the IGH mutant and non-IGH group, relative to the non-IGH patient group. Small, but strongly significant decreases in most MG, DG, and TG were associated with anomalies at the IGH locus. Moreover, larger and significant increases in PC, PE, PS, and SM species were associated with IGH locus aberrations. Of note, for MG, PS, and SM, only one or two species were statistically significant, thus the global contributions of these classes remain unclear. Overall, these data indicate that patients with IGH locus mutations have unique lipid profiles that are characterized by diminished quantities of DG and TG species and significantly increased abundances of PC and PE species.

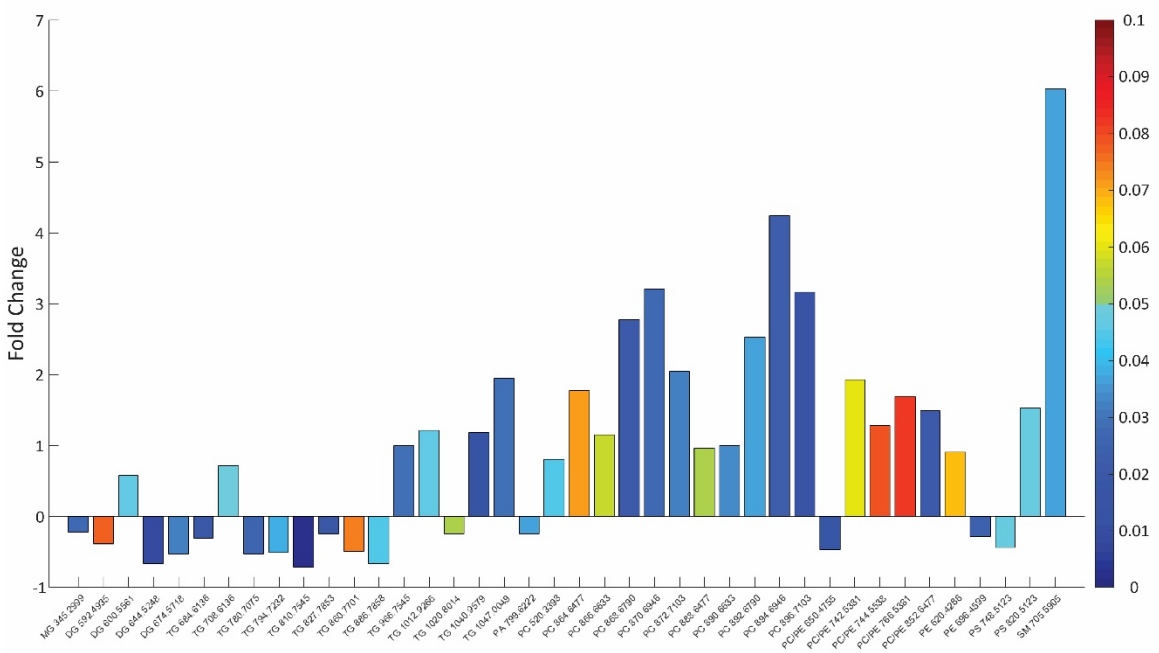

Figure 3.3: Fold change differences in lipid concentrations between BCP-ALL patients with chromosomal anomalies at the IGH locus and non-IGH mutants
Color bar indicates p-value calculated by independent Student's t-test. Fold change was calculated relative to the non-IGH mutant group. Numeric value indicates the *m/z* of the lipid species identified. BCP-ALL, precursor B-cell acute lymphoblastic leukemia; IGH, immunoglobulin heavy chain; MG, monoglyceride; DG, diglyceride; TG, triglyceride; PA, phosphatidic acid; PC, phosphatidylcholine; PE, phosphatidylethanolamine; PS, phosphatidylserine; SM, sphingomyelin.

3.4.5 Cambridge cancer compound library (CCL) screening

A customized version of the Cambridge cancer compound library (CCL) composed of 291 unique compounds was assessed for cytotoxicity as measured by ATP luminescence in two BCP-ALL cell lines carrying cytogenetic anomalies at the IGH locus. BALL-1 was established from the peripheral blood of a 75 year-old-man with BCP-ALL and carries a biallelic rearrangement of IGH with *CCND1* (Cyclin D1; t(11;14)(q13;q32)) and *MYC* (t(8;14)(q24;q32)) [217, 218]. Tanoue was established from the peripheral blood of an 11 year-old-boy with BCP-ALL and carries a single copy of the IGH-MYC translocation t(8;14)(q24;q32) [219]. Cells were treated with a final concentration of 100 nM and

efficacy was assessed 24 hours after treatment. There were 62 compounds that resulted in an average relative viability of ≤90% in BALL-1 and Tanoue cells (**Figure 3.4**). Of those, 13 compounds yielded an average relative viability of ≤70% in both cell lines (**Table 3.4**). Importantly, the most effective compounds appear to target heat shock protein (HSP; 2), proteasome (2), mammalian target of rapamycin (mTOR; 4), and histone deacetylase (HDAC; 3) activities. The two remaining compounds were an inhibitor of survivin (YM155, sepantronium bromide) and the anti-folate anti-metabolite, methotrexate, currently used for induction therapy in both AALL0932 and AALL1131. Three of these compounds have been FDA approved: bortezomib, panobinostat, and methotrexate. Bortezomib is approved by the FDA for treatment of multiple myeloma and mantle cell lymphoma. Similarly, panobinostat is FDA approved for use in patients with multiple myeloma. Finally, methotrexate is FDA approved for treatment of many cancers including leukemia and lymphoma. Nine of the remaining 10 compounds are in Phase 1 or 2 clinical trials in one or more malignancies, indicating their promise as novel therapeutics. Only Torin 2 is not currently being investigated in clinical trial.

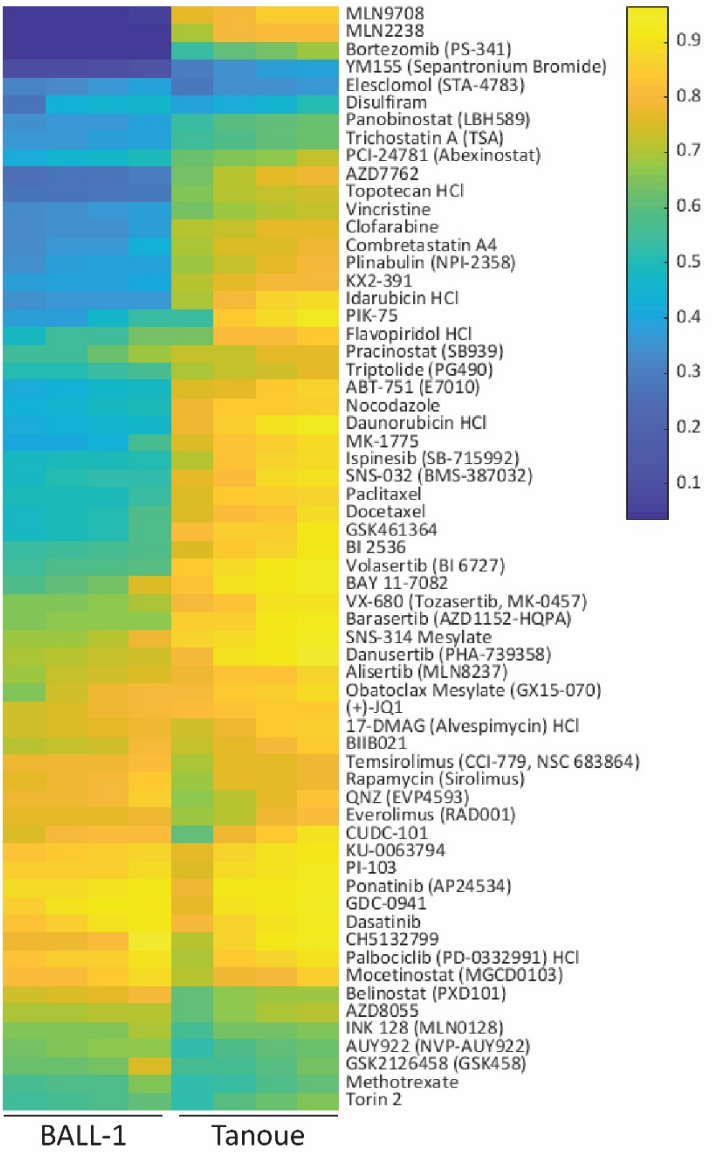

Figure 3.4: Screening of CCL indicated similar cell viability patterns in BCP-ALL cell lines carrying IGH locus anomalies

Viability measured by ATP luminescence 24 hours after treatment will 100 nM CCL. A total of 291 compounds were evaluated. Shown are the 62 compounds that inhibited viability in both BALL-1 and Tanoue by ≥10% relative to vehicle control. CCL, Cambridge cancer compound library; BCP-ALL, precursor B-cell acute lymphoblastic leukemia; IGH, immunoglobulin heavy chain.

Table 3.4: CCL candidates that decreased viability in cell lines carrying IGH locus aberrations were inhibitors of heat shock protein, proteasome, mTOR, and HDAC activities

Mean viability of four replicates reported relative to vehicle control. HSP, heat shock protein; mTOR, mammalian target of rapamycin; DHFR, dihydrofolate reductase; HDAC, histone deacetylases.

Compound	*Alias*	*Target*	*BALL-1*	*Tanoue*
AUY922 (NVP-AUY922)	Luminespib	HSP	0.65	0.58
AZD8055		mTOR	0.70	0.67
Bortezomib (PS-341)	Velcade	Proteasome	0.04	0.61
Disulfiram	Antabuse	Proteasome	0.40	0.44
Elesclomol (STA-4783)		HSP	0.35	0.35
GSK2126458 (GSK458)	Omipalisib	mTOR	0.66	0.59
INK 128 (MLN0128)	Sapanisertib	mTOR	0.66	0.62
Methotrexate		DHFR	0.59	0.56
Panobinostat (LBH589)	Farydak	HDAC	0.37	0.59
PCI-24781 (Abexinostat)		HDAC	0.46	0.66
Torin 2		mTOR	0.58	0.60
Trichostatin A (TSA)		HDAC	0.37	0.59
YM155 (Sepantronium Bromide)		Survivin	0.09	0.35

3.5 DISCUSSION

Pediatric patients with hematological malignancies were recruited at the time of diagnosis. For this analysis, patients were grouped based on their primary cytogenetic anomalies. Preliminary evidence suggested distinct metabolic profiles of leukemia cells derived from patients with aberrations at the IGH locus. Overall, patient characteristics and demographics were similar between groups. There were minimal differences in age, weight, and BMI. Using the standard clinical cutoff for statistical significance (p-value $\leq$0.1) only weight was statistically significant between the IGH mutant group and the non-IGH group. This is most likely explained by the fact that two of the patients in the IGH group were obese and ranked at or above the 99th percentile for their age and sex. Similarly, sex, race, and ethnicity were similar between groups. Thus, differences in the metabolic

profiles do not appear to be attributable to these clinical features. The one important distinction between the groups was that patients harboring an IGH locus aberration were more likely to be classified as high or very high risk whereas the distribution was more even in the non-IGH group. This finding is consistent with previous studies indicating poorer outcomes for patients with IGH locus anomalies [44, 185, 201, 209, 210].

Metabolomics and pathway analyses of the polar and non-polar fractions of bone marrow-derived BCP-ALL cells collected from patients at the time of diagnosis indicated distinct profiles in patients with anomalies at the IGH locus. Metabolomics analysis indicated significant increases in the IGH group of several amino acids, amino acid-related compounds, and glucose. Significant increases were also observed in PC and PE lipid species and polar metabolites important in lipid metabolism. Nucleotides were generally decreased in in the IGH group as were intermediates in central energy metabolism (glycolysis and TCA cycle). Pathway analysis confirmed the central importance of amino acid, nucleotide, and energy metabolism. Combined these results indicate that aberrations at the IGH locus result in a unique metabolic profile. IGH locus anomalies often result in overexpression of partner genes due to the proximity of the IGH enhancer region. While recurrent translocations into the IGH locus are not directly involved in metabolism, many have important roles in cell cycle, apoptosis and survival, proliferation, and differentiation. Cytokine receptor-like factor 2 (CRLF2), erythropoietin receptor (EPOR), and interleukin 3 (IL3) activate the JAK-STAT signaling pathway which has been shown to directly regulate lipid metabolism in adipocytes [220, 221]. This activity has not been observed in BCL-ALL and our findings may be the result of either dysregulated lipid metabolism in leukemia cells and/or crosstalk between leukemia cells and adipocytes in the bone marrow tumor microenvironment. The translocation partner, B-cell lymphoma 2 (BCL2), primarily know for inhibiting apoptosis also controls metabolic activity and insulin under cellular

stress [222]. Another member of the BCL2 family, BCL-XL, has been shown to alter mitochondrial physiology to promote survival under stress [223]. Further studies will be needed to determine whether either of these activities contribute to dysregulated metabolism in BCP-ALL cells. Lastly, MYC translocations at the IGH locus account for the majority of Burkitt's lymphoma cases and many BCP-ALL cases harboring an IGH translocation. MYC is a proto-oncogene involved in cell cycle progression, apoptosis, and cellular transformation. MYC has also been shown regulate the expression of enzyme involved in glycolysis, nucleotide synthesis, and lipid synthesis [60, 224]. Furthermore, MYC appears to work in concert with mTOR to exacerbate metabolic dysregulation in cancer cells. While MYC upregulates glycolysis and biosynthesis of lipids and nucleotides, mTOR increases uptake of glucose and amino acids and upregulates protein synthesis [60].

The concerted upregulation of biosynthetic pathways and energy production for rapid proliferation by MYC and mTOR may explain the efficacy of mTOR inhibitors on IGH mutant cells screened with the customized library. Of 291 total compounds, 13 compounds yielded an average viability of ≤70% of control, in both cell lines. Four of the top candidates were mTOR inhibitors, indicating that the increased uptake of small molecules to support proliferation is essential for survival of IGH mutants. Related, two proteasome inhibitors were also top candidates, confirming a dependence on free amino acids for protein synthesis. There were also three histone deacetylase inhibitors in the top candidates. HDAC inhibitors target multiple processes important in IGH mutant BCP-ALL including intrinsic apoptosis, cell cycle arrest, and regulation of ROS [225]. Moreover, HDAC inhibitors disrupt the protein chaperone function of heat shock proteins (HSP) [226]. Two HSP inhibitors were also top candidates for inhibiting leukemia cell viability. In addition to functioning as chaperones for new and misfolded proteins, there is evidence that ROS regulate HSP activity [227]. Taken together, the top library candidates identified

by high-throughput screening support the central role of amino acid, nucleotide, energy, and lipid metabolism to support the survival of BCP-ALL cells harboring an aberration at the IGH locus. More importantly, several novel therapeutic targets were identified that could decrease the toxic burden and improve both short- and long- term outcomes for patients with an IGH locus anomalies.

Chapter 4: Concluding Remarks

4.1 Conclusions

The aim of this research was to elucidate targetable metabolic vulnerabilities in BCP-ALL to improve outcomes in pediatric patients. This was achieved by combining high-throughput screening, ultrahigh performance liquid chromatography-mass spectrometry, direct infusion mass spectrometry, metabolic flux analysis, and pathway analysis. These tools were combined to investigate two main avenues of research. First, a non-toxic therapeutic strategy was explored by identifying a synergistic combination of natural products by high-throughput screening followed by untargeted metabolomics and metabolic flux analysis to provide mechanistic insights. Second, untargeted metabolomics analyses were performed on bone marrow-derived BCP-ALL patient cells to support the clinical use of metabolic markers for risk stratification. This was followed up with high-throughput screening of a customized chemotherapeutic compound library to identify novel drug targets. Together these avenues of research address the central challenge in pediatric leukemia – administering a robust treatment to induce remission while causing minimal physiological and psychological harm to young patients.

The first study identified a synergistic combination of DMAPT and SHK. This combination resulted in the net reduction of many nucleotides, amino acids, and TCA cycle intermediates. Pathway analysis confirmed the central role of amino acid and nucleotide metabolism in BCP-ALL. Metabolic flux analysis demonstrated that the combination of DMAPT and SHK resulted in decreased shunting of metabolites from glycolysis into the pentose phosphate pathway for nucleotide synthesis. Glutaminolysis was also reduced leading to a decrease in both oxidative and reductive TCA cycle flux as well as downstream

pathways. In combination, DMAPT and SHK induced measurable changes in intracellular metabolism that promoted pro-apoptotic signaling and resulted in leukemia cell death.

The second study aimed to correlate metabolic profiles with recurrent cytogenetic anomalies in pediatric BCP-ALL patients. Intracellular metabolic profiles of patients with IGH locus anomalies were distinct from patients without an aberration at this locus. Interrogation of identified metabolites indicated significant increases in amino acids, amino acid-related compounds, and glucose in IGH mutants. Polar metabolites involved in lipid metabolism were also significantly increased. Analysis of nonpolar metabolites indicated small, but significant decreases in DG and TG in addition to larger significant increases in PC and PE. Pathway analysis corroborated the vital role of amino acid and nucleotide metabolism. High-throughput screening of a customized chemotherapeutic compound library identified several promising novel therapeutics for patients harboring IGH locus anomalies that target HSP, proteasome, mTOR, and HDAC activities. Collectively, these findings indicate the clinical relevance and application of metabolomics for improving patient stratification.

4.2 Future Directions

The ongoing collaboration with the Children's Blood and Cancer Center has resulted in a large number of peripheral blood (PB) and bone marrow (BM) aspirates collected at diagnosis and throughout treatment. Future studies will evaluate the intracellular profiles of leukemia cells in circulation, the extracellular environment in BM and PB, and patient stratification based on other relevant and recurring cytogenetic anomalies. Finally, intracellular and extracellular PB specimens have been collected from a cohort of heathy children to interrogate the differences in metabolic profiles in leukemia patients at diagnosis and following induction as compared to their healthy counterparts.

Appendix A: Supplementary Tables

Table A1: Comprehensive list of compounds included in the natural products library Screening library was purchased from Selleck Chemicals, formatted in to 384-well plates, and diluted in DMSO prior to treatment.

Compound	CAS Number
(-)-Epigallocatechin gallate	989-51-5
(+)-Usniacin (D-Usnic acid)	7562-61-0
10-Hydroxycamptothecin	19685-09-7
3-Indolebutyric acid (IBA)	133-32-4
4-Methylumbelliferone (4-MU)	90-33-5
5-hydroxytryptophan (5-HTP)	56-69-9
Aesculin (Esculin)	531-75-9
Aloin (Barbaloin)	1415-73-2
Ammonium Glycyrrhizinate (AMGZ)	1407-03-0
Amygdalin	29883-15-6
Andrographolide	5508-58-7
Apigenin	520-36-5
Apocynin (Acetovanillone)	498-02-2
Arbutin (Uva, p-Arbutin)	497-76-7
Artesunate	88495-63-0
Asiatic acid	464-92-6
Astragaloside A	83207-58-3
Azomycin (2-Nitroimidazole)	527-73-1
Baicalein	491-67-8
Baicalin	21967-41-9
Berberine Hydrochloride	633-65-8
Bergenin (Cuscutin)	477-90-7
Betulinic acid	472-15-1
Bilobalide	33570-04-6
Biochanin A (4-Methylgenistein)	491-80-5
Butylscopolamine bromide (Scopolamine butylbromide)	149-64-4
Caffeic acid	331-39-5
Caffeic acid phenylethyl ester	104594-70-9
Chlorogenic acid	327-97-9
Chrysin	480-40-0
Chrysophanic acid (Chrysophanol)	481-74-3
Cinchonidine	485-71-2
Cryptotanshinone	35825-57-1
Curcumol	4871-97-0
Cyclocytidine HCl	10212-25-6
Cyclosporin A (Cyclosporine A)	59865-13-3, 55126-45-9, 56645-58-0
Cytisine (Baphitoxine, Sophorine)	485-35-8
Dihydroartemisinin (DHA)	71939-50-9
Dihydromyricetin (Ampeloptin)	27200-12-0
Dioscin (Collettiside III)	19057-60-4
Diosmetin (Luteolin 4-methyl ether)	520-34-3
Diosmin	520-27-4
DL-Carnitine hydrochloride	461-05-2
D-Mannitol (Osmitrol)	69-65-8

Table A1, continued

Compound	CAS Number
Emodin	518-82-1
Enoxolone (Glycyrrhetin)	471-53-4
Fisetin (Fustel)	528-48-3
Formononetin (Formononetol)	485-72-3
Fumalic acid (Ferulic acid)	1135-24-6
Gastrodin (Gastrodine)	62499-27-8
Genistein	446-72-0
Glycyrrhizic acid	1405-86-3
Gossypol	303-45-7, 40112-23-0, 732279-01-5
Gramine	87-52-5
Guanosine	118-00-3
Gynostemma Extract	80321-63-7
Hematoxylin (Hydroxybrazilin)	517-28-2
Hesperetin	520-33-2
Hesperidin	520-26-3
Honokiol	35354-74-6
Hordenine	539-15-1
Hyodeoxycholic acid (HDCA)	83-49-8
Hypoxanthine	68-94-0
Icariin	489-32-7
Indirubin	479-41-4
Indole-3-carbinol	700-06-1
Inosine	58-63-9
Ipriflavone	35212-22-7
Isoliquiritigenin	961-29-5, 78918-29-3
Kaempferol	520-18-3
Kinetin (6-Furfuryladenine)	525-79-1
L (+)-Rhamnose Monohydrate	10030-85-0
Lappaconite Hydrobromide	97792-45-5
Limonin	1180-71-8
Luteolin	491-70-3
Magnolol	528-43-8
Matrine ((+)-Matrine)	519-02-8
Methyl-Hesperidin	11013-97-1
Morin hydrate (Aurantica)	6202-27-3
Myricetin (Cannabiscetin)	529-44-2
Myricitrin (Myricitrine)	17912-87-7
Nalidixic acid (NegGram)	389-08-2
Naringenin	480-41-1
Naringin (Naringoside)	10236-47-2
Naringin Dihydrochalcone (Naringin DC)	18916-17-1
Neohesperidin	13241-33-3
Neohesperidin dihydrochalcone (Nhdc)	20702-77-6
Nobiletin (Hexamethoxyflavone)	478-01-3
Oleanolic Acid (Caryophyllin)	508-02-1
Oridonin (Isodonol)	28957-04-2
Orotic acid (6-Carboxyuracil)	65-86-1
Osthole (Osthol)	484-12-8
Oxymatrine (Matrine N-oxide)	16837-52-8

Table A1, continued

Compound	CAS Number
Paeonol (Peonol)	552-41-0
Palmatine chloride	10605-02-4
Parthenolide ((-)-Parthenolide)	20554-84-1
Phloretin (Dihydronaringenin)	60-82-2
Phlorizin (Phloridzin)	60-81-1
Piperine (1-Piperoylpiperidine)	94-62-2
Polydatin(Piceid)	65914-17-2
Puerarin (Kakonein)	3681-99-0
Quercetin (Sophoretin)	117-39-5
Quercetin dihydrate (Sophoretin)	6151-25-3
Resveratrol	501-36-0
Rheochrysidin (Physcione)	521-61-9, 140670-52-6
Rotundine	483-14-7
Rutaecarpine (Rutecarpine)	84-26-4
Rutin (Rutoside)	153-18-4
Salicin (Salicoside, Salicine)	138-52-3
Salidroside (Rhodioloside)	10338-51-9
Sclareol	515-03-7
Sclareolide (Norambreinolide)	564-20-5
Sesamin (Fagarol)	607-80-7
Shikimic acid (Shikimate)	138-59-0
Shikonin	54952-43-1
Silibinin (Silybin)	22888-70-6
Silymarin (Silybin B)	65666-07-1
Sinomenine (Cucoline)	115-53-7
Sodium Danshensu	67920-52-9, 23028-17-3
Sophocarpine	6483-15-4, 33823-32-4 (HCl)
Sorbitol (Glucitol)	50-70-4
Synephrine (Oxedrine)	94-07-5
Tangeretin (Tangeritin)	481-53-8
Tanshinone I	568-73-0
Tanshinone IIA (Tanshinone B)	568-72-9
Taxifolin (Dihydroquercetin)	480-18-2
Tetrahydropapaverine hydrochloride	6429-04-5
Tetrandrine (Fanchinine)	518-34-3, 32434-13-2 (2HCL)
Triptolide	38748-32-2
Troxerutin	7085-55-4
Ursolic acid (Malol)	77-52-1
Vanillin	121-33-5
Vanillylacetone	122-48-5
Xanthone (Genicide)	90-47-1
Yohimbine hydrochloride (Antagonil)	65-19-0
β-Sitosterol	83-46-5

Table A2: Bliss indices demonstrate strong synergism between parthenolide and shikonin in BCP-ALL

Selectively toxic compounds were evaluated between 250 nM - 15 µM. Broadly toxic compounds were evaluated between 10 nM - 5 µM. Bliss indices were calculated from cell viability data following 24-hour combination treatment. Values >0.1 are shown in **bold**. BCP-ALL, precursor B-cell acute lymphoblastic leukemia.

Cell Line	Compound		Parthenolide						
			0 nM	50 nM	250 nM	500 nM	750 nM	1 µM	5 µM
Kasumi-2	10-Hydroxycamptothecin	250 nM	-0.0069	0.0102	0.0340	0.0210	0.0067	-0.0002	-0.0901
		500 nM	-0.0065	-0.0020	0.0233	-0.0139	-0.0074	-0.0164	-0.0073
		750 nM	-0.0065	-0.0016	0.0217	0.0113	0.0040	-0.0191	-0.0049
		1 µm	-0.0068	-0.0025	0.0389	0.0229	0.0139	0.0091	-0.0040
		5 µM	-0.0062	0.0007	0.0057	-0.0143	-0.0200	-0.0345	-0.0026
		10 µm	-0.0067	-0.0064	0.0198	0.0288	0.0039	0.0096	-0.0005
		15 µm	-0.0074	0.0236	0.0396	0.0234	0.0659	***0.1931***	0.0009
	Cyclocytidine HCl	250 nM	-0.0201	-0.0198	0.0444	-0.0054	-0.0210	-0.0086	0.0084
		500 nM	-0.0173	-0.0074	0.0157	-0.0223	-0.0319	0.0041	0.0071
		750 nM	-0.0141	-0.0518	-0.0340	-0.0433	-0.0678	-0.0431	0.0045
		1 µm	-0.0143	0.0166	0.0264	0.0154	-0.0337	0.0113	0.0055
		5 µM	-0.0088	0.0180	0.0301	0.0081	-0.0116	-0.0150	0.0026
		10 µm	-0.0065	0.0146	0.0221	-0.0140	-0.0252	-0.0465	0.0008
		15 µm	-0.0058	0.0081	0.0244	-0.0182	-0.0246	-0.0294	-0.0010
	Dioscin	10 nM	-0.0269	0.0243	0.0660	0.0310	0.0245	0.0622	0.0034
		50 nM	-0.0267	-0.0145	0.0418	0.0426	0.0020	0.0657	0.0029
		100 nM	-0.0271	-0.0101	0.0782	0.0758	0.0718	-0.0878	0.0006
		250 nM	-0.0261	0.0328	0.0751	***0.1936***	0.0666	***0.1072***	0.0087
		500 nM	-0.0221	***0.1748***	***0.1413***	***0.1684***	0.0901	0.0386	0.0083
		1 µM	-0.0028	-0.2233	-0.0231	-0.2358	-0.1843	0.0012	-0.0026
		5 µM	-0.0058	0.0672	***0.2152***	0.0062	***0.1139***	0.0414	0.0005
	Shikonin	10 nM	-0.0255	-0.0047	0.0403	0.0017	0.0064	0.0007	0.0001
		50 nM	-0.0241	-0.0023	***0.1467***	***0.1877***	***0.2923***	***0.4710***	0.0042
		100 nM	-0.0234	0.0125	***0.2371***	***0.4440***	***0.5623***	***0.5251***	0.0050
		250 nM	-0.0100	0.0819	***0.1312***	***0.2929***	***0.2778***	***0.2937***	-0.0063
		500 nM	-0.0065	0.0826	***0.1184***	***0.1898***	***0.1861***	***0.1977***	-0.0095
		1 µM	-0.0053	0.0158	***0.1110***	***0.1523***	***0.1613***	***0.1580***	-0.0103
		5 µM	-0.0058	***0.1134***	***0.1200***	***0.1598***	***0.1747***	***0.1750***	-0.0093
	Tetrandrine	10 nM	-0.0254	-0.0116	0.0193	-0.0095	-0.0657	-0.0192	-0.0001
		50 nM	-0.0262	-0.0087	0.0246	-0.0014	-0.0085	-0.0207	-0.1106
		100 nM	-0.0263	-0.0150	0.0318	0.0229	0.0272	-0.0208	-0.0035
		250 nM	-0.0262	-0.0366	0.0225	-0.0814	-0.1112	-0.0148	-0.0007
		500 nM	-0.0273	-0.0149	0.0275	-0.0336	-0.0733	-0.0632	-0.0485
		1 µM	-0.0266	-0.0346	0.0458	-0.0506	-0.0614	0.0182	-0.0016
		5 µM	-0.0259	-0.0315	-0.0056	-0.0144	-0.0405	-0.0064	-0.0022
	Triptolide	250 nM	-0.0007	0.0038	0.0110	0.0146	0.0154	0.0167	-0.0107
		500 nM	-0.0007	0.0055	0.0142	0.0219	0.0215	0.0201	-0.0116
		750 nM	-0.0005	0.0007	0.0117	0.0135	0.0130	0.0128	-0.0124
		1 µm	-0.0005	0.0003	0.0131	0.0134	0.0120	0.0139	-0.0122
		5 µM	-0.0005	0.0030	0.0115	0.0147	0.0134	0.0123	-0.0104
		10 µm	-0.0005	0.0019	0.0104	0.0128	0.0136	0.0105	-0.0094
		15 µm	-0.0008	0.0025	0.0125	0.0147	0.0129	0.0133	-0.0026

Table A2, continued

Cell Line	Compound		Parthenolide						
			0 nM	50 nM	250 nM	500 nM	750 nM	1 µM	5 µM
KOPN-8	10-Hydroxycamptothecin	250 nM	-0.0057	-0.0099	-0.0230	-0.0228	-0.0256	-0.0322	-0.0044
		500 nM	-0.0060	-0.0056	-0.0089	-0.0172	-0.0288	-0.0365	-0.0065
		750 nM	-0.0063	0.0019	-0.0056	-0.0087	-0.0226	-0.0195	-0.0062
		1 µm	-0.0061	-0.0133	-0.0141	-0.0145	-0.0308	-0.0159	-0.0038
		5 µM	-0.0064	0.0316	-0.0080	-0.0127	0.0018	-0.0146	-0.0024
		10 µm	-0.0063	-0.0142	-0.0154	-0.0034	-0.0141	-0.0192	-0.0029
		15 µm	-0.0064	-0.0096	-0.0102	-0.0010	0.0119	0.0091	-0.0032
	Cyclocytidine HCl	250 nM	-0.0266	-0.0248	-0.0220	-0.0244	-0.0390	-0.0368	0.0030
		500 nM	-0.0267	-0.0177	-0.0203	-0.0343	-0.0010	0.0123	0.0043
		750 nM	-0.0248	-0.0304	-0.0375	0.0035	-0.0195	0.0344	0.0028
		1 µm	-0.0236	-0.0437	-0.0158	-0.0020	-0.0326	0.0840	0.0029
		5 µM	-0.0136	-0.0012	0.0111	-0.0132	-0.0336	-0.0125	0.0007
		10 µm	-0.0105	-0.0205	-0.0343	-0.0212	-0.0322	-0.0385	0.0003
		15 µm	-0.0101	-0.0103	0.0054	-0.0160	-0.0122	0.0080	-0.0005
	Dioscin	10 nM	-0.0291	-0.0382	-0.0166	-0.0086	-0.0097	0.0213	0.0002
		50 nM	-0.0289	-0.0806	-0.0227	-0.0194	-0.0541	0.0116	-0.0005
		100 nM	-0.0292	-0.0460	-0.0186	-0.0146	0.0474	-0.1068	-0.0038
		250 nM	-0.0289	0.0186	-0.0438	0.0855	0.0029	***0.1024***	-0.0009
		500 nM	-0.0289	***0.2008***	***0.2951***	***0.4401***	***0.1345***	***0.4816***	0.0044
		1 µM	-0.0200	***0.1614***	***0.2103***	***0.2371***	***0.4403***	***0.3081***	0.0023
		5 µM	-0.0008	-0.2454	-0.3716	-0.1089	-0.5082	-0.1447	-0.0049
	Shikonin	10 nM	-0.0286	-0.0534	-0.0429	-0.0368	-0.0362	-0.0267	-0.0033
		50 nM	-0.0290	-0.0034	0.0666	0.0624	0.0856	***0.2586***	-0.0025
		100 nM	-0.0285	-0.0141	***0.1054***	***0.1654***	***0.2590***	***0.2178***	-0.0025
		250 nM	-0.0208	0.0097	0.0586	***0.2179***	***0.2364***	***0.3191***	-0.0012
		500 nM	-0.0173	0.0167	0.0946	***0.2490***	***0.2078***	***0.2917***	-0.0018
		1 µM	-0.0168	0.0229	0.0820	***0.2069***	***0.2409***	***0.2816***	-0.0018
		5 µM	-0.0144	-0.0232	0.0336	0.0991	***0.2197***	***0.2453***	-0.0016
	Tetrandrine	10 nM	-0.0290	-0.0187	-0.0288	-0.0352	-0.0216	-0.0122	-0.0001
		50 nM	-0.0289	-0.0655	-0.0398	-0.0394	-0.0478	-0.0480	-0.0050
		100 nM	-0.0291	-0.0363	-0.0432	-0.0189	0.0546	-0.0272	-0.0045
		250 nM	-0.0293	-0.0295	-0.0047	-0.0483	-0.0529	0.0158	-0.0033
		500 nM	-0.0288	-0.0515	-0.0243	-0.0571	-0.0742	-0.0793	-0.0018
		1 µM	-0.0294	-0.0508	-0.0146	-0.0224	0.0298	0.0450	-0.0010
		5 µM	-0.0286	-0.0379	-0.0179	0.0025	0.0717	0.0512	-0.0031
	Triptolide	250 nM	-0.0001	0.0007	0.0013	0.0018	0.0021	0.0016	-0.0061
		500 nM	-0.0001	0.0004	0.0007	0.0010	0.0007	0.0006	-0.0067
		750 nM	0.0000	0.0002	0.0002	0.0007	0.0004	0.0003	-0.0071
		1 µm	-0.0001	-0.0003	0.0006	0.0005	0.0004	0.0004	-0.0057
		5 µM	0.0000	0.0002	0.0001	0.0005	0.0004	0.0000	-0.0048
		10 µm	-0.0001	0.0000	0.0002	0.0004	0.0001	0.0002	-0.0049
		15 µm	-0.0002	-0.0024	-0.0008	-0.0009	-0.0008	-0.0014	-0.0021

Table A2, continued

Cell Line	Compound		Parthenolide						
			0 nM	50 nM	250 nM	500 nM	750 nM	1 µM	5 µM
NALM-6	10-Hydroxycamptothecin	250 nM	0.0020	0.0119	0.0019	0.0023	0.0125	0.0209	-0.0023
		500 nM	0.0023	0.0048	0.0128	0.0122	0.0194	0.0325	0.0015
		750 nM	0.0024	0.0087	0.0168	0.0086	0.0256	0.0302	0.0020
		1 µm	0.0022	-0.0157	0.0002	0.0033	0.0132	0.0256	0.0028
		5 µM	0.0026	-0.0091	0.0153	0.0053	0.0277	0.0313	0.0061
		10 µm	0.0025	0.0143	0.0059	0.0191	0.0380	0.0436	0.0052
		15 µm	0.0025	0.0082	0.0120	0.0086	0.0115	-0.0093	0.0034
	Cyclocytidine HCl	250 nM	0.0111	0.0674	0.0499	0.0175	0.0108	0.0500	0.0176
		500 nM	0.0064	-0.0028	-0.0275	-0.0744	-0.0902	-0.0325	-0.0180
		750 nM	0.0047	0.0096	0.0029	-0.0043	-0.0394	-0.0185	-0.0124
		1 µm	0.0040	-0.0196	-0.0081	-0.0337	-0.0288	-0.0405	-0.0048
		5 µM	0.0035	-0.0075	-0.0065	-0.0143	-0.0002	0.0123	0.0029
		10 µm	0.0037	0.0155	0.0013	-0.0005	0.0181	0.0321	0.0100
		15 µm	0.0035	0.0057	0.0100	0.0013	0.0120	0.0358	0.0082
	Dioscin	10 nM	0.0187	0.0388	0.0484	0.0584	0.0991	***0.1278***	0.0541
		50 nM	0.0182	0.0809	0.0075	-0.0173	0.0513	0.0626	0.0625
		100 nM	0.0175	-0.0409	0.0054	0.0103	0.0046	0.0339	-0.0040
		250 nM	0.0119	0.0119	-0.0987	-0.2503	-0.2728	-0.2432	0.0065
		500 nM	0.0068	***0.3209***	0.0844	0.0192	***0.1534***	-0.0129	0.0027
		1 µM	0.0024	-0.0961	-0.1519	-0.2143	-0.3960	-0.1586	0.0048
		5 µM	0.0053	-0.0909	-0.2003	-0.6052	-0.0354	-0.1587	0.0115
	Shikonin	10 nM	0.0171	0.0086	0.0305	-0.0130	0.0690	0.0827	0.0491
		50 nM	0.0168	0.0082	0.0241	0.0064	0.0493	0.0983	0.0528
		100 nM	0.0160	-0.0201	-0.0063	-0.0548	0.0342	0.0962	0.0729
		250 nM	0.0153	-0.0043	0.0499	0.0604	***0.1557***	***0.2301***	0.0751
		500 nM	0.0134	0.0485	0.0566	***0.1243***	***0.1813***	***0.2939***	0.0670
		1 µM	0.0126	0.0348	0.0623	0.0809	***0.2257***	***0.3156***	0.0615
		5 µM	0.0112	-0.0139	0.0298	0.0114	***0.1192***	***0.2156***	0.0451
	Tetrandrine	10 nM	0.0160	-0.0244	-0.0049	-0.0313	0.0034	0.0016	0.0386
		50 nM	0.0166	0.0080	0.0169	-0.0173	0.0075	0.0573	0.0336
		100 nM	0.0164	0.0081	0.0225	-0.0421	0.0172	0.0434	-0.0035
		250 nM	0.0165	0.0132	0.0122	-0.0115	0.0178	0.0505	0.0458
		500 nM	0.0163	0.0201	0.0007	-0.0350	0.0176	0.0256	0.0460
		1 µM	0.0164	0.0119	-0.0149	-0.0326	0.0458	0.0420	0.0382
		5 µM	0.0162	0.0163	0.0334	-0.0146	0.0281	0.0660	0.0749
	Triptolide	250 nM	0.0050	0.0016	0.0139	0.0081	0.0286	0.0370	-0.0110
		500 nM	0.0044	-0.0064	-0.0065	-0.0049	0.0109	0.0168	-0.0151
		750 nM	0.0043	0.0091	0.0198	0.0087	0.0227	0.0310	-0.0108
		1 µm	0.0042	0.0056	0.0177	0.0081	0.0213	0.0330	-0.0224
		5 µM	0.0039	0.0097	0.0133	-0.0003	0.0225	0.0238	-0.0179
		10 µm	0.0039	0.0114	0.0102	0.0043	0.0148	0.0243	0.0029
		15 µm	0.0036	-0.0117	-0.0077	-0.0226	0.0050	0.0078	-0.0023

Table A2, continued

Cell Line	Compound		Parthenolide						
			0 nM	50 nM	250 nM	500 nM	750 nM	1 µM	5 µM
RCH-ACV	10-Hydroxycamptothecin	250 nM	-0.0047	-0.0055	0.0036	0.0002	-0.0010	-0.0064	-0.0761
		500 nM	-0.0047	-0.0029	-0.0022	0.0006	-0.0055	-0.0014	-0.0708
		750 nM	-0.0053	0.0074	0.0130	0.0090	0.0137	0.0104	-0.0611
		1 µm	-0.0049	-0.0068	-0.0032	0.0069	0.0030	0.0037	-0.0638
		5 µM	-0.0053	-0.0066	0.0062	0.0005	0.0049	0.0035	-0.0645
		10 µm	-0.0054	0.0047	0.0162	0.0111	0.0081	0.0096	-0.0559
		15 µm	-0.0053	-0.0002	-0.0076	-0.0323	-0.0073	-0.0289	-0.0707
	Cyclocytidine HCl	250 nM	-0.0430	-0.0404	0.0056	-0.0389	-0.0578	-0.0114	0.0170
		500 nM	-0.0393	-0.0331	0.0051	-0.0577	-0.0515	-0.0275	0.0197
		750 nM	-0.0314	-0.0146	0.0207	-0.0116	-0.0289	-0.0319	0.0535
		1 µm	-0.0266	-0.0688	-0.0431	-0.0569	-0.1144	-0.0818	0.0645
		5 µM	-0.0164	-0.0033	0.0068	-0.0013	-0.0080	0.0082	0.0079
		10 µm	-0.0154	-0.0201	0.0138	-0.0065	-0.0160	0.0016	0.0160
		15 µm	-0.0159	-0.0046	0.0109	-0.0064	-0.0134	0.0037	0.0159
	Dioscin	10 nM	-0.0493	-0.0534	-0.0107	-0.0195	-0.0202	-0.0027	***0.2587***
		50 nM	-0.0515	-0.0207	0.0379	0.0244	0.0091	0.0459	***0.2171***
		100 nM	-0.0509	-0.0526	0.0213	-0.0318	-0.0029	0.0297	0.0946
		250 nM	-0.0509	-0.0144	0.0629	-0.0076	0.0095	0.0461	***0.2251***
		500 nM	-0.0499	-0.0787	***0.1357***	0.0256	***0.2402***	***0.2281***	***0.3362***
		1 µM	-0.0481	-0.0885	***0.1766***	***0.1580***	0.0716	***0.2155***	***0.2062***
		5 µM	-0.0510	-0.0362	***0.1414***	***0.3836***	0.0130	0.0336	***0.1865***
	Shikonin	10 nM	-0.0498	-0.0306	0.0107	-0.0377	-0.0345	0.0410	***0.1898***
		50 nM	-0.0503	-0.0319	0.0217	-0.0241	0.0056	0.0650	***0.2500***
		100 nM	-0.0501	-0.0345	0.0358	-0.0075	0.0434	***0.1139***	***0.3815***
		250 nM	-0.0459	-0.0683	0.0573	-0.0166	0.0943	***0.1744***	***0.3111***
		500 nM	-0.0435	-0.0141	0.0927	0.0604	***0.1420***	***0.1588***	***0.3636***
		1 µM	-0.0438	0.0074	0.0919	0.0876	***0.1579***	***0.2143***	***0.3588***
		5 µM	-0.0416	-0.0166	0.0782	0.0137	***0.1062***	***0.1912***	***0.3662***
	Tetrandrine	10 nM	-0.0492	-0.0341	0.0607	-0.0221	0.0062	0.0306	0.0241
		50 nM	-0.0504	-0.0214	0.0262	-0.0075	-0.0121	0.0283	***0.2384***
		100 nM	-0.0494	-0.0231	0.0067	-0.0324	-0.0115	0.0142	-0.0441
		250 nM	-0.0489	-0.0549	0.0066	-0.0349	-0.0227	-0.0124	0.0466
		500 nM	-0.0486	-0.0515	0.0056	-0.0525	-0.0431	-0.0185	***0.1758***
		1 µM	-0.0484	-0.0519	0.0063	-0.0507	-0.0192	-0.0375	-0.0323
		5 µM	-0.0477	-0.0517	-0.0097	-0.0407	-0.0484	-0.0495	0.0517
	Triptolide	250 nM	-0.0066	0.0042	0.0272	0.0306	0.0369	0.0563	0.0637
		500 nM	-0.0066	0.0003	0.0201	0.0215	0.0251	0.0509	0.0618
		750 nM	-0.0067	-0.0036	0.0199	0.0189	0.0367	0.0533	0.0721
		1 µm	-0.0066	-0.0014	0.0164	0.0277	0.0349	0.0495	0.0668
		5 µM	-0.0065	0.0017	0.0195	0.0271	0.0433	0.0535	0.0675
		10 µm	-0.0065	-0.0005	0.0173	0.0248	0.0335	0.0560	0.0696
		15 µm	-0.0067	-0.0074	0.0072	0.0180	0.0297	0.0348	0.0645

Table A2, continued

Cell Line	Compound		Parthenolide						
			0 nM	50 nM	250 nM	500 nM	750 nM	1 µM	5 µM
Reh	10-Hydroxycamptothecin	250 nM	0.0033	0.0065	-0.0009	-0.0038	-0.0022	-0.0095	-0.0556
		500 nM	0.0034	-0.0048	0.0064	-0.0093	-0.0025	-0.0051	-0.0714
		750 nM	0.0036	-0.0062	0.0075	-0.0128	-0.0004	-0.0017	-0.0560
		1 µm	0.0035	-0.0048	0.0007	-0.0149	-0.0037	-0.0052	-0.0554
		5 µM	0.0035	0.0354	0.0059	-0.0049	0.0039	0.0064	-0.0450
		10 µm	0.0036	-0.0124	0.0014	0.0063	0.0137	0.0079	-0.0491
		15 µm	0.0036	-0.0072	-0.0042	-0.0040	0.0848	0.0761	-0.0447
	Cyclocytidine HCl	250 nM	0.0193	-0.0210	0.0580	0.0117	0.0316	0.0263	0.0218
		500 nM	0.0177	-0.0088	0.0577	0.0056	0.0213	0.0220	0.0069
		750 nM	0.0150	0.0295	0.0710	0.0480	0.0478	0.0437	0.0446
		1 µm	0.0121	-0.0547	-0.0319	0.0104	-0.0296	-0.0594	0.0147
		5 µM	0.0019	-0.0124	0.0087	-0.0011	-0.0176	-0.0145	-0.0437
		10 µm	0.0010	-0.0028	0.0038	-0.0025	-0.0069	-0.0039	-0.0312
		15 µm	0.0009	-0.0039	-0.0004	-0.0048	-0.0064	-0.0079	-0.0303
	Dioscin	10 nM	0.0201	-0.0413	0.0530	0.0082	0.0652	0.0464	0.0711
		50 nM	0.0199	-0.0369	0.0291	-0.0158	0.0373	0.0419	0.0538
		100 nM	0.0203	-0.0214	0.0564	0.0038	0.0182	0.0763	-0.0315
		250 nM	0.0199	-0.0597	***0.1053***	0.0171	***0.2110***	0.0749	0.0530
		500 nM	0.0183	-0.0747	***0.3808***	***0.2719***	-0.0071	0.0506	0.0968
		1 µM	0.0200	0.0165	***0.1470***	***0.1443***	***0.3004***	0.0340	-0.0338
		5 µM	0.0203	0.0789	***0.2944***	0.0612	***0.3246***	0.0089	-0.0431
	Shikonin	10 nM	0.0198	-0.0218	0.0244	-0.0184	0.0418	0.0823	***0.1014***
		50 nM	0.0197	-0.0181	0.0295	0.0290	0.0404	0.0393	0.0932
		100 nM	0.0199	-0.0068	0.0694	-0.0336	0.0577	0.0897	***0.1248***
		250 nM	0.0189	-0.0282	0.0869	-0.0092	***0.1214***	***0.1756***	***0.1310***
		500 nM	0.0176	-0.0142	0.0663	-0.0071	***0.1034***	***0.1271***	***0.1401***
		1 µM	0.0177	-0.0483	***0.1054***	0.0596	***0.1375***	***0.1900***	***0.1097***
		5 µM	0.0174	-0.0424	0.0887	0.0128	0.0960	***0.1007***	***0.1425***
	Tetrandrine	10 nM	0.0198	0.0043	0.0537	0.0231	0.0775	0.0644	0.0095
		50 nM	0.0196	-0.0350	0.0525	0.0077	0.0427	0.0520	***0.1465***
		100 nM	0.0197	0.0015	0.0367	-0.0047	0.0538	0.0531	-0.0690
		250 nM	0.0197	-0.0215	0.0622	0.0074	0.0926	0.0399	-0.0164
		500 nM	0.0197	-0.0219	0.0273	-0.0006	0.0545	0.0262	***0.1119***
		1 µM	0.0200	-0.0401	0.0514	-0.0097	0.0470	0.0196	-0.0669
		5 µM	0.0200	-0.0327	0.0410	-0.0068	0.0186	-0.0008	-0.0073
	Triptolide	250 nM	0.0012	0.0027	0.0128	0.0069	0.0111	0.0135	-0.0162
		500 nM	0.0009	-0.0005	0.0045	0.0011	0.0050	0.0070	-0.0220
		750 nM	0.0010	-0.0008	0.0050	0.0017	0.0068	0.0068	-0.0221
		1 µm	0.0010	-0.0015	0.0072	0.0056	0.0072	0.0086	-0.0231
		5 µM	0.0008	0.0004	0.0043	0.0008	0.0032	0.0045	-0.0244
		10 µm	0.0009	0.0014	0.0083	0.0044	0.0056	0.0078	-0.0217
		15 µm	0.0011	0.0011	0.0098	0.0037	0.0082	0.0089	-0.0162

Table A2, continued

Cell Line	Compound		Parthenolide						
			0 nM	50 nM	250 nM	500 nM	750 nM	1 µM	5 µM
HS-5	10-Hydroxycamptothecin	250 nM	-0.0083	0.0243	0.0964	-0.0491	-0.0273	0.0224	-0.0915
		500 nM	-0.0083	-0.0783	0.0275	-0.0677	-0.0880	-0.0623	-0.1701
		750 nM	-0.0083	-0.0455	0.0114	-0.1042	-0.0874	-0.0542	-0.1979
		1 µm	-0.0083	-0.0383	0.0141	-0.1231	-0.0786	-0.0696	-0.1434
		5 µM	-0.0079	-0.0143	***0.1574***	0.0369	0.0684	***0.1386***	0.0415
		10 µm	-0.0049	-0.0481	0.0055	-0.0631	-0.0615	-0.0413	-0.0900
		15 µm	-0.0050	-0.0217	0.0034	-0.0375	-0.0119	-0.0266	-0.0394
	Cyclocytidine HCl	250 nM	-0.0104	-0.0463	***0.1014***	-0.0213	-0.0312	-0.0002	-0.0081
		500 nM	-0.0107	-0.0205	0.0754	-0.0533	-0.0694	0.0152	-0.0175
		750 nM	-0.0109	0.0112	***0.1006***	-0.0820	0.0185	0.0972	0.0095
		1 µm	-0.0106	-0.0045	0.0909	-0.1091	-0.0821	-0.0154	-0.0246
		5 µM	-0.0105	0.0253	0.0918	-0.0734	-0.0561	-0.0140	-0.0776
		10 µm	-0.0098	-0.0440	0.0219	-0.0640	-0.1536	-0.0555	-0.1222
		15 µm	-0.0098	-0.0360	0.0708	-0.1240	-0.0763	-0.0468	-0.1249
	Dioscin	10 nM	-0.0111	-0.0208	0.0376	-0.1030	-0.1021	-0.0613	-0.1017
		50 nM	-0.0111	0.0041	0.0151	-0.0814	-0.0957	-0.0781	-0.0704
		100 nM	-0.0112	-0.0567	0.0467	-0.1189	-0.1075	-0.0370	-0.1147
		250 nM	-0.0113	-0.0616	0.0706	-0.0932	-0.0288	-0.0109	-0.0548
		500 nM	-0.0115	0.0072	0.0885	-0.0301	0.0557	0.0278	-0.0064
		1 µM	-0.0118	0.0462	***0.1308***	0.0382	0.0208	0.0487	0.0613
		5 µM	-0.0110	-0.0109	0.0731	-0.0182	0.0723	0.0162	0.0092
	Shikonin	10 nM	-0.0118	0.0218	***0.1146***	-0.0848	0.0011	-0.0019	0.0149
		50 nM	-0.0115	-0.0599	0.0621	-0.0782	-0.0046	0.0443	-0.0134
		100 nM	-0.0117	-0.0228	0.0386	-0.1529	-0.0300	0.0312	-0.0101
		250 nM	-0.0114	-0.0354	-0.0351	-0.0974	-0.0020	0.0193	-0.0174
		500 nM	-0.0114	0.0304	0.0794	-0.0950	-0.0452	0.0332	0.0383
		1 µM	-0.0115	0.0254	***0.1024***	-0.0755	0.0289	0.0743	0.0196
		5 µM	-0.0114	-0.0333	***0.1023***	-0.0714	0.0127	0.0585	-0.0047
	Tetrandrine	10 nM	-0.0112	-0.0646	0.0451	-0.0969	-0.0439	0.0433	0.0293
		50 nM	-0.0114	-0.0340	0.0260	-0.1290	-0.0495	0.0434	-0.0161
		100 nM	-0.0112	-0.0686	0.0881	-0.0906	-0.0111	0.0279	0.0591
		250 nM	-0.0114	0.0134	***0.1134***	-0.0478	0.0102	0.0639	0.0007
		500 nM	-0.0112	-0.0347	0.0852	-0.1333	-0.0475	-0.0005	-0.0359
		1 µM	-0.0112	0.0249	0.0856	-0.0685	-0.0493	-0.0108	-0.0105
		5 µM	-0.0111	0.0075	***0.1285***	-0.0974	-0.0644	-0.0139	-0.0101
	Triptolide	250 nM	-0.0044	-0.0287	-0.0128	-0.0798	-0.0296	-0.0181	-0.0177
		500 nM	-0.0043	-0.0382	0.0079	-0.0462	-0.0256	-0.0027	-0.0419
		750 nM	-0.0046	0.0005	0.0204	-0.0513	-0.0054	0.0125	-0.0282
		1 µm	-0.0046	-0.0128	0.0297	-0.0343	0.0119	0.0203	-0.0050
		5 µM	-0.0045	-0.0006	0.0296	-0.0339	0.0021	0.0247	0.0069
		10 µm	-0.0044	-0.0167	0.0224	-0.0348	-0.0137	0.0127	-0.0038
		15 µm	-0.0044	-0.0260	0.0414	-0.0241	-0.0163	0.0071	0.0119

Table A2, continued

Cell Line	Compound		Parthenolide						
			0 nM	50 nM	250 nM	500 nM	750 nM	1 µM	5 µM
HS-27A	10-Hydroxycamptothecin	250 nM	-0.0457	0.0025	0.0330	-0.0066	0.0139	-0.0167	-0.1013
		500 nM	-0.0439	-0.0741	-0.0014	-0.0298	-0.0082	-0.0564	-0.1584
		750 nM	-0.0448	-0.0200	0.0242	-0.0156	-0.0054	-0.0573	-0.1602
		1 µm	-0.0436	-0.0303	-0.0150	-0.0411	-0.0611	-0.0825	-0.1530
		5 µM	-0.0393	-0.0246	0.0123	-0.0428	0.0131	-0.0150	-0.1679
		10 µm	-0.0345	-0.0460	-0.0214	-0.0098	-0.0263	-0.0350	-0.1276
		15 µm	-0.0340	0.0060	0.0133	-0.0079	-0.0104	-0.0291	-0.1012
	Cyclocytidine HCl	250 nM	-0.0667	-0.0329	-0.0131	-0.0356	-0.0218	-0.0920	-0.0070
		500 nM	-0.0677	-0.0985	-0.0460	-0.0865	-0.0802	-0.0838	-0.0556
		750 nM	-0.0693	-0.0568	-0.0394	-0.0653	0.0299	-0.0766	0.0414
		1 µm	-0.0700	-0.0244	-0.0167	-0.1084	-0.0571	-0.0336	0.0460
		5 µM	-0.0618	-0.0148	-0.0355	-0.0685	-0.0412	-0.0475	-0.0345
		10 µm	-0.0590	-0.0804	-0.0663	-0.0835	-0.0882	-0.0789	-0.0736
		15 µm	-0.0627	-0.0187	0.0726	-0.0167	0.0802	0.0312	0.0719
	Dioscin	10 nM	-0.0685	-0.0204	-0.0093	-0.0325	-0.0161	-0.0226	-0.0565
		50 nM	-0.0695	-0.0017	0.0239	0.0022	0.0739	-0.0746	0.0020
		100 nM	-0.0705	-0.0487	0.0693	-0.0050	0.0084	-0.0155	-0.0699
		250 nM	-0.0698	-0.0563	-0.0338	0.0189	0.0479	-0.0589	-0.0805
		500 nM	-0.0728	-0.0758	0.0217	0.0568	0.0990	0.0163	0.0831
		1 µM	-0.0662	-0.1043	***0.1083***	-0.0346	-0.0214	-0.0832	-0.0244
		5 µM	-0.0654	-0.0535	0.0552	0.0449	***0.1243***	0.0009	***0.1027***
	Shikonin	10 nM	-0.0732	0.0262	-0.0362	-0.0554	-0.0794	-0.0623	0.0220
		50 nM	-0.0731	0.0270	0.0671	-0.0076	0.0598	-0.0102	0.0346
		100 nM	-0.0729	0.0071	0.0947	0.0202	0.0336	0.0252	0.0701
		250 nM	-0.0724	-0.0424	0.0200	0.0153	-0.0040	0.0272	0.0680
		500 nM	-0.0726	-0.0649	0.0158	-0.0011	-0.0154	-0.0274	0.0266
		1 µM	-0.0725	0.0008	0.0555	-0.0428	0.0203	0.0495	0.0846
		5 µM	-0.0707	0.0347	0.0488	0.0166	0.0625	0.0503	0.0589
	Tetrandrine	10 nM	-0.0708	-0.0395	0.0518	-0.0409	0.0599	0.0275	0.0347
		50 nM	-0.0736	-0.0296	0.0235	-0.0622	0.0121	-0.0612	0.0329
		100 nM	-0.0689	-0.0427	0.0249	-0.0272	0.0045	-0.0834	0.0046
		250 nM	-0.0709	-0.0018	-0.0418	-0.0169	0.0186	0.0062	0.0420
		500 nM	-0.0744	0.0500	0.0434	0.0171	-0.0013	0.0271	0.0582
		1 µM	-0.0722	-0.0296	0.0323	-0.0170	0.0572	-0.0694	-0.0279
		5 µM	-0.0664	-0.0538	-0.0497	-0.0406	-0.0400	-0.0811	-0.0256
	Triptolide	250 nM	-0.0395	0.0158	-0.0095	-0.0172	0.0150	0.0078	-0.0866
		500 nM	-0.0393	-0.0173	-0.0154	-0.0694	-0.0309	-0.0035	-0.1031
		750 nM	-0.0415	-0.0100	-0.0129	0.0045	0.0157	-0.0119	-0.0519
		1 µm	-0.0432	0.0049	0.0536	-0.0006	0.0457	0.0148	-0.0383
		5 µM	-0.0414	-0.0055	-0.0171	-0.0254	0.0233	-0.0524	-0.0999
		10 µm	-0.0389	-0.0224	-0.0006	-0.0484	-0.0136	-0.0004	-0.0589
		15 µm	-0.0408	-0.0180	-0.0073	-0.0416	-0.0125	-0.0221	-0.0825

Table A3: Comprehensive list of compounds included in the Cambridge cancer compound library

Screening library was purchased from Selleck Chemicals, formatted in to 384-well plates, and diluted in dimethyl sulfoxide (DMSO) & phosphate buffered solution (PBS) prior to treatment.

Compound	CAS Number
(-)-Epigallocatechin Gallate	989-51-5
(+)-JQ1	1268524-70-4
17-DMAG (Alvespimycin) HCl	467214-21-7
2-Methoxyestradiol (2-MeOE2)	362-07-2
3-Methyladenine	5142-23-4
A-769662	844499-71-4
ABT-263 (Navitoclax)	923564-51-6
ABT-737	852808-04-9
ABT-751 (E7010)	141430-65-1
AC3-019	
AEE788 (NVP-AEE788)	497839-62-0
Afatinib (BIBW2992)	439081-18-2
Ivosidenib (AG-120)	1448347-49-6
AG-14361	328543-09-5
AGI-6780	1432660-47-3
Alisertib (MLN8237)	1028486-01-2
Altretamine	645-05-6
AMG-900	945595-80-2
Aminoglutethimide	125-84-8
Amuvatinib (MP-470)	850879-09-3
Anagrelide HCl	58579-51-4
Anastrozole	120511-73-1
Andarine	401900-40-1
Aprepitant	170729-80-3
AR-A014418	487021-52-3
AT7519	844442-38-2
AUY922 (NVP-AUY922)	747412-49-3
Axitinib	319460-85-0
AZ 3146	1124329-14-1
AZ 628	878739-06-1
Azacitidine	320-67-2
Azathioprine	446-86-6
AZD7762	860352-01-8
AZD8055	1009298-09-2
Bafetinib (INNO-406)	859212-16-1
Barasertib (AZD1152-HQPA)	722544-51-6
BAY 11-7082	19542-67-7
Bay 11-7085	196309-76-9
Belinostat (PXD101)	414864-00-9
BI 2536	755038-02-9
BIBR 1532	321674-73-1
Bicalutamide	90357-06-5
BIIB021	848695-25-0
BIRB 796 (Doramapimod)	285983-48-4
Bitopertin	845614-11-1
BIX 01294	1392399-03-9
BKM120 (NVP-BKM120, Buparlisib)	944396-07-0
Bleomycin Sulfate	9041-93-4
BMS-777607	1025720-94-8

Table A3, continued

Compound	CAS Number
BMS-794833	1174046-72-0
Bortezomib (PS-341)	179324-69-7
Bosutinib (SKI-606)	380843-75-4
BX-795	702675-74-9
CAL-101 (Idelalisib, GS-1101)	870281-82-6
Canagliflozin	842133-18-0
Capecitabine	154361-50-9
CB-839	1439399-58-2
Celecoxib	169590-42-5
CEP-33779	1257704-57-6
CH5132799	1007207-67-1
CHIR-99021 (CT99021) HCl	252917-06-9 (free base)
Chrysophanic Acid	481-74-3
Cladribine	4291-63-8
Clofarabine	123318-82-1
Combretastatin A4	117048-59-6
Crenolanib (CP-868596)	670220-88-9
Crizotinib (PF-02341066)	877399-52-5, 877399-53-6 (acetate)
CUDC-101	1012054-59-9
CX-4945 (Silmitasertib)	1009820-21-6
CYC116	693228-63-6
Cyclophosphamide Monohydrate	6055-19-2
Cyclosporin A	59865-13-3
CYT387	1056634-68-4
Dacomitinib (PF299804, PF299)	1110813-31-4
Dalcetrapib (JTT-705, RO4607381)	211513-37-0
Danusertib (PHA-739358)	827318-97-8
Dapagliflozin	461432-26-8
DAPT (GSI-IX)	208255-80-5
Dasatinib	302962-49-8
Daunorubicin HCl	23541-50-6
DCC-2036 (Rebastinib)	1020172-07-9
Decitabine	2353-33-5
Degrasyn (WP1130)	856243-80-6
Dexamethasone (DHAP)	50-02-2
Disulfiram	97-77-8
Docetaxel	114977-28-5
Dovitinib (TKI-258, CHIR-258)	405169-16-6
Doxercalciferol	54573-75-0
Doxorubicin (Adriamycin)	25316-40-9
DR4-089	
Elesclomol (STA-4783)	488832-69-5
ENMD-2076	934353-76-1
Entinostat (MS-275)	209783-80-2
Enzalutamide (MDV3100)	915087-33-1
Enzastaurin (LY317615)	170364-57-5
Erlotinib HCl (OSI-744)	183319-69-9
Estradiol	50-28-2
Estrone	53-16-7

Table A3, continued

Compound	CAS Number
Etoposide	33419-42-0
Everolimus (RAD001)	159351-69-6
EX 527 (Selisistat)	49843-98-3
Exemestane	107868-30-4
Ezetimibe	163222-33-1
Febuxostat	144060-53-7
Fingolimod (FTY720) HCl	162359-56-0
Flavopiridol HCl	131740-09-5
Fludarabine	21679-14-1
Fluorouracil (5-Fluoracil, 5-FU)	51-21-8
Flutamide	13311-84-7
Fluvastatin Sodium	93957-55-2
Formestane	566-48-3
FR 180204	865362-74-9
GDC-0879	905281-76-7
GDC-0941	957054-30-7
Gefitinib (ZD1839)	184475-35-2
Setanaxib (GKT137831)	1218942-37-0
Gossypol	12542-36-8
GSK1904529A	1089283-49-7
GSK2126458 (GSK458)	1086062-66-9
GSK3787	188591-46-0
GSK461364	929095-18-1
GSK650394	890842-28-1
GSK690693	937174-76-0
GW3965 HCl	405911-17-3
GW4064	278779-30-9
GW9508	885101-89-3
Hydrocortisone	50-23-7
IACS-10759	1570496-34-2
Ibrutinib (PCI-32765)	936563-96-1
Idarubicin HCl	57852-57-0
Imatinib (STI571)	220127-57-1
Iniparib (BSI-201)	160003-66-7
INK 128 (MLN0128)	1224844-38-5
Irinotecan HCl Trihydrate	136572-09-3
Ispinesib (SB-715992)	336113-53-2
Itraconazole	84625-61-6
JNJ-26854165 (Serdemetan)	881202-45-5
JNJ-38877605	943540-75-8
JNJ-7706621	443797-96-4
KU-0063794	938440-64-3
KU-55933 (ATM Kinase Inhibitor)	587871-26-9
KU-60019	925701-49-1
KX2-391	897016-82-9
LDE225 (NVP-LDE225,Erismodegib)	956697-53-3
Lenalidomide (CC-5013)	191732-72-6
Lenvatinib (E7080)	417716-92-8
Letrozole	112809-51-5

Table A3, continued

Compound	CAS Number
Linifanib (ABT-869)	796967-16-3
Lomeguatrib	192441-08-0
Lomustine	13010-47-4
Lonidamine	50264-69-2
LY2157299	700874-72-2
LY2603618	911222-45-2
LY294002	154447-36-6
Maraviroc	376348-65-1
Medroxyprogesterone acetate	71-58-9
Megestrol Acetate	595-33-5
Methotrexate	59-05-2
MG149	1243583-85-8
Mifepristone	84371-65-3
Mitoxantrone HCl	70476-82-3
MK-0752	471905-41-6
MK-1775	955365-80-7
MK-2206 2HCl	1032350-13-2
MLN2238	1072833-77-2
MLN9708	1201902-80-8
Mocetinostat (MGCD0103)	726169-73-9
Motesanib Diphosphate (AMG-706)	857876-30-3
Mycophenolate Mofetil	128794-94-5
Mycophenolic acid	24280-93-1
Napabucasin	83280-65-3
Necrostatin-1	4311-88-0
Nilotinib (AMN-107)	641571-10-0
Nintedanib (BIBF 1120)	656247-17-5
Nocodazole	31430-18-9
NSC 23766	1177865-17-6
NU6027	220036-08-8
NU7441 (KU-57788)	503468-95-9
Nutlin-3	548472-68-0
NVP-BSK805 2HCl	1092499-93-8 (free base)
Obatoclax Mesylate (GX15-070)	803712-79-0
Olaparib (AZD2281, Ku-0059436)	763113-22-0
OSI-906 (Linsitinib)	867160-71-2
OSI-930	728033-96-3
Oxaliplatin	61825-94-3
PAC-1	315183-21-2
Paclitaxel	33069-62-4
Palbociclib (PD-0332991) HCl	827022-32-2, 571190-30-2 (free base)
Panobinostat (LBH589)	404950-80-7
Pazopanib	444731-52-6
PCI-24781 (Abexinostat)	783355-60-2
PD0325901	391210-10-9
PD173074	219580-11-7
Pelitinib (EKB-569)	257933-82-7
PF-04217903	956905-27-4
PF-3845	1196109-52-0

Table A3, continued

Compound	CAS Number
PF-4708671	1255517-76-0
PF-562271	717907-75-0
PF-573228	869288-64-2
PH-797804	586379-66-0
PHA-665752	477575-56-7
PHA-793887	718630-59-2
Phloretin	60-82-2
PI-103	371935-74-9
PIK-75	372196-77-5
PIK-93	593960-11-3
Pioglitazone	111025-46-8
Plinabulin (NPI-2358)	714272-27-2
Ponatinib (AP24534)	943319-70-8
Ponesimod	854107-55-4
Pracinostat (SB939)	929016-96-6
QNZ (EVP4593)	545380-34-5
Quercetin	117-39-5
Quizartinib (AC220)	950769-58-1
R406 (free base)	841290-80-0
Raloxifene HCl	82640-04-8
Ranolazine	95635-55-5
Rapamycin (Sirolimus)	53123-88-9
RG108	48208-26-0
RG-7112	939981-39-2
Ro 61-8048	199666-03-0
Roscovitine (Seliciclib,CYC202)	186692-46-6
Rosiglitazone	122320-73-4
Rucaparib (AG-014699,PF-01367338)	459868-92-9
Ruxolitinib (INCB018424)	941678-49-5
SANT-1	304909-07-7
Saracatinib (AZD0530)	379231-04-6
SB203580	152121-47-6
SB216763	280744-09-4
SB431542	301836-41-9
SB525334	356559-20-1
SB590885	405554-55-4
SecinH3	853625-60-2
Selumetinib (AZD6244)	606143-52-6
SGI-1776 free base	1025065-69-3
SGX-523	1022150-57-7
Simvastatin	79902-63-9
Sirtinol	410536-97-9
SKI II	312636-16-1
SMI-4a	438190-29-5
SNS-032 (BMS-387032)	345627-80-7
SNS-314 Mesylate	1146618-41-8
Sodium Phenylbutyrate	1716-12-7
Sorafenib Tosylate	475207-59-1
Sotrastaurin	425637-18-9

Table A3, continued

Compound	CAS Number
SRT1720	1001645-58-4
S-Ruxolitinib (INCB018424)	941685-37-6
SU11274	658084-23-2
Sunitinib Malate	341031-54-7
TAK-733	1035555-63-5
TAME	901-47-3
Tamoxifen Citrate	54965-24-1
Telatinib	332012-40-5
Temozolomide	85622-93-1
Temsirolimus (CCI-779, NSC 683864)	162635-04-3
TG101348 (SAR302503)	936091-26-8
Evofosfamide (TH-302)	918633-87-1
Tie2 kinase inhibitor	948557-43-5
Tipifarnib	192185-72-1
Tivozanib (AV-951)	475108-18-0
Tofacitinib (CP-690550,Tasocitinib)	477600-75-2
Topotecan HCl	119413-54-6
Toremifene Citrate	89778-27-8
Torin 2	1223001-51-1
TPCA-1	507475-17-4
Trametinib (GSK1120212)	871700-17-3
Trichostatin A (TSA)	58880-19-6
Triptolide (PG490)	38748-32-2
TW-37	877877-35-5
Valproic acid sodium salt (Sodium valproate)	1069-66-5
Vandetanib (ZD6474)	443913-73-3
Vatalanib (PTK787) 2HCl	212141-51-0
Veliparib (ABT-888)	912444-00-9
Vemurafenib (PLX4032, RG7204)	918504-65-1
Venetoclax (ABT-199, GDC-0199)	1257044-40-8
Vincristine	2068-78-2
Vismodegib (GDC-0449)	879085-55-9
Volasertib (BI 6727)	755038-65-4
Vorinostat (SAHA, MK0683)	149647-78-9
VX-680 (Tozasertib, MK-0457)	639089-54-6
WYE-354	1062169-56-5
WZ4002	1213269-23-8
XAV-939	284028-89-3
XL335	629664-81-9
Y-27632 2HCl	129830-38-2
YM155 (Sepantronium Bromide)	781661-94-7
YM201636	371942-69-7
YO-01027	209984-56-5
Zibotentan (ZD4054)	186497-07-4
Zileuton	111406-87-2
ZSTK474	475110-96-4

Appendix B: Supplementary Figures

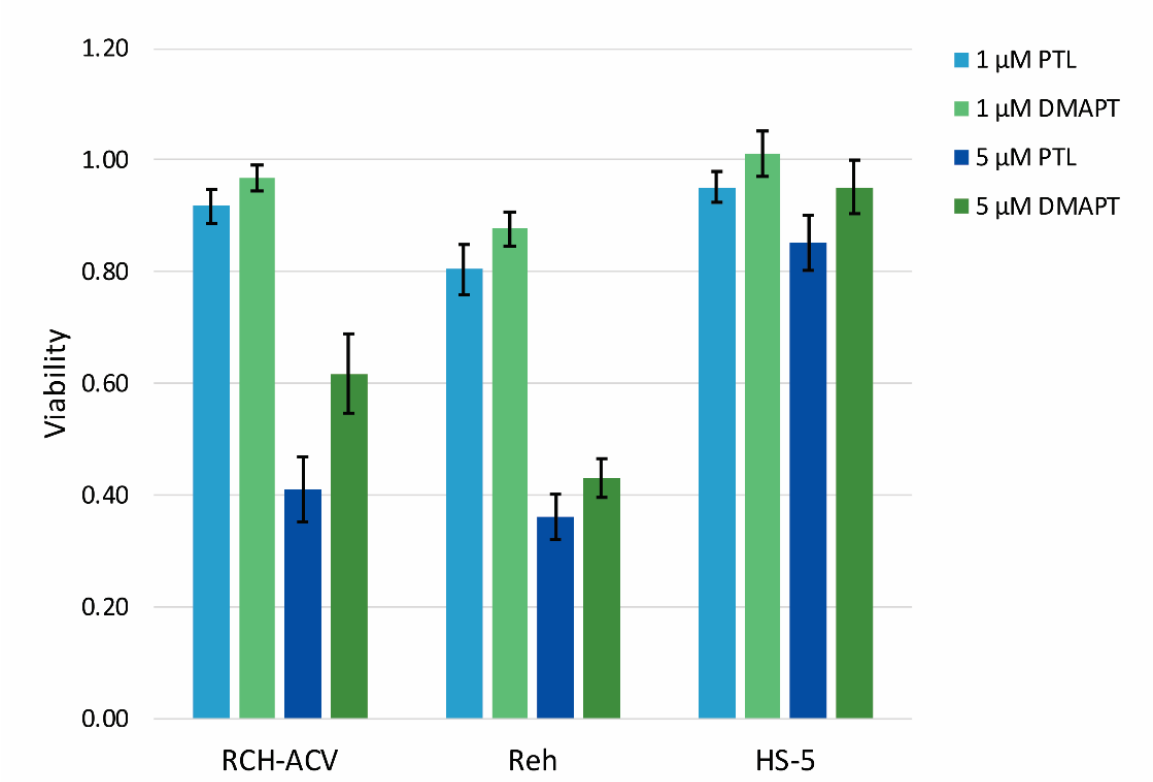

Figure B1: Minimal differences in viability were observed between PTL and DMAPT in leukemia and normal cells

Viability was assessed by ATP luminescence following 24-hour treatment with PTL or DMAPT at 1 or 5 µM final concentration. Viability is expressed relative to vehicle control for each cell line. Standard deviation calculated from 6 replicates. High reproducibility led to statistical significance between PTL and DMAPT at both concentrations. However, the difference was small (<10% in most cases) and was considered acceptable given the improvements in solubility and expected bioavailability *in vivo*. PTL, parthenolide; DMAPT, dimethylaminoparthenolide.

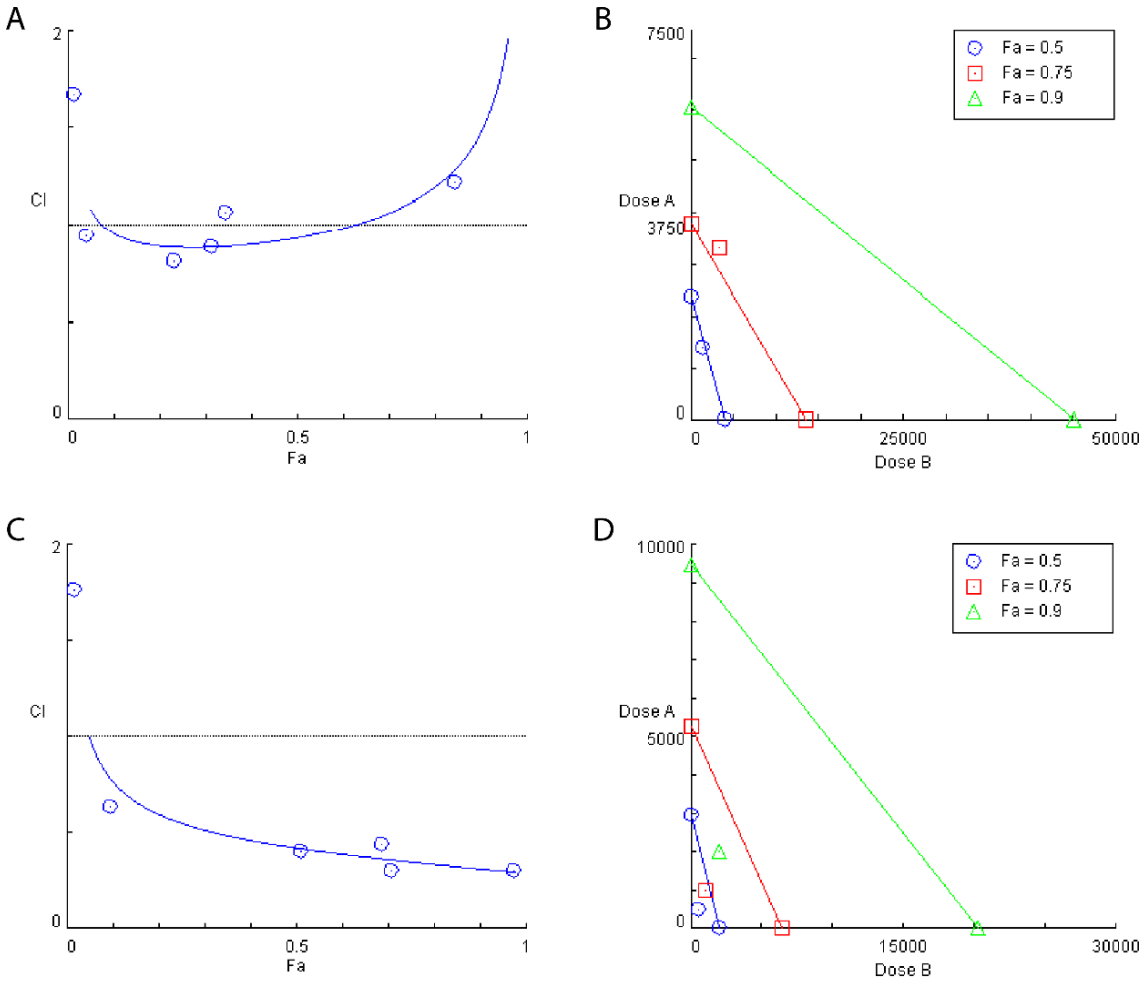

Figure B2: DMAPT and SHK are synergistic at a 1:1 ratio in RCH-ACV and Reh cells according to Chou-Talalay combination index analysis

Combination index plots for RCH-ACV (A) and Reh (C) demonstrate the synergistic window for DMAPT:SHK. CI >1 indicates antagonism, CI equal to one indicates an additive effect, and CI <1 indicates synergism. Synergism was found between Fa 0.1 – 0.6 and >0.1 for RCH-ACV and Reh cells, respectively. Isobologram for RCH-ACV (B) indicates synergism at Fa = 0.5 and below. Isobologram for Reh (D) indicates synergism at Fa = 0.9 and below. CI, combination index; Fa, fraction affected; DMAPT, dimethylaminoparthenolide; SHK, shikonin; Dose A (nM), DMAPT; Dose B (nM), SHK.

Appendix C: Induction Therapy Roadmap Forms

Form C1: AALL0932 Induction Therapy Roadmap

CHILDREN'S ONCOLOGY GROUP

THIS PROTOCOL IS FOR RESEARCH PURPOSES ONLY, SEE PAGE 1 FOR USAGE POLICY

AALL0932

4.2.1 Induction (35 days).- B-ALL Patients

All patients without DS receive common Induction Therapy.

For patients with Down syndrome see Section 4.20.

Patient name or initials _____ DOB _____

Induction therapy lasts 5 weeks (35 days). See Section 4.1 for full details regarding assignment to treatment arms and subsequent therapy. This Therapy Delivery Map is on one (1) page

DRUG	ROUTE	DOSAGE	DAYS	IMPORTANT NOTES	OBSERVATIONS
Intrathecal Cytarabine (IT ARAC)	IT	Age (yrs) Dose 1-1.99 30 mg 2-2.99 50 mg ≥ 3 70 mg	Given at time of diagnostic LP OR Day 1*	See Section 4.2 for administration guidelines **Note age-based dosing**	a. Hx, PE, Wt, Ht b. CBC/diff/platelets c. BM eval[1] d. PB sample[1] e. CSF cell count, cytospin[2] f. Creatinine, Bili, Albumin & ALT g. Varicella titer h. TPMT and NUDT15 genotype[#] [1]See Section 7.1 for details [2] Obtain with each IT administration **OBTAIN OTHER STUDIES AS REQUIRED FOR GOOD PATIENT CARE**
Intrathecal Cytarabine (IT ARAC)	IT	CNS2 patients ONLY Age (yrs) Dose 1-1.99 20 mg 2-2.99 30 mg ≥ 3 40 mg	CNS2: twice weekly[†]	† The initial dose is followed by twice weekly IT ARAC except during weeks when Days 8 & 29 IT MTX is administered **Note:** IT therapy is administered until 3 consecutive CSF samples are clear of blasts.	
VinCRIStine (VCR)	IV push over 1 minute[+]	1.5 mg/m²/dose	Days 1, 8, 15 &22	+ Or infusion via minibag as per institutional policy **Maximum dose: 2 mg**	
Dexamethasone (DEX)	PO (may give IV)	3 mg/m²/dose BID	Days 1-28 (do not taper)	Total daily dose: 6 mg/m²/day, divided BID See Section 4.2 for administration guidelines	
Pegaspargase (PEG-ASP)	IV over 1-2 hours	2500 International units/m²/dose	Day 4	**Note: pegaspargase should be administered on Day 4.** Administer through the tubing of a freely infusing solution of D_5W or 0.9% NaCl	
Intrathecal Methotrexate (IT MTX)	IT	Age (yrs) Dose 1-1.99 8 mg 2-2.99 10 mg 3-8.99 12 mg ≥ 9 15 mg	Days 8 and 29	See Section 4.2 for administration guidelines **Note age-based dosing** **Note:** All patients receive Day 8 and 29 IT MTX regardless of CSF evaluation.	

Ht ____ cm Wt ____ kg BSA ____ m²

Date Due	Date Given	Day	IT ARAC ____ mg	IT ARAC ____ mg	VCR ____ mg	DEX (BID dosing) ____ mg ____ mg	PEG-ASP ____ IU	IT MTX ____ mg	Studies	Comments
			Enter calculated dose above and actual dose administered below							
									(a[%], c, e-g)[@]	
		-2/-1/0/LP*	____mg							
		1			____mg	____mg ____mg				
		2								
		3								
		4'		____mg'			____IU		e'	
		--								
		8			____mg			____mg	a[%], b, d^**, e	
		9								
		--								
		11'		____mg'					e'	
		--								
		15			____mg				a[%], b, h	
		--								
		22			____mg				a[%], b	
		--								
		28								
		29						____mg	a[%], b, c**, d***, e	
		--								
		35								
		36		Begin Consolidation (Section 4.3) for AR B-ALL (without PD) or LR B-ALL patients randomized to Arm LR-C on Day 36 or when blood count parameters have been met (whichever occurs later). Begin Consolidation (Section 4.12) for LR B-ALL patients randomized to Arm LR-M on Day 36 regardless of blood counts.						

*On Day 1 **OR** at the time of diagnostic lumbar puncture (LP) if ≤ 72 hours from the start of protocol therapy. @Baseline

' **CNS2 patients only: administer IT therapy twice weekly until 3 consecutive CSF are clear of blasts. Day 8 & 29 IT therapy will remain IT MTX for all patients.**

Note: CNS2 patients receive IT ARAC on Days 4, 5, or 6 and 11 or 12, etc., depending on treatment schedule. Log additional IT-ARAC doses in the comments section.

** Note: For B-ALL patients, if Day 8 PB and 29 BM MRD samples are not obtained and shipped to a COG Approved ALL flow cytometry laboratory, then the patient will not be eligible to continue on a COG ALL trial following completion of Induction therapy. **Day 8 PB sample must be collected prior to Day 8 IV/IT chemotherapy.**

*** Day 29 PB specimen should be shipped to the COG ALL Molecular Reference Laboratory for all B-ALL patients that consented to studies of genomic variation on AALL08B1 or APEC14B1 (if open for classification of ALL patients) (see Section 14.0 for specimen shipping and handling). ***This specimen is very important.***

% Note: Height (Ht) is only required at the beginning of this course.

TPMT and NUDT15 genotype (TPMT highly recommended for all subjects; NUDT15 is highly recommended for subjects of Hispanic/Native American or East Asian ancestry, and optional for all other subjects (See Section 5.9)

DO CALL-BACK PRIOR TO BEGINNING CONSOLIDATION THERAPY FOR ALL B-ALL PATIENTS WHO HAVE SIGNED CONSENT FOR POST-INDUCTION THERAPY.

SEE SECTION 5.0 FOR DOSE MODIFICATIONS AND TOXICITIES. SEE SECTION 8.0 FOR SUPPORTIVE CARE GUIDELINES.

Form C2: AALL1131 Induction Therapy Roadmap

CHILDREN'S ONCOLOGY GROUP

THIS PROTOCOL IS FOR RESEARCH PURPOSES ONLY, SEE PAGE 1 FOR USAGE POLICY AALL1131

4.2.1 INDUCTION

This Induction therapy is for all patients **without** Down syndrome. **For patients with Down syndrome see Section 4.26.1**

Patient name or initials _____ DOB _____

Induction is 5 weeks (35 days). This Therapy Delivery Map is on **one (1)** page.

DRUG	ROUTE	DOSAGE	DAYS	IMPORTANT NOTES	OBSERVATIONS
Intrathecal Cytarabine (IT ARAC)	IT	At LP or Day1: Age (yrs) Dose 1-1.99 30 mg 2-2.99 50 mg ≥ 3 70 mg	Given at time of diagnostic lumbar puncture (LP) OR Day 1♦	**Note age-based dosing**	a. Hx, PE, Wt., Ht. b. CBC/diff/platelets c. BM eval[1] d. PB sample[1] e. CSF cell count, cytospin[2] f. Bilirubin, ALT & Creatinine g. Echocardiogram h. TPMT and NUDT15 genotype[θ] i. Pregnancy test [1]See Section 7.0 for further details [2] Obtain with each IT administration **OBTAIN OTHER STUDIES AS REQUIRED FOR GOOD PATIENT CARE**
Intrathecal Cytarabine (IT ARAC)	IT	CNS2 ONLY: Age (yrs) Dose 1-1.99 20 mg 2-2.99 30 mg ≥ 3 40 mg	**CNS2:** twice weekly[ß]	[1]The initial dose is followed by 2x weekly IT ARAC except on Days 8 & 29 when IT MTX is administered. **Note:** IT therapy is administered until 3 consecutive CSF samples are clear of blasts.	
VinCRIStine (VCR)	IV push over 1 minute*	1.5 mg/m²/dose	Days 1, 8, 15 &22	+ Or infusion via minibag as per institutional policy **Maximum dose: 2 mg**	
Dexamethasone (DEX) **Patients < 10 years ONLY**	PO (may be given IV)	5 mg/m²/dose BID	Days 1-14	Total daily dose: 10 mg/m²/day, divided BID See Section 4.2 for admin guidelines	
PrednISONE (PRED) **Patients ≥ 10 years ONLY**	PO (may be given IV)	30 mg/m²/dose BID	Days 1-28	Total daily dose: 60 mg/m²/day, divided BID See Section 4.2 for admin guidelines Note: IV methylprednisolone may be substituted for oral prednISONE at 80% of the oral dose	
DAUNOrubicin (DAUN)	IV push/infusion over 1-15 min	25 mg/m²/dose	Days 1, 8, 15 & 22	See Section 4.2 for admin guidelines	
Pegaspargase (PEG-ASP)	IV over 1-2 hours	2500 International Units/m²/dose	Day 4	**Note: pegaspargase must be administered on Day 4.** Administer through the tubing of a freely infusing solution of D_5W or 0.9% NaCl	
Intrathecal Methotrexate (IT MTX)	IT	Age (yrs) Dose 1-1.99 8 mg 2-2.99 10 mg 3-8.99 12 mg ≥ 9 15 mg	Days 8 & 29 CNS3 also on Days 15 & 22	See Section 4.2 for admin guidelines **Note age-based dosing** Note: All patients receive Day 8 and 29 IT MTX regardless of CSF evaluation.	

Ht_____cm Wt_____kg BSA_____m²

Date Due	Date Given	Day	IT ARAC ____mg	IT ARAC ____mg	VCR ____mg	DEX ____mg ____mg **Patients < 10 yrs ONLY**	PRED ____mg ____mg **Patients ≥ 10 yrs ONLY**	DAUN ____mg	PEG-ASP ____IU	IT MTX ____mg	Studies	Comments
			Enter calculated dose above and actual dose administered below									
		-2/-1/0/LP*	____mg								(a, b, c, e, f, g, i)[θ]	*Note any additional IT ARAC doses here.
		1			____mg	____mg ____mg	____mg ____mg	____mg				
		2										
		3										
		4♦		____mg♦					____IU		e♦	
		8			____mg			____mg		____mg	a%, b, e	
		9										
		10										
		11♦		____mg♦							e♦	
		12										
		13										
		14										
		15^♦		____mg♦	____mg			____mg		____mg^	a%, b, e^♦, h	
		22^			____mg			____mg		____mg^	a%, b, e^	
		28										
		29								____mg	a%, b, c**, d[θ], e, f	
		36	**VHR EOI MRD positive (excluding hypodiploid and induction failures), begin next course Consolidation (based upon Day 29 evaluation results for risk stratification and treatment randomization) on Day 36 or when blood count parameters are met (whichever occurs later). VHR EOI MRD negative patients go off-protocol therapy and proceed to receive standard of care therapy.**									

*On Day 1 **OR** at the time of diagnostic lumbar puncture (LP) if ≤ than 72 hours from the start of protocol therapy. ^ CNS3 patients only [θ] Baseline

% **Note:** Height (Ht) is only required at the beginning of this course. [ß] TPMT and NUDT15 genotype (TPMT highly recommended for all subjects; NUDT15 is highly recommended for subjects of Hispanic/Native American or East Asian ancestry, and optional for all other subjects (See Section 5.9)

♦**CNS2 patients only: administer IT therapy twice weekly until 3 consecutive CSF are clear of blasts. Day 8 & 29 IT therapy will remain IT MTX for all patients.**

Note: **CNS2 patients receive IT ARAC on Days 4, 5, or 6 and 11 or 12, etc., depending on treatment schedule. Log additional IT-ARAC doses in the comments section.**

****NOTE: IF THE DAY 29 BM MRD SAMPLE IS NOT OBTAINED AND SHIPPED TO A COG-APPROVED ALL FLOW CYTOMETRY LABORATORY, THEN THE PATIENT WILL NOT BE ELIGIBLE TO CONTINUE ON A COG ALL TRIAL FOLLOWING COMPLETION OF INDUCTION THERAPY. THESE SAMPLES ARE ABSOLUTELY ESSENTIAL.**

[θ]Day 29 PB specimen should be shipped to the COG ALL Molecular Reference Laboratory for all patients that consented to studies of genomic variation on AALL08B1 or APEC14B1 (*if available for ALL patients). This specimen is very important.*

SEE PROTOCOL SECTION 5.0 FOR DOSE MODIFICATIONS. SEE SECTION 8.0 FOR SUPPORTIVE CARE

Form C3: AALL1122 Induction Therapy Roadmap

AALL1122

Induction Therapy Phase IA (approx 29-33 days depending on institutional standard of care) Version 17-Apr-13				Patient's Name or Initials:		Patient's DOB:
Requirements for beginning Inductijon phase I:	All patients will receive the first induction according to the cooperative group protocol. See Appendix 11 for examples of induction phase IA regimens.					
Drug	Route	Dosage	Days	Important notes		observations
Dasatinib	po	60mg/m^2 once daily	daily	Dasatinib will be introduced on day 15 from the start of induction IA or no later than when the day 15 induction chemotherapy is administered to accommodate any delays for toxicity or scheduling/logistics. The dasatinib dose will be recalculated based on BSA every 12 weeks, or more often if necessary. Dose may be rounded up to the nearest 5 mg dose. Dasatinib should only be interrupted for toxicity.		
Therapy Delivery Map		Ht____—____cm		Wt_____ kg		BSA____m2

Due Date	Date Given	Week	Day	Dasatinib					
		Week 1	1	%					
			2	%					
			3	%					
			4	%					
			5	%					
			6	%					
			7	%					
		Week 2	8	%					
			9	%					
			10	%					
			11	%					
			12	%					
			13	%					
			14	%					
		Week 3	15	____mg					
			16	____mg					
			17	____mg					
			18	____mg					
			19	____mg					
			20	____mg					
			21	____mg					
		Week 4	22	____mg					
			23	____mg					
			24	____mg					
			25	____mg					
			26	____mg					
			27	____mg					
			28	____mg					
		week 5	29	____mg					
			30	____mg					
			31	____mg					
			32	____mg					
			33	____mg					

Form C3: AALL1122 Induction Therapy Roadmap, continued

AALL1122

Induction Therapy Phase IB (28 days, 4 weeks) Starts no sooner than Day 33 from start of Induction A Version 17-Apr-13				Patient's Name or Initials:	Patient's DOB:
Requirements for beginning of phase IB:	Pneumocystis (jirovecii) pneumonia (PCP) prophylaxis is recommended withtrimethoprim/sulfamethoxazole, cotrimoxazole or other appropriate agent against Pneumocystis jirovecii according to the institutional standard of care. Note that pentamidine use is prohibited in this trial due to potential interaction with dasatinib (see Section 3.4.11). **Induction IB therapy should begin no sooner than day 33 from the start of Induction 1A or when the following requirements are met: 1) Good general condition without serious infections; 2) Creatinine level within normal limits according to age; 3) ANC > 500/µl; platelets > 50,000/µl.**				
Drug	Route	Dosage	Days	Important notes	observations
Dasatinib	po	60mg/m^2 once daily	Daily	Dose may be rounded up to the nearest 5 mg dose	
Cyclophosphamide (CPM)	iv/(1hr)	1000mg/m^2	1 and 28	There are no blood count requirements for the initiation of day 28 cyclophosphamide. Please consider adequate anti-emetic supportive therapy. Optional hydration guidelines are in Appendix 12.	
Mercaptopurine (6-MP)	po	60 mg/m^2/d	1-28	To be taken in the evening on an empty stomach not together with milk. If the start of Ara-C is delayed or interrupted, 6-MP should be withheld until the start of Ara-C.	
Cytarbine (ARA-C)	iv or sc	75 mg/m^2/d	3-6, 10-13, 17-20, 24-27	The 4-day cycles that **begin on days 10, 17, and 24** should be started when WBC > 500/µl and platelets > 30,000/µl; each cycle when started should not be stopped unless for acute infection (please consider that fever might be also induced by the drug). **Note: For the cycle starting on day 3, the WBC and platelet counts do not need to be rechecked if adequate to begin this Induction 1B block.**	
Methotrexate (IT MTX)	it	Dose by Age (see Table 4.3.1.2)	3, 17	Start with the 4-day cycle of ARAC in cycles 1 and 3 Dose by Age (see Table 4.3.1.2) ≥1 yr < 2 yrs 8 mg ≥ 2 yrs < 3 yrs 10 mg ≥ 3 yrs 12mg	
See second page for Dosing Schedule					

Form C3: AALL1122 Induction Therapy Roadmap, continued

AALL1122

Therapy Delivery Map		Ht____ --- ____ cm		Wt_____ kg		BSA_____ m^2		
Due Date	Date Give	Week	Day	Dasatinib	CPM	6-MP	ARA-C	IT MTX
		Week 1	1	___mg	___mg	___mg	x	x
			2	___mg	x	___mg	x	x
			3	___mg	x	___mg	___mg	___mg
			4	___mg	x	___mg	___mg	x
			5	___mg	x	___mg	___mg	x
			6	___mg	x	___mg	___mg	x
			7	___mg	x	___mg	x	x
		Week 2	8	___mg	x	___mg	x	x
			9	___mg	x	___mg	x	x
			10	___mg	x	___mg	___mg	x
			11	___mg	x	___mg	___mg	x
			12	___mg	x	___mg	___mg	x
			13	___mg	x	___mg	___mg	x
			14	___mg	x	___mg	x	x
		Week 3	15	___mg	x	___mg	x	x
			16	___mg	x	___mg	x	x
			17	___mg	x	___mg	___mg	___mg
			18	___mg	x	___mg	___mg	x
			19	___mg	x	___mg	___mg	x
			20	___mg	x	___mg	___mg	x
			21	___mg	x	___mg	x	x
		Week 4	22	___mg	x	___mg	x	x
			23	___mg	x	___mg	x	x
			24	___mg	x	___mg	___mg	x
			25	___mg	x	___mg	___mg	x
			26	___mg	x	___mg	___mg	x
			27	___mg	x	___mg	___mg	x
			28	___mg	___mg	___mg	x	x

References

1. Siegel, R.L., K.D. Miller, and A. Jemal, *Cancer statistics, 2020.* CA: A Cancer Journal for Clinicians, 2020. **70**(1): p. 7-30.

2. Heron, M., *Deaths: Leading causes for 2017*, N.C.f.H. Statistics, Editor. 2019: Hyattsville, MD.

3. Hanahan, D. and R.A. Weinberg, *The hallmarks of cancer.* Cell, 2000. **100**(1): p. 57-70.

4. Hanahan, D. and R.A. Weinberg, *Hallmarks of Cancer: The Next Generation.* Cell, 2011. **144**(5): p. 646-674.

5. Campisi, J., *Aging, Cellular Senescence, and Cancer*, in *Annual Review of Physiology, Vol 75*, D. Julius, Editor. 2013. p. 685-705.

6. Hoeijmakers, J.H.J., *Molecular origins of cancer - DNA Damage, Aging, and Cancer.* New England Journal of Medicine, 2009. **361**(15): p. 1475-1485.

7. Armitage, P. and R. Doll, *The age distribution of cancer and a multi-stage theory of carcinogenesis.* British Journal of Cancer, 1954. **8**(1): p. 1-12.

8. Pitot, H.C., *The molecular biology of carcinogenesis.* Cancer, 1993. **72**(3): p. 962-970.

9. Vogelstein, B. and K.W. Kinzler, *The multistep nature of cancer.* Trends in Genetics, 1993. **9**(4): p. 138-141.

10. Collado, M., M.A. Blasco, and M. Serrano, *Cellular senescence in cancer and aging.* Cell, 2007. **130**(2): p. 223-233.

11. Finkel, T., M. Serrano, and M.A. Blasco, *The common biology of cancer and ageing.* Nature, 2007. **448**(7155): p. 767-774.

12. Rabbitts, T.H., *Chromosomal translocations in human cancer.* Nature, 1994. **372**(6502): p. 143-149.

13. Grobner, S.N., et al., *The landscape of genomic alterations across childhood cancers.* Nature, 2018. **555**(7696): p. 321-+.

14. Zhang, J.H., et al., *Germline Mutations in Predisposition Genes in Pediatric Cancer.* New England Journal of Medicine, 2015. **373**(24): p. 2336-2346.

15. Inaba, H., M. Greaves, and C.G. Mullighan, *Acute lymphoblastic leukaemia.* Lancet, 2013. **381**(9881): p. 1943-1955.

16. Winters, A.C. and K.M. Bernt, *MLL-Rearranged Leukemias-An Update on Science and Clinical Approaches.* Frontiers in Pediatrics, 2017. **5**.

17. Ma, X.T., et al., *Pan-cancer genome and transcriptome analyses of 1,699 paediatric leukaemias and solid tumours.* Nature, 2018. **555**(7696): p. 371-+.

18. Bleyer, A., et al., *The distinctive biology of cancer in adolescents and young adults.* Nature Reviews Cancer, 2008. **8**(4): p. 288-298.

19. Howlader N, N.A., Krapcho M, Miller D, Brest A, Yu M, Ruhl J, Tatalovich Z, Mariotto A, Lewis DR, Chen HS, Feuer EJ, Cronin KA (eds), *SEER Cancer Statistics Review, 1975-2016*. 2019, https://seer.cancer.gov/csr/1975_2016/ based on November 2018 SEER data submission, posted to the SEER web site, April 2019: National Cancer Institute. Bethesda, MD.

20. Ward, E., et al., *Childhood and adolescent cancer statistics, 2014.* Ca-a Cancer Journal for Clinicians, 2014. **64**(2): p. 83-103.

21. Hudson, M.M., et al., *Clinical Ascertainment of Health Outcomes Among Adults Treated for Childhood Cancer.* Jama-Journal of the American Medical Association, 2013. **309**(22): p. 2371-2381.

22. Cheung, Y.T., et al., *Chronic Health Conditions and Neurocognitive Function in Aging Survivors of Childhood Cancer: A Report from the Childhood Cancer Survivor Study.* Jnci-Journal of the National Cancer Institute, 2018. **110**(4): p. 411-419.

23. Hutchinson, A.D., S.M. Pfeiffer, and C. Wilson, *Cancer-related cognitive impairment in children.* Current Opinion in Supportive and Palliative Care, 2017. **11**(1): p. 70-75.

24. Chow, E.J., et al., *New Agents, Emerging Late Effects, and the Development of Precision Survivorship.* Journal of Clinical Oncology, 2018. **36**(21).

25. Nathan, P.C., et al., *Adverse Mental Health Outcomes in a Population-Based Cohort of Survivors of Childhood Cancer.* Cancer, 2018. **124**(9): p. 2045-2057.

26. Smith, M.A., et al., *Outcomes for Children and Adolescents With Cancer: Challenges for the Twenty-First Century.* Journal of Clinical Oncology, 2010. **28**(15): p. 2625-2634.

27. Hunger, S.P. and C.G. Mullighan, *Acute Lymphoblastic Leukemia in Children.* New England Journal of Medicine, 2015. **373**(16): p. 1541-1552.

28. Al-Tubaikh, J., *Leukemia*, in *Internal Medicine*, J. Al-Tubaikh, Editor. 2010, Springer Berlin Heidelberg. p. 313-318.

29. Bozzone, D.M., *Leukemia*. The Biology of Cancer. 2009, New York, NY: Chelsea House.

30. Mejía-Aranguré, J.M., ed. *Etiology of Acute Leukemias in Children*. 1 ed. 2016, Springer International Publishing. XIII, 320.

31. Siegel, R.L., K.D. Miller, and A. Jemal, *Cancer Statistics, 2018.* Ca-a Cancer Journal for Clinicians, 2018. **68**(1): p. 7-30.

32. Ries, L., et al., *Cancer Incidence and Survival among Children and Adolescents: United States SEER Program 1975-1995*, S.P. National Cancer Institute, Editor. 1999, NIH Pub: Bethesda, MD.

33. Pui, C.H., et al., *Challenging issues in pediatric oncology.* Nature Reviews Clinical Oncology, 2011. **8**(9): p. 540-549.

34. Mody, R., et al., *Twenty-five-year follow-up among survivors of childhood acute lymphoblastic leukemia: a report from the Childhood Cancer Survivor Study.* Blood, 2008. **111**(12): p. 5515-5523.

35. Getz, K.D., et al., *Occurrence of Treatment-Related Cardiotoxicity and Its Impact on Outcomes Among Children Treated in the AAML0531 Clinical Trial: A Report From the Children's Oncology Group.* Journal of Clinical Oncology, 2019. **37**(1): p. 12-+.

36. Taylor, O.A., et al., *Disparities in Neurotoxicity Risk and Outcomes among Pediatric Acute Lymphoblastic Leukemia Patients.* Clinical Cancer Research, 2018. **24**(20): p. 5012-5017.

37. Anestin, A.S., et al., *Psychological risk in long-term survivors of childhood acute lymphoblastic leukemia and its association with functional health status: A PETALE cohort study.* Pediatric Blood & Cancer, 2018. **65**(11).

38. Huang, I.C., et al., *Child symptoms, parent behaviors, and family strain in long-term survivors of childhood acute lymphoblastic leukemia.* Psycho-Oncology, 2018. **27**(8): p. 2031-2038.

39. Jacola, L.M., et al., *Cognitive, behaviour, and academic functioning in adolescent and young adult survivors of childhood acute lymphoblastic leukaemia: a report from the Childhood Cancer Survivor Study.* Lancet Psychiatry, 2016. **3**(10): p. 965-972.

40. Pui, C.H., et al., *Biology, Risk Stratification, and Therapy of Pediatric Acute Leukemias: An Update.* Journal of Clinical Oncology, 2011. **29**(5): p. 551-565.

41. Schultz, K.R., et al., *Risk- and response-based classification of childhood B-precursor acute lymphoblastic leukemia: a combined analysis of prognostic markers from the Pediatric Oncology Group (POG) and Children's Cancer Group (CCG).* Blood, 2007. **109**(3): p. 926-935.

42. Moorman, A.V., *New and emerging prognostic and predictive genetic biomarkers in B-cell precursor acute lymphoblastic leukemia.* Haematologica, 2016. **101**(4): p. 407-416.

43. van Dongen, J.J.M., et al., *Minimal residual disease diagnostics in acute lymphoblastic leukemia: need for sensitive, fast, and standardized technologies.* Blood, 2015. **125**(26): p. 3996-4009.

44. Chapiro, E., et al., *Chromosomal translocations involving the IGH@ locus in B-cell precursor acute lymphoblastic leukemia: 29 new cases and a review of the literature.* Cancer Genetics, 2013. **206**(5): p. 162-173.

45. Kiossoglou, K.A., W.J. Mitus, and W. Dameshek, *Chromosomal aberrations in acute leukemia.* Blood-the Journal of Hematology, 1965. **26**(5): p. 610-+.

46. Greaves, M.F. and J. Wiemels, *Origins of chromosome translocations in childhood leukaemia.* Nature Reviews Cancer, 2003. **3**(9): p. 639-649.

47. Moorman, A.V., *The clinical relevance of chromosomal and genomic abnormalities in B-cell precursor acute lymphoblastic leukaemia.* Blood Reviews, 2012. **26**(3): p. 123-135.

48. Harrison, C.J., *Cytogenetics of paediatric and adolescent acute lymphoblastic leukaemia.* British Journal of Haematology, 2009. **144**(2): p. 147-156.

49. Pui, C.H., L.L. Robison, and A.T. Look, *Acute lymphoblastic leukaemia.* Lancet, 2008. **371**(9617): p. 1030-1043.

50. Speicher, M.R. and N.P. Carter, *The new cytogenetics: Blurring the boundaries with molecular biology.* Nature Reviews Genetics, 2005. **6**(10): p. 782-792.

51. Kallioniemi, A., et al., *Comparative genomic hybridization for molecular cytogenetic analysis of solid tumors.* Science, 1992. **258**(5083): p. 818-821.

52. Wu, C. and W. Li, *Genomics and pharmacogenomics of pediatric acute lymphoblastic leukemia.* Critical Reviews in Oncology Hematology, 2018. **126**: p. 100-111.

53. Hogan, L.E., et al., *Integrated genomic analysis of relapsed childhood acute lymphoblastic leukemia reveals therapeutic strategies.* Blood, 2011. **118**(19): p. 5218-5226.

54. Warburg, O., *On Respiratory Impairment in Cancer Cells.* Science, 1956. **124**(3215): p. 269-270.

55. Warburg, O., *On the Origins of Cancer Cells.* Science, 1956. **123**(3191): p. 309-314.

56. Samudio, I., et al., *The Warburg effect in leukemia-stroma cocultures is mediated by mitochondrial uncoupling associated with uncoupling protein 2 activation.* Cancer Research, 2008. **68**(13): p. 5198-5205.

57. Samudio, I., M. Fiegl, and M. Andreeff, *Mitochondrial Uncoupling and the Warburg Effect: Molecular Basis for the Reprogramming of Cancer Cell Metabolism.* Cancer Research, 2009. **69**(6): p. 2163-2166.

58. Hsu, P.P. and D.M. Sabatini, *Cancer cell metabolism: Warburg and beyond.* Cell, 2008. **134**(5): p. 703-707.

59. Vander Heiden, M.G., L.C. Cantley, and C.B. Thompson, *Understanding the Warburg Effect: The Metabolic Requirements of Cell Proliferation.* Science, 2009. **324**(5930): p. 1029-1033.

60. DeBerardinis, R.J., et al., *The biology of cancer: Metabolic reprogramming fuels cell growth and proliferation.* Cell Metabolism, 2008. **7**(1): p. 11-20.

61. Wise, D.R. and C.B. Thompson, *Glutamine addiction: a new therapeutic target in cancer.* Trends in Biochemical Sciences, 2010. **35**(8): p. 427-433.

62. Samudio, I. and M. Konopleva, *Asparaginase unveils glutamine-addicted AML.* Blood, 2013. **122**(20): p. 3398-3400.

63. Iwamoto, S., et al., *Mesenchymal cells regulate the response of acute lymphoblastic leukemia cells to asparaginase.* J Clin Invest, 2007. **117**(4): p. 1049-57.

64. Ehsanipour, E.A., et al., *Adipocytes cause leukemia cell resistance to L-asparaginase via release of glutamine.* Cancer Res, 2013. **73**(10): p. 2998-3006.

65. Zhang, W., et al., *Stromal control of cystine metabolism promotes cancer cell survival in chronic lymphocytic leukaemia.* Nat Cell Biol, 2012. **14**(3): p. 276-86.

66. Fiehn, O., *Metabolomics - the link between genotypes and phenotypes.* Plant Molecular Biology, 2002. **48**(1-2): p. 155-171.

67. Fernie, A.R., et al., *Innovation - Metabolite profiling: from diagnostics to systems biology.* Nature Reviews Molecular Cell Biology, 2004. **5**(9): p. 763-769.

68. Tiziani, S., et al., *Optimized metabolite extraction from blood serum for H-1 nuclear magnetic resonance spectroscopy.* Analytical Biochemistry, 2008. **377**(1): p. 16-23.

69. Forcisi, S., et al., *Liquid chromatography–mass spectrometry in metabolomics research: Mass analyzers in ultra high pressure liquid chromatography coupling.* Journal of Chromatography A, 2013. **1292**(0): p. 51-65.

70. Gibney, M.J., et al., *Metabolomics in human nutrition: opportunities and challenges.* American Journal of Clinical Nutrition, 2005. **82**(3): p. 497-503.

71. Kell, D.B., *Metabolomics and systems biology: making sense of the soup.* Current Opinion in Microbiology, 2004. **7**(3): p. 296-307.

72. Joyce, A.R. and B.O. Palsson, *The model organism as a system: integrating 'omics' data sets.* Nature Reviews Molecular Cell Biology, 2006. **7**(3): p. 198-210.

73. Beger, R.D., *A review of applications of metabolomics in cancer.* Metabolites, 2013. **3**(3): p. 552-574.

74. Schuhmacher, R., et al., *Metabolomics and metabolite profiling.* Analytical and Bioanalytical Chemistry, 2013. **405**(15): p. 5003-5004.

75. Nicholson, J.K., J.C. Lindon, and E. Holmes, *'Metabonomics': understanding the metabolic responses of living systems to pathophysiological stimuli via multivariate statistical analysis of biological NMR spectroscopic data.* Xenobiotica, 1999. **29**(11): p. 1181-1189.

76. Ludwig, C., et al., *Birmingham Metabolite Library: a publicly accessible database of 1-D H-1 and 2-D H-1 J-resolved NMR spectra of authentic metabolite standards (BML-NMR).* Metabolomics, 2012. **8**(1): p. 8-18.

77. Madhavan, S., et al., *Integrative Analysis Workflow for Untargeted Metabolomics in Translational Research.* Metabolomics, 2014. **4**(130): p. 2153-0769.1000130.

78. Jones, D.P., Y. Park, and T.R. Ziegler, *Nutritional Metabolomics: Progress in Addressing Complexity in Diet and Health.* Annual Review of Nutrition, Vol 32, 2012. **32**: p. 183-+.

79. Bino, R.J., et al., *Potential of metabolomics as a functional genomics tool.* Trends in Plant Science, 2004. **9**(9): p. 418-425.

80. Kind, T. and O. Fiehn, *Metabolomic database annotations via query of elemental compositions: Mass accuracy is insufficient even at less than 1 ppm.* Bmc Bioinformatics, 2006. **7**.

81. Patti, G.J., O. Yanes, and G. Siuzdak, *Metabolomics: the apogee of the omics trilogy.* Nature Reviews Molecular Cell Biology, 2012. **13**(4): p. 263-269.

82. Bouatra, S., et al., *The Human Urine Metabolome.* Plos One, 2013. **8**(9).

83. Psychogios, N., et al., *The Human Serum Metabolome.* Plos One, 2011. **6**(2).

84. Saito, K. and F. Matsuda, *Metabolomics for Functional Genomics, Systems Biology, and Biotechnology.* Annual Review of Plant Biology, Vol 61, 2010. **61**: p. 463-489.

85. Brennan, L., *Metabolomics in nutrition research: current status and perspectives.* Biochemical Society Transactions, 2013. **41**: p. 670-673.

86. Beckonert, O., et al., *Metabolic profiling, metabolomic and metabonomic procedures for NMR spectroscopy of urine, plasma, serum and tissue extracts.* Nature Protocols, 2007. **2**(11): p. 2692-2703.

87. McNiven, E.M.S., J.B. German, and C.M. Slupsky, *Analytical metabolomics: nutritional opportunities for personalized health.* Journal of Nutritional Biochemistry, 2011. **22**(11): p. 995-1002.

88. Saccenti, E., et al., *Reflections on univariate and multivariate analysis of metabolomics data.* Metabolomics, 2014. **10**(3): p. 361-374.

89. Zhang, S., et al., *Advances in NMR-based biofluid analysis and metabolite profiling.* Analyst, 2010. **135**(7): p. 1490-8.

90. Whitfield, P.D., A.J. German, and P.J.M. Noble, *Metabolomics: an emerging post-genomic tool for nutrition.* British Journal of Nutrition, 2004. **92**(4): p. 549-555.

91. Wishart, D.S., *Quantitative metabolomics using NMR.* Trac-Trends in Analytical Chemistry, 2008. **27**(3): p. 228-237.

92. Tiziani, S., et al., *Metabolomic high-content nuclear magnetic resonance-based drug screening of a kinase inhibitor library.* Nature Communications, 2011. **2**.

93. Tiziani, S., et al., *Metabolomics of the Tumor Microenvironment in Pediatric Acute Lymphoblastic Leukemia.* Plos One, 2013. **8**(12).

94. Emsley, J.W. and J. Feeney, *Milestones in the first fifty years of NMR.* Progress in Nuclear Magnetic Resonance Spectroscopy, 1995. **28**: p. 1-9.

95. Levitt, M.H., *The signs of frequencies and phases in NMR.* Journal of Magnetic Resonance, 1997. **126**(2): p. 164-182.

96. Kovacs, H., D. Moskau, and M. Spraul, *Cryogenically cooled probes - a leap in NMR technology.* Progress in Nuclear Magnetic Resonance Spectroscopy, 2005. **46**(2-3): p. 131-155.

97. Fullerton, G.D., J.L. Potter, and N.C. Dornbluth, *NMR relaxation of protons in tissues and other macromolecular water solutions.* Magnetic resonance imaging, 1982. **1**(4): p. 209-26.

98. Arnold, J.T., S.S. Dharmatti, and M.E. Packard, *Chemical effects on nuclear induction signals from organic compounds.* Journal of Chemical Physics, 1951. **19**(4): p. 507-507.

99. Wilkens, S.J., et al., *Natural J-coupling analysis: Interpretation of scalar J-couplings in terms of natural bond orbitals.* Journal of the American Chemical Society, 2001. **123**(48): p. 12026-12036.

100. Sattler, M., J. Schleucher, and C. Griesinger, *Heteronuclear multidimensional NMR experiments for the structure determination of proteins in solution employing pulsed field gradients.* Progress in Nuclear Magnetic Resonance Spectroscopy, 1999. **34**(2): p. 93-158.

101. Emsley, J.W. and J. Feeney, *Forty years of Progress in Nuclear Magnetic Resonance Spectroscopy.* Progress in Nuclear Magnetic Resonance Spectroscopy, 2007. **50**(4): p. 179-198.

102. Grzesiek, S., et al., *Multiple-quantum line narrowing for measurement of H-alpha-H-beta J-coupling in isotopically enriched proteins.* Journal of the American Chemical Society, 1995. **117**(19): p. 5312-5315.

103. Lindon, J.C., J.K. Nicholson, and J.R. Everett, *NMR spectroscopy of biofluids.* Annual Reports on Nmr Spectroscopy, Vol 38, 1999. **38**: p. 1-88.

104. Hurd, R.E., *Gradient-enhanced spectroscopy.* Journal of Magnetic Resonance, 1990. **87**(2): p. 422-428.

105. Price, W.S., *Pulsed-field gradient nuclear magnetic resonance as a tool for studying translational diffusion .1. Basic theory.* Concepts in Magnetic Resonance, 1997. **9**(5): p. 299-336.

106. Hwang, T.L. and A.J. Shaka, *Water suppression that works - Excitation sculpting using arbitrary wave-forms and pulsed-field gradients* Journal of Magnetic Resonance Series A, 1995. **112**(2): p. 275-279.

107. Molinski, T.F., *NMR of natural products at the 'nanomole-scale'.* Natural Product Reports, 2010. **27**(3): p. 321-329.

108. Oresic, M., *Metabolomics, a novel tool for studies of nutrition, metabolism and lipid dysfunction.* Nutrition Metabolism and Cardiovascular Diseases, 2009. **19**(11): p. 816-824.

109. Bird, S.S., et al., *Qualitative characterization of the rat liver mitochondrial lipidome using LC-MS profiling and high energy collisional dissociation (HCD) all ion fragmentation.* Metabolomics, 2013. **9**(1): p. S67-S83.

110. Gallart-Ayala, H., et al., *Versatile lipid profiling by liquid chromatography-high resolution mass spectrometry using all ion fragmentation and polarity switching. Preliminary application for serum samples phenotyping related to canine mammary cancer.* Analytica Chimica Acta, 2013. **796**: p. 75-83.

111. Schuhmann, K., et al., *Shotgun lipidomics on a LTQ Orbitrap mass spectrometer by successive switching between acquisition polarity modes.* Journal of Mass Spectrometry, 2012. **47**(1): p. 96-104.

112. Yamada, T., et al., *Development of a lipid profiling system using reverse-phase liquid chromatography coupled to high-resolution mass spectrometry with rapid polarity switching and an automated lipid identification software.* Journal of Chromatography A, 2013. **1292**: p. 211-218.

113. Tiziani, S., S.J. Schwartz, and Y. Vodovotz, *Profiling of carotenoids in tomato juice by one- and two-dimensional NMR.* Journal of Agricultural and Food Chemistry, 2006. **54**(16): p. 6094-6100.

114. Zeisel, S.H., *Nutrigenomics and metabolomics will change clinical nutrition and public health practice: insights from studies on dietary requirements for choline.* American Journal of Clinical Nutrition, 2007. **86**(3): p. 542-548.

115. Bylesjo, M., et al., *OPLS discriminant analysis: combining the strengths of PLS-DA and SIMCA classification.* Journal of Chemometrics, 2006. **20**(8-10): p. 341-351.

116. Mahadevan, S., et al., *Analysis of metabolomic data using support vector machines.* Analytical Chemistry, 2008. **80**(19): p. 7562-7570.

117. Westerhuis, J.A., et al., *Multivariate paired data analysis: multilevel PLSDA versus OPLSDA.* Metabolomics, 2010. **6**(1): p. 119-128.

118. Manach, C., et al., *The complex links between dietary phytochemicals and human health deciphered by metabolomics.* Molecular Nutrition & Food Research, 2009. **53**(10): p. 1303-1315.

119. Wishart, D.S., et al., *HMDB 4.0: the human metabolome database for 2018.* Nucleic Acids Research, 2018. **46**(D1): p. D608-D617.

120. Wishart, D.S., et al., *HMDB 3.0-The Human Metabolome Database in 2013.* Nucleic Acids Research, 2013. **41**(D1): p. D801-D807.

121. Wishart, D.S., et al., *HMDB: a knowledgebase for the human metabolome.* Nucleic Acids Research, 2009. **37**: p. D603-D610.

122. Wishart, D.S., et al., *HMDB: the human metabolome database.* Nucleic Acids Research, 2007. **35**: p. D521-D526.

123. Kanehisa, M., *Toward understanding the origin and evolution of cellular organisms.* Protein Science, 2019. **28**(11): p. 1947-1951.

124. Kanehisa, M., et al., *New approach for understanding genome variations in KEGG.* Nucleic Acids Research, 2019. **47**(D1): p. D590-D595.

125. Kanehisa, M. and S. Goto, *KEGG: Kyoto Encyclopedia of Genes and Genomes.* Nucleic Acids Research, 2000. **28**(1): p. 27-30.

126. Romero, P., et al., *Computational prediction of human metabolic pathways from the complete human genome.* Genome Biology, 2004. **6**(1): p. R2.

127. Smith, C.A., et al., *METLIN: a metabolite mass spectral database.* Therapeutic drug monitoring, 2005. **27**(6): p. 747-751.

128. Sentandreu, E., et al., *A Survey of Orbitrap All Ion Fragmentation Analysis Assessed by an R MetaboList Package to Study Small-Molecule Metabolites.* Chromatographia, 2018. **81**(7): p. 981-994.

129. Peris-Diaz, M.D., et al., *R-MetaboList 2: A Flexible Tool for Metabolite Annotation from High-Resolution Data-Independent Acquisition Mass Spectrometry Analysis.* Metabolites, 2019. **9**(9).

130. Sumner, L.W., et al., *Proposed minimum reporting standards for chemical analysis.* Metabolomics, 2007. **3**(3): p. 211-221.

131. Fiehn, O., et al., *The metabolomics standards initiative (MSI).* Metabolomics, 2007. **3**(3): p. 175-178.

132. Clayton, T.A., et al., *Pharmaco-metabonomic phenotyping and personalized drug treatment.* Nature, 2006. **440**(7087): p. 1073-1077.

133. Sugimoto, M., et al., *Bioinformatics Tools for Mass Spectroscopy-Based Metabolomic Data Processing and Analysis.* Current Bioinformatics, 2012. **7**(1): p. 96-108.

134. Serkova, N.J., T.J. Standiford, and K.A. Stringer, *The Emerging Field of Quantitative Blood Metabolomics for Biomarker Discovery in Critical Illnesses.* American Journal of Respiratory and Critical Care Medicine, 2011. **184**(6): p. 647-655.

135. Dunn, W.B. and D.I. Ellis, *Metabolomics: Current analytical platforms and methodologies.* Trac-Trends in Analytical Chemistry, 2005. **24**(4): p. 285-294.

136. Lenz, E.M. and I.D. Wilson, *Analytical strategies in metabonomics.* Journal of Proteome Research, 2007. **6**(2): p. 443-458.

137. Ewald, J.C., S. Heux, and N. Zamboni, *High-Throughput Quantitative Metabolomics: Workflow for Cultivation, Quenching, and Analysis of Yeast in a Multiwell Format.* Analytical Chemistry, 2009. **81**(9): p. 3623-3629.

138. Wu, H.F., et al., *High-throughput tissue extraction protocol for NMR- and MS-based metabolomics.* Analytical Biochemistry, 2008. **372**(2): p. 204-212.

139. Janzen, L.A., *Long-term neurocognitive and functional effects of treatment for childhood acute lymphoblastic leukaemia.* Lancet Psychiatry, 2016.

140. Pui, C.H., et al., *Extended follow-up of long-term survivors of childhood acute lymphoblastic leukemia.* New England Journal of Medicine, 2003. **349**(7): p. 640-649.

141. Phillips, S.M., et al., *Survivors of childhood cancer in the United States: prevalence and burden of morbidity.* Cancer Epidemiol Biomarkers Prev, 2015. **24**(4): p. 653-63.

142. Surh, Y.J., *Cancer chemoprevention with dietary phytochemicals.* Nature Reviews Cancer, 2003. **3**(10): p. 768-780.

143. Yang, K.C., et al., *Apple Polyphenol Phloretin Potentiates the Anticancer Actions of Paclitaxel Through Induction of Apoptosis in Human Hep G2 Cells.* Molecular Carcinogenesis, 2009. **48**(5): p. 420-431.

144. Sweeney, S.R., J. Digiovanni, and S. Tiziani, *Metabolomics, Bioactives, and Cancer*, in *Genomics, Proteomics and Metabolomics in Nutraceuticals and Functional Foods*. 2015. p. 365-378.

145. Bishayee, A. and G. Sethi, *Bioactive natural products in cancer prevention and therapy: Progress and promise.* Semin Cancer Biol, 2016.

146. Collins, A.R., *Antioxidant intervention as a route to cancer prevention.* European Journal of Cancer, 2005. **41**(13): p. 1923-1930.

147. D'Incalci, M., W.P. Steward, and A.J. Gescher, *Use of cancer chemopreventive phytochemicals as antineoplastic agents.* Lancet Oncology, 2005. **6**(11): p. 899-904.

148. Elamin, M.H., et al., *Curcumin Inhibits the Sonic Hedgehog Signaling Pathway and Triggers Apoptosis in Medulloblastoma Cells.* Molecular Carcinogenesis, 2010. **49**(3): p. 302-314.

149. Kim, S.H., M. Danilenko, and T.S. Kim, *Differential enhancement of leukaemia cell differentiation without elevation of intracellular calcium by plant-derived sesquiterpene lactone compounds.* British Journal of Pharmacology, 2008. **155**(6): p. 814-825.

150. Lodi, A., et al., *Combinatorial treatment with natural compounds in prostate cancer inhibits prostate tumor growth and leads to key modulations of cancer cell metabolism.* Npj Precision Oncology, 2017. **1**.

151. Agarwal, C., Y. Sharma, and R. Agarwal, *Anticarcinogenic effect of a polyphenolic fraction isolated from grape seeds in human prostate carcinoma DU145 cells: Modulation of mitogenic signaling and cell-cycle regulators and induction of G1 arrest and apoptosis.* Molecular Carcinogenesis, 2000. **28**(3): p. 129-138.

152. Spagnuolo, C., et al., *Dietary polyphenols in cancer prevention: the example of the flavonoid quercetin in leukemia*, in *Environmental Stressors in Biology and Medicine*, G. Valacchi, Editor. 2012. p. 95-103.

153. Li, J.W.H. and J.C. Vederas, *Drug Discovery and Natural Products: End of an Era or an Endless Frontier?* Science, 2009. **325**(5937): p. 161-165.

154. Spratlin, J.L., N.J. Serkova, and S.G. Eckhardt, *Clinical Applications of Metabolomics in Oncology: A Review.* Clinical Cancer Research, 2009. **15**(2): p. 431-440.

155. Macarron, R., et al., *Impact of high-throughput screening in biomedical research.* Nature Reviews Drug Discovery, 2011. **10**(3): p. 188-195.

156. Dean, R.B. and W.J. Dixon, *Simplified statistics for small numbers of obervations.* Analytical Chemistry, 1951. **23**(4): p. 636-638.

157. Zhao, W., et al., *A New Bliss Independence Model to Analyze Drug Combination Data.* Journal of Biomolecular Screening, 2014. **19**(5): p. 817-821.

158. Chou, T.C. and P. Talalay, *Analysis of combined drug effects - A new look at a very old problem.* Trends in Pharmacological Sciences, 1983. **4**(11): p. 450-454.

159. Team, R.C., *R: A Language and Environment for Statistical Computing*. 2018, R Foundation for Statistical Computing.

160. Zhang, N., J.N. Fu, and T.C. Chou, *Synergistic combination of microtubule targeting anticancer fludelone with cytoprotective panaxytriol derived from panax ginseng against MX-1 cells in vitro: experimental design and data analysis using the combination index method.* American Journal of Cancer Research, 2016. **6**(1): p. 97-104.

161. Pandey, R., et al., *Highly sensitive and selective determination of redox states of coenzymes Q(9) and Q(10) in mice tissues: Application of orbitrap mass spectrometry.* Analytica Chimica Acta, 2018. **1011**: p. 68-76.

162. Di Guida, R., et al., *Non-targeted UHPLC-MS metabolomic data processing methods: a comparative investigation of normalisation, missing value imputation, transformation and scaling.* Metabolomics, 2016. **12**(5).

163. Chong, J., et al., *MetaboAnalyst 4.0: towards more transparent and integrative metabolomics analysis.* Nucleic Acids Research, 2018. **46**(W1): p. W486-W494.

164. Lu, X.Y., et al., *Three-Dimensional Leukemia Co-Culture System for In Vitro High-Content Metabolomics Screening.* Slas Discovery, 2019. **24**(8): p. 817-828.

165. Guzman, M.L., et al., *An orally bioavailable parthenolide analog selectively eradicates acute myelogenous leukemia stem and progenitor cells.* Blood, 2007. **110**(13): p. 4427-4435.

166. Neelakantan, S., et al., *Aminoparthenolides as novel anti-leukemic agents: Discovery of the NF-kappa B inhibitor, DMAPT (LC-1).* Bioorganic & Medicinal Chemistry Letters, 2009. **19**(15): p. 4346-4349.

167. Dang, L., et al., *Cancer-associated IDH1 mutations produce 2-hydroxyglutarate.* Nature, 2009. **462**(7274): p. 739-U52.

168. Lu, X.H., et al., *Cellular ATP depletion by LY309887 as a predictor of growth inhibition in human tumor cell lines.* Clinical Cancer Research, 2000. **6**(1): p. 271-277.

169. Liu, B., et al., *Shikonin exerts antitumor activity by causing mitochondrial dysfunction in hepatocellular carcinoma through PKM2-AMPK-PGC1 alpha signaling pathway.* Biochemistry and Cell Biology, 2019. **97**(4): p. 397-405.

170. Zhao, X.Y., et al., *Shikonin Inhibits Tumor Growth in Mice by Suppressing Pyruvate Kinase M2-mediated Aerobic Glycolysis.* Scientific Reports, 2018. **8**.

171. Guzman, M.L., et al., *The sesquiterpene lactone parthenolide induces apoptosis of human acute myelogenous leukemia stem and progenitor cells.* Blood, 2005. **105**(11): p. 4163-4169.

172. Zunino, S.J., J.M. Ducore, and D.H. Storms, *Parthenolide induces significant apoptosis and production of reactive oxygen species in high-risk pre-B leukemia cells.* Cancer Letters, 2007. **254**(1): p. 119-127.

173. Fukuda, S., et al., *Pyruvate Kinase M2 Modulates Esophageal Squamous Cell Carcinoma Chemotherapy Response by Regulating the Pentose Phosphate Pathway.* Annals of Surgical Oncology, 2015. **22**: p. S1461-S1468.

174. Iqbal, M.A. and R.N.K. Bamezai, *Resveratrol Inhibits Cancer Cell Metabolism by Down Regulating Pyruvate Kinase M2 via Inhibition of Mammalian Target of Rapamycin.* Plos One, 2012. **7**(5).

175. Merfort, I., *Perspectives on Sesquiterpene Lactones in Inflammation and Cancer.* Current Drug Targets, 2011. **12**(11): p. 1560-1573.

176. Ren, Y.H., et al., *Parthenolide regulates oxidative stress-induced mitophagy and suppresses apoptosis through p53 signaling pathway in C2C12 myoblasts.* Journal of Cellular Biochemistry, 2019. **120**(9): p. 15695-15708.

177. Zhang, S.Y., et al., *Suppressed NF-kappa B and sustained JNK activation contribute to the sensitization effect of parthenolide to TNF-alpha-induced apoptosis in human cancer cells.* Carcinogenesis, 2004. **25**(11): p. 2191-2199.

178. Takahashi, H., et al., *Autophagy is required for cell survival under L-asparaginase-induced metabolic stress in acute lymphoblastic leukemia cells.* Oncogene, 2017. **36**(30): p. 4267-4276.

179. Valvezan, A.J., et al., *mTORC1 Couples Nucleotide Synthesis to Nucleotide Demand Resulting in a Targetable Metabolic Vulnerability.* Cancer Cell, 2017. **32**(5): p. 624-+.

180. Sen, S., et al., *Novel mTOR inhibitory activity of ciclopirox enhances parthenolide antileukemia activity.* Experimental Hematology, 2013. **41**(9): p. 799-807.

181. Hassane, D.C., et al., *Chemical genomic screening reveals synergism between parthenolide and inhibitors of the PI-3 kinase and mTOR pathways.* Blood, 2010. **116**(26): p. 5983-5990.

182. Arber, D.A., et al., *The 2016 revision to the World Health Organization classification of myeloid neoplasms and acute leukemia.* Blood, 2016. **127**(20): p. 2391-2405.

183. Moorman, A.V., H.M. Ensor, and S.M. Richards, *Prognostic effect of chromosomal abnormalities in childhood B-cell precursor acute lymphoblastic leukaemia: results from the UK Medical Research Council ALL97/99 randomised trial. (vol 11, pg 429, 2010).* Lancet Oncology, 2010. **11**(6): p. 516-516.

184. Russell, L.J., et al., *IGH@ Translocations Are Prevalent in Teenagers and Young Adults With Acute Lymphoblastic Leukemia and Are Associated With a Poor Outcome.* Journal of Clinical Oncology, 2014. **32**(14): p. 1453-+.

185. Harvey, R.C., et al., *Rearrangement of CRLF2 is associated with mutation of JAK kinases, alteration of IKZF1, Hispanic/Latino ethnicity, and a poor outcome in pediatric B-progenitor acute lymphoblastic leukemia.* Blood, 2010. **115**(26): p. 5312-5321.

186. Mrozek, K., N.A. Heerema, and C.D. Bloomfield, *Cytogenetics in acute leukemia.* Blood Reviews, 2004. **18**(2): p. 115-136.

187. Kuiper, R.P., et al., *High-resolution genomic profiling of childhood ALL reveals novel recurrent genetic lesions affecting pathways involved in lymphocyte differentiation and cell cycle progression.* Leukemia, 2007. **21**(6): p. 1258-1266.

188. Schwab, C.J., et al., *Genes commonly deleted in childhood B-cell precursor acute lymphoblastic leukemia: association with cytogenetics and clinical features.* Haematologica, 2013. **98**(7): p. 1081-1088.

189. Sindelarova, L., et al., *Incidence of chromosomal anomalies detected with FISH and their clinical correlations in B-chronic lymphocytic leukemia.* Cancer Genetics and Cytogenetics, 2005. **160**(1): p. 27-34.

190. Seckerwalker, L.M., S.D. Lawler, and R.M. Hardisty, *Prognostic implications of chromosomal findings in acute lymphoblastic leukemia at diagnosis.* British Medical Journal, 1978. **2**(6151): p. 1529-1530.

191. Arico, M., et al., *Outcome of treatment in children with philadelphia chromosome-positive acute lymphoblastic leukemia.* New England Journal of Medicine, 2000. **342**(14): p. 998-1006.

192. Druker, B.J., et al., *Activity of a specific inhibitor of the BCR-ABL tyrosine kinase in the blast crisis of chronic myeloid leukemia and acute lymphoblastic leukemia with the philadelphia chromosome.* New England Journal of Medicine, 2001. **344**(14): p. 1038-1042.

193. Jain, P., et al., *Clinical implications of cytogenetic heterogeneity in Philadelphia chromosome positive (Ph plus) adult B cell acute lymphoblastic leukemia following tyrosine kinase inhibitors and chemotherapy regimens.* Leukemia Research, 2019. **84**.

194. Gu, Z.H., et al., *PAX5-driven subtypes of B-progenitor acute lymphoblastic leukemia.* Nature Genetics, 2019. **51**(2): p. 296-+.

195. Othman, M.A.K., et al., *A novel IGH@ gene rearrangement associated with CDKN2A/B deletion in young adult B-cell acute lymphoblastic leukemia.* Oncology Letters, 2016. **11**(3): p. 2117-2122.

196. Huh, J., et al., *Submicroscopic Deletions of Immunoglobulin Heavy Chain Gene (IGH) in Precursor B Lymphoblastic Leukemia with IGH Rearrangements.* Annals of Laboratory Medicine, 2015. **35**(1): p. 128-131.

197. Jeffries, S.J., et al., *IGH@ translocations co-exist with other primary rearrangements in B-cell precursor acute lymphoblastic leukemia.* Haematologica, 2014. **99**(8): p. 1334-1342.

198. Akasaka, T., et al., *Five members of the CEBP transcription factor family are targeted by recurrent IGH translocations in B-cell precursor acute lymphoblastic leukemia (BCP-ALL).* Blood, 2007. **109**(8): p. 3451-3461.

199. Russell, L.J., et al., *Characterisation of the genomic landscape of CRLF2-rearranged acute lymphoblastic leukemia.* Genes Chromosomes & Cancer, 2017. **56**(5): p. 363-372.

200. Maifrede, S., et al., *IGH/MYC Translocation Associates with BRCA2 Deficiency and Synthetic Lethality to PARP1 Inhibitors.* Molecular Cancer Research, 2017. **15**(8): p. 967-972.

201. Moorman, A.V., et al., *IGH@ Translocations, CRLF2 Deregulation, and Microdeletions in Adolescents and Adults With Acute Lymphoblastic Leukemia.* Journal of Clinical Oncology, 2012. **30**(25): p. 3100-3108.

202. Nishida, K., et al., *The Ig heavy chain gene is frequently involved in chromosomal translocations in multiple myeloma and plasma cell leukemia as detected by in situ hybridization.* Blood, 1997. **90**(2): p. 526-534.

203. Gu, G.Y., et al., *IGF2BP1: a novel IGH translocation partner in B acute lymphoblastic leukemia.* Cancer Genetics, 2014. **207**(7-8): p. 332-334.

204. Russell, L.J., et al., *A novel translocation, t(14;19)(q32;p13), involving IGH@ and the cytokine receptor for erythropoietin.* Leukemia, 2009. **23**(3): p. 614-617.

205. Russell, L.J., et al., *t(6;14)(p22;q32): a new recurrent IGH@ translocation involving ID4 in B-cell precursor acute lymphoblastic leukemia (BCP-ALL).* Blood, 2008. **111**(1): p. 387-391.

206. Yoda, A., et al., *Functional screening identifies CRLF2 in precursor B-cell acute lymphoblastic leukemia.* Proceedings of the National Academy of Sciences of the United States of America, 2010. **107**(1): p. 252-257.

207. Dyer, M.J.S., et al., *Immunoglobulin heavy chain locus chromosomal translocations in B-cell precursor acute lymphoblastic leukemia: rare clinical curios or potent genetic drivers?* Blood, 2010. **115**(8): p. 1490-1499.

208. Andersson, A., et al., *Molecular signatures in childhood acute leukemia and their correlations to expression patterns in normal hematopoietic subpopulations.* Proceedings of the National Academy of Sciences of the United States of America, 2005. **102**(52): p. 19069-19074.

209. Schmah, J., et al., *Molecular characterization of acute lymphoblastic leukemia with high CRLF2 gene expression in childhood.* Pediatric Blood & Cancer, 2017. **64**(10).

210. Cavazzini, F., et al., *Chromosome 14q32 translocations involving the immunoglobulin heavy chain locus in chronic lymphocytic leukaemia identify a disease subset with poor prognosis.* British Journal of Haematology, 2008. **142**(4): p. 529-537.

211. Gibbons, J.D. and S. Chakraborti, *Nonparametric Statistical Inference*. 5th ed. 2011, Boca Raton, FL: Chapman & Hall/CRC Press, Taylor & Francis Group.

212. Hollander, M., D.A. Wolfe, and E. Chicken, *Nonparametric Statistical Methods*. 3rd ed. 2013, Hoboken, NJ: John Wiley & Sons, Inc.

213. Jewison, T., et al., *SMPDB 2.0: Big Improvements to the Small Molecule Pathway Database.* Nucleic Acids Research, 2014. **42**(D1): p. D478-D484.

214. Frolkis, A., et al., *SMPDB: The Small Molecule Pathway Database.* Nucleic Acids Research, 2010. **38**: p. D480-D487.

215. Kessner, D., et al., *ProteoWizard: open source software for rapid proteomics tools development.* Bioinformatics, 2008. **24**(21): p. 2534-2536.

216. Sweeney, S.R., et al., *Identification of a synergistic combination of dimethylaminoparthenolide and shikonin alters metabolism and inhibits proliferation of pediatric precursor B-cell acute lymphoblastic leukemia.* Molecular Carcinogenesis, 2020. **59**(4): p. 399-411.

217. Hiraki, S., et al., *Establishment of an Epstein-Barr Virus-Determined Nuclear Antigen-Negative Human B-Cell Line From Acute Lymphoblastic Leukemia: Brief Communication2.* JNCI: Journal of the National Cancer Institute, 1977. **59**(1): p. 93-94.

218. Miyoshi, I., et al., *Human B cell, T cell and null cell leukaemic cell lines derived from acute lymphoblastic leukaemias.* Nature, 1977. **267**(5614): p. 843.

219. El-Sonbaty, S.S., et al., *Exogenous expression of human granulocyte colonystimulating factor receptor in a B-lineage acute lymphoblastic leukemia cell line: A possible model for mixed lineage leukemia.* Leukemia Research, 1995. **19**(4): p. 249-256.

220. Xu, D., et al., *JAK-STAT in lipid metabolism of adipocytes.* JAK-STAT, 2013. **2**(4): p. e27203.

221. McGillicuddy, F.C., et al., *Interferon gamma Attenuates Insulin Signaling, Lipid Storage, and Differentiation in Human Adipocytes via Activation of the JAK/STAT Pathway.* Journal of Biological Chemistry, 2009. **284**(46): p. 31936-31944.

222. He, C.C., et al., *Exercise-induced BCL2-regulated autophagy is required for muscle glucose homeostasis.* Nature, 2012. **481**(7382): p. 511-U126.

223. Plas, D.R., et al., *Akt and Bcl-x(L) promote growth factor-independent survival through distinct effects on mitochondrial physiology.* Journal of Biological Chemistry, 2001. **276**(15): p. 12041-12048.

224. Stine, Z.E., et al., *MYC, Metabolism, and Cancer.* Cancer Discovery, 2015. **5**(10): p. 1024-1039.

225. Bolden, J.E., M.J. Peart, and R.W. Johnstone, *Anticancer activities of histone deacetylase inhibitors.* Nature Reviews Drug Discovery, 2006. **5**(9): p. 769-784.

226. Bali, P., et al., *Inhibition of histone deacetylase 6 acetylates and disrupts the chaperone function of heat shock protein 90 - A novel basis for antileukemia activity of histone deacetylase inhibitors.* Journal of Biological Chemistry, 2005. **280**(29): p. 26729-26734.

227. Martindale, J.L. and N.J. Holbrook, *Cellular response to oxidative stress: Signaling for suicide and survival.* Journal of Cellular Physiology, 2002. **192**(1): p. 1-15.